1-1-2011

Shoe embedded air pump type piezoelectric power harvester

Naser Haghbin
Ryerson University

SHOE EMBEDDED AIR PUMP TYPE PIEZOELECTRIC POWER HARVESTER

by

Naser Haghbin

Bachelor of Mechanical Engineering, Iran University of Science and Technology, 1995

A thesis

presented to Ryerson University

in partial fulfillment of the

requirement for the degree of

Master of Applied Science

in the Program of

Mechanical Engineering

Toronto, Ontario, Canada, 2011

Author's declaration

I hereby declare that I am the sole author of this thesis.

I authorize Ryerson University to lend this thesis to other institutions or individuals for the purpose of scholarly research.

Naser Haghbin

I further authorize Ryerson University to reproduce this thesis by photocopying or by other means, in total or in part, at the request of other institutions or individuals for the purpose of scholarly research.

Naser Haghbin

SHOE EMBEDDED AIR PUMP TYPE PIEZOELECTRIC POWER HARVESTER

Naser Haghbin

Master of Applied Science, 2011

Mechanical Engineering

Ryerson University

Abstract

Conventional shoe embedded PZT (Lead Zirconate Titanate) power harvesters have the problem of low reliability and short life time due to the fragility of the PZT material for bending and the high stepping force which directly acts on the PZT-metal structure. In this thesis, a novel shoe embedded PZT power harvester is presented, which is able to solve the problem of low reliability and short life time associated with conventional designs. This harvester uses an air pump to squeeze the air into a fixed chamber to deform a PZT diaphragm to generate electricity. Thus the high stepping force is directly taken by the housing of the harvester instead of the PZT material. A power of 1.12 mW is generated at a speed of 4 mph on a treadmill. The stepping force acting on the harvester is also measured, which indicates the power harvester can survive a very high stepping force.

Key Words: Piezoelectric power harvesting, Shoe-embedded, Air pump, high reliability

Acknowledgements

I would like to thank:

- Dr. Siyuan He, for giving me the opportunity to work in the field of Power Harvesting and for his encouragements, support, and guidance throughout the course of this research project.
- Devin Ostrom and Joseph Amankrah for their technical advice and fabricating the harvester parts.
- Special thanks to Yuan Xue and Chao Fan for their prompt assistance in times of need. Without them, the countless hours of treadmill tests were not possible.
- My good friend Soonho Park for his great technical supports especially during working with different engineering software.
- All my graduate friends Zewdu Hailu, James Chong, Soonho Park, Yuan Xue, and Chao Fan for making my graduate studies enjoyable throughout my time at Ryerson University.
- Most deeply, I thank my wife, Dr. Negin Etehad, for her guidance, unconditional support, and friendship over the years. Through her example, I came to believe that I could, with God's help, accomplish any task to which I set my mind.

Table of Contents

Author's declaration ii
Abstract iii
Acknowledgements iv
List of Tables vii
List of Figures viii
Nomenclature xii
Chapter 1 Introduction 1
1.1 Power Harvesting 1
1.2 Power Harvesting From Human Motion 1
1.3 Existing Shoe Embedded Power Generators 3
1.4 Problems With Existing Shoe Embedded Piezoelectric Power Generators 11
1.5 Objectives 12
Chapter 2 Design and Modeling of the Harvester 14
2.1 Principle of Operation 14
2.2 Piezo Diaphragm Design 16
2.3 Air Chamber Design 18
2.4 Finite Element Simulation 19
2.5 Theoretical Prediction of Generated Power 21
2.5.1 Modeling of Piezoelectric Generator 21
2.5.2 Principle of Piezoelectric Composite Diaphragm 23
2.5.3 Transverse Displacement of the Piezo Diaphragm 25
2.5.4 Total Kinetic Energy of Bimorph Piezo Diaphragm 26
2.5.5 Total Potential Energy of Bimorph Piezo Diaphragm 27
2.5.6 Generated Voltage and Charge for a Clamped Bimorph Piezo Diaphragm 29
Chapter 3 Prototype of Air Pump Piezo Power Generator 31
3.1 Prototype and Fabrication 31
3.2 Modification of the Power Harvester 35
3.2.1 Fabrication and Assembly Process of New Parts 37
3.3 Integration in a Shoe 38
Chapter 4 Experimental Tests and Results Analysis 41

4.1 Voltage and Power Measurement Tests 41
4.1.1 Experimental Test Setup for Measuring Voltage 41
4.1.2 First Trial With Hand Impact Force 42
4.1.3 First Experimental Test on a Treadmill 43
4.1.4 More Experimental Tests on a Treadmill 43
4.1.5 Experimental Tests after Harvester Modification 45
4.2 Theoretical Simulation and Comparison 49
4.2.1 Results Analysis and Discussion 51
4.3 Foot Stepping Force 52
4.3.1 Force Experimental Test Set Up 52
4.3.2 Force Test Results 55
Chapter 5 Summary and Future Work 57
5.1 Summary 57
5.2 Future Work 58
Appendix A Piezoelectric Configurations 59
Appendix B The Harvester Drawings 69
References 78

List of Tables

Table 1.1 Comparing three method of harvesting energy from vibration [1-2] 4

Table 2.1 Material properties and structural parameters of the diaphragm 18

Table 2.2 The dimensions of air pump and bottom and upper chambers 19

Table 2.3 Element types for piezo and substrate in ANSYS. 20

Table 2.4 Compared the result of ANSYS modeling with design theories. 21

Table 3.1 Different parts of the harvester (refer to Figure 3.1) 31

Table 3.2 Added parts to the harvester after modification (Figure 3.9). 36

Table 4.1. Test results by applying hand force. 42

Table 4.2. Measured maximum force when walking on the treadmill. 55

Table A.1 Comparison of piezoelectric materials [3]. 60

Table A.2 Some researches based on materials. 61

Table A.3 Some researches based on using piezoelectric patches. 62

Table A.4 Some researches based on various geometries. 63

Table A.5 Some bulk transducer structures for energy harvesting [1-2][12-14][45][63-66] 64

List of Figures

Figure 1.1 Possible reachable power from human body (footfalls can give the most power) [2]. . 2

Figure 1.2 Schematic of electromagnetic power generator [13]. 3

Figure 1.3 Schematic of electrostatic power generator [14]. 3

Figure 1.4 Schematic of piezoelectric power generator [3]. 4

Figure 1.5 Two sets of prestressed PZT unimorph under the heel [15]. 5

Figure 1.6 Schematic layout of PVDF harvester [15] [19]. 5

Figure 1.7 Two sets of PZT unimorph and PVDF harvester inside the shoes [15]. 6

Figure 1.8 Two piezo films connected in parallel and inserted in shoes [16]. 6

Figure 1.9 Dielectric elastomer acts as an electrostatic generator. When it deforms it produces power due to changing in plate distance [17]. 6

Figure 1.10 Two PVDF films above the shoe sole and an electrostatic generator under the sole [18]. 7

Figure 1.11 Microstructure polymer film is rolled into 120 layers of 1-cm thick [19]. 7

Figure 1.12 Custom clamp system with rectangular bimorph piezo beam inside the shoe [22]. ... 8

Figure 1.13 Bimorph piezo beam with the curved L-shaped mass [23]. 8

Figure 1.14 A schematic of rotary power generators [24]. 9

Figure 1.15 A rotary generator system [26]. 9

Figure 1.16 Improved rotary generator with gears and two magnetic generators [24]. 9

Figure 1.17 Cross section of generator with 2 magnet and 2 coils [27]. 10

Figure 1.18 Prototype of tubular linear generator. (a) Stator coils, (b) mover magnets [28]. 10

Figure 1.19 (a) Generator coil, fonner and magnet, (b) Generator integrated in a shoe [29]. 10

Figure 1.20 Demonstrator generator with 3 coils (150 turns of copper enamelled Wire) [30]. ... 10

Figure 1.21 Two disk magnets facing each other in opposition: one is fixed and the other one is free to move through the coil [30]. 11

Figure 2.1 Cross section schematic of circular air pump piezo power generator with a circular bimorph piezo diaphragm before and after applying foot impact force (a) the piezo diaphragm before deformation in normal condition, (b) The Piezo diaphragm is deformed with air pressure, (c) the harvester completely embedded inside the shoe without increasing the shoe size. 15

Figure 2.2 (a) Schematic of circular clamped bimorph piezo diaphragm (connected in parallel). (b) Schematic of positive and negative stress distribution on the diaphragm. 17

Figure 2.3 ANSYS modeling and deflection of the diaphragm after maximum deformation...... 20

Figure 2.4. ANSYS stress analysis of the diaphragm after maximum deformation..................... 21

Figure 2.5 An equivalent model for a piezoelectric energy harvester. 22

Figure 3.1 Prototype of the harvester. (a) Outside looking of the harvester. (b) Internal view of the harvester (also look at Table 3.1)... 32

Figure 3.2 (a) the bottom circular plate of the harvester (part 5) (b) the upper circular plate of the harvester (Item 4).. 33

Figure 3.3 (a) the wave spring (Item 1) and the spring connection plate (Item 2), (b) the top circular plate (Item 7)... 34

Figure 3.4 The seal ring (Item 6) to keep and seal the rubber bottom surrounding...................... 34

Figure 3.5 Bimorph piezo diaphragm with shim plate (Item 8) is parallel extension operation which means three wires are connected (two of them to Piezo layers and one to brass shim). (a) Upside of piezo diaphragm. (b) Downside of the piezo diaphragm 35

Figure 3.6 The initial wave spring without end shim plate (model C-150 Smalley Co.) 35

Figure 3.7 The wave spring with end shim plate (model CS-137 Smalley Co.). 36

Figure 3.8 (a) The bottom aluminum ring to keep the bottom of spring, (b) The top aluminum ring to fix the top of spring. 37

Figure 3.9 Cross section of modified power harvester. 37

Figure 3.10 Fabrication process of the harvester parts; the cure time between each step is 24 hours due to required time for epoxy hardness.. 38

Figure 3.11 (a) A 55 mm hole inside the heel for placing the power generator, (b) A hole for wire path.. 39

Figure 3.12 (a) The harvester is embedded in the shoe heel, (b) The level of harvester is the same as shoe pad level. 40

Figure 4.1 Experimental test set up on treadmill for measuring the voltage: The wearer walks with speed ranging from 1mph to 4 mph.. 41

Figure 4.2 Experimental test set up on treadmill: Electrical connection of the testing setup....... 42

Figure 4.3 Power versus resistance in different speeds (first experimental test on treadmill). ... 43

Figure 4.4 Power versus resistance (second test).. 44

Figure 4.5 Power versus resistance (third test). 44

Figure 4.6 First test after modification (power versus resistance)... 45

Figure 4.7 First test after modification (voltage versus resistance).. 46

Figure 4.8 Second test after modification (power versus resistance). 46

Figure 4.9 Second test after modification (voltage versus resistance).. 47

Figure 4.10 Slut was made due to edge of epoxy. 47

Figure 4.11 (a) Vrms (voltage) versus resistance and (b) Power versus resistance for four speeds of 1 mph, 2 mph, 3 mph, and 4 mph on the treadmill.. 48

Figure 4.12 Comparing experimental output powers with predicted theoretical power values in different resistances for 1 mile/hour. 50

Figure 4.13 Comparing experimental output powers with predicted theoretical power values in different resistances for 2 mile/hour. 50

Figure 4.14 Comparing experimental output powers with predicted theoretical power values in different resistances for 3 mile/hour. 51

Figure 4.15 Comparing experimental output powers with predicted theoretical power values in different resistances for 4 mile/hour. 51

Figure 4.16 (a) A force measurement sensor with a 50 mm diameter poly carbonates plate, (b) The poly carbonate plate is covered the sensing area. 53

Figure 4.17 (a) Force measurement device (wireless ELF system from Tekscan, INC.), (b) Force experimental test set up on a treadmill. 54

Figure 4.18 Heel force on harvester for speed 1mile/hour to 4 miles/hour. 55

Figure 4.19 Measured steeping force for random stepping on the floor...................................... 56

Figure 5.1 Moulded air below is applicable for air pump... 58

Figure A.2 Operating modes of piezoelectric transducer [12]... 60

Figure A.3 (a) A series triple layer type piezoelectric sensor, (b) A parallel triple layer type piezoelectric sensor, (c) A unimorph piezoelectric sensor [3], [32]. 66

Figure A.4 Section of a homogeneous bimorph beam. tc/2 corresponds to a piezoelectric film thickness [69]. 66

Figure A.5 Cross section of symmetric heterogeneous bimorph beam. tc/2 corresponds to piezoelectric film thickness whereas ts correspond to non-piezoelectric film thickness [69]...... 66

Figure A.6 Cross section of asymmetric heterogeneous bimorph beam. tc corresponds to piezoelectric film thickness whereas ts correspond to non-piezoelectric film thickness. Yc is the Young's modulus for the piezoelectric material and Ys is the Young's modulus for the non-piezoelectric material. W0 is the width of the beam [69]. 66

Figure A.7 Cantilever beam designs with (a) trapezoidal, and (b) rectangular footprints [1], [69]. 67

Figure A.8 Unimorph piezoelectric circular harvester: (a) Cross section view, (b) Top view [5].67
Figure A.9 Cross section of PZT composite diaphragm [57]. 67
Figure A.10 Cross section of decoupled piezo diaphragm [50-52]. 67
Figure A.11 Ceramic fibers of various cross-sections [66]. 68

Nomenclature

ω	Natural frequency (rad/s)
$\varepsilon/\varepsilon_o$	Dielectric constant
ϵ_{33}^{T}	The permittivity in the z-direction
ε_o	Permittivity of free space (F/m)
ρ_c	Density of piezoelectric layer (kg/m^3)
ρ_m	Density of shim(brass) layer (kg/m^3)
η	Mechanical damping ratio
S_{yp}	Yield strength of the piezo (MPa)
S_{ym}	Yield strength of the substrate (MPa)
a	The radius of the diaphragm
α	Thickness ratio of piezo and substrate
a_i	The Raleigh coefficient
Λ_{eff}^{D}	The potential-energy factor of the whole composite diaphragm
b	Distance from the center of the shim to the center of the piezo (mm)
β	Diameter ratio of piezo and substrate
β_{33}^{T}	The impermeability ($\beta_{33}^{T} = \frac{1}{\epsilon_{33}^{T}}$)
C_f	Free piezo capacitance (C/V)
C_P	Capacitive of piezoelectric element
D	Electric displacement (C/m^2)
d_{31}	Strain coefficient (m/V)
E	Electric field (V/m)
E^D	The young's modulus of the piezoelectric membrane
E_m	The young's modulus of the substrate membrane
F	Force (N)
f	Frequency (Hz)
g_{31}	The piezoelectric voltage constant
H_{mass}	Height of the mass (mm)
i	Current (A)

I	Moment of inertia (m^4)
k_{31}	Piezoelectric coupling coefficient
K	Spring effective stiffness
K_1 and K_2	Kinetic-energy factors
l_b	Length of the beam (mm)
l_e	Length of the electrode (mm)
L_{mass}	Length of the mass (mm)
L_m	Equivalent inductance (H)
l_m	Length of the mass contacting the beam (mm)
$M(x)$	Moment (Nm)
M	Effective mass (kg)
m	The substrate thickness
n	Transformer turns ratio
P	Power output (W)
Po	Pressure (Kpa)
P_i	Initial pressure before air chamber deformation (Kpa)
P_f	Final pressure after air chamber deformation (Kpa)
Q_o	The generated charge
R_b	Equivalent resistance (Ω)
R_{opt}	Optimal external load
r	The distance from the center of the diaphragm to the point of the deflection
S	Strain (mm/mm)
S_1	The strains in the radial directions
S_2	The strains in the angular directions
$\dot{S}$	Strain rate
s	Compliance (m/N)
σ^D	Poison’s ratio of the piezoelectric membrane
σ_m	Poison’s ratio of the substrate membrane
T	Stress induced by electrical effects (N/m^2)

T_1	The stresses in the radial directions
T_2	The stresses in the angular directions
T_P^D	The kinetic energy for piezo and substrate (J)
U_C^D	The potential energy of the two piezoelectric membranes (J)
V_i	Initial volume before air chamber deformation (m3)
V_f	Final Volume before air chamber deformation (m3)
V_{oc}	Open circuit voltage
V_{rms}	The root mean square voltage (V)
wb	Width of the beam (mm)
wm	Width of the mass (mm)
Yc	Young's modulus of piezoelectric layer (GPa)
Ym	Young's modulus of mass (GPa)
Ysh	Young's modulus of shim (brass) layer (GPa)
$\ddot{y}$	Input acceleration (m/s2)
W(r)	Deflection of the piezoelectric diaphragm in Z direction (mm)
$\ddot{w}$	Acceleration in Z direction (m/s2)
PVDF	Polyvinylidine Fluoride
PZN − PT	Lead Zinc Niobate – Leate Titanate
PZT	Lead Zirconate Titanate

Chapter 1 Introduction

1.1 Power Harvesting

The interest in power harvesting technology has been increasing in recent years. Power harvesting is the act of scavenging energy from the surrounding environment energy sources such as heat, light, vibration, and movement and converting these energies into electrical energy. Harvesting energy from vibration and mechanical movements (low frequency vibration) is the most attractive method of power harvesting [1] [2]. These power generators harvest electricity from vibration or motion and the output can be used for small electronic devices such as a Bio-MEMS device, a cell phone or a GPS.

The goal of this type of power generation is to replace batteries and make small electronic systems battery-less [1]. The two main battery problems are [3]:

- A battery has limited operation time for the sensor and wireless communication devices.
- The chemicals in batteries are a pollution source and their recycling process is very difficult and expensive.

Because of these disadvantages, the total cost of ownership for battery-powered devices is much higher than for self-powered electronic devices. Battery-less systems overcome these limitations and have additional advantages of being maintenance-free and environmental friendly.

1.2 Power Harvesting From Human Motion

One of the main power sources for harvesting energy is body motion (such as breathing, chest motion, and footsteps during walking). Human chest motion during breathing has been used for wearable computer applications [2]. Scavenging electricity from heel strikes during walking is another method of human power harvesting [4]. Join motion has also been evaluated for power generation [5]. An experimental study of energy harvesting in an artificial knee joint after total knee replacement surgery has been carried out [6]. Knee movement has been used to power a DC electric generator [7]. Electrical energy has been derived from the vertical movement of suspended-load backpack carried by a walking person using a linear-to-rotary resistor load to a DC motor [8]. Sodano [9] has presented an energy harvester in a backpack that can generate electrical energy from the differential forces on a stack piezo between the wearer and the pack. The motion of a magnet in a linear permanent magnet generator has been utilized to convert the vertical motion energy to electricity [10] [11]. Starner and Paradiso [2] have also theoretically calculated the output power from different parts of human bodies. They have concluded that maximum power can be derived from footsteps (Figure 1.1).

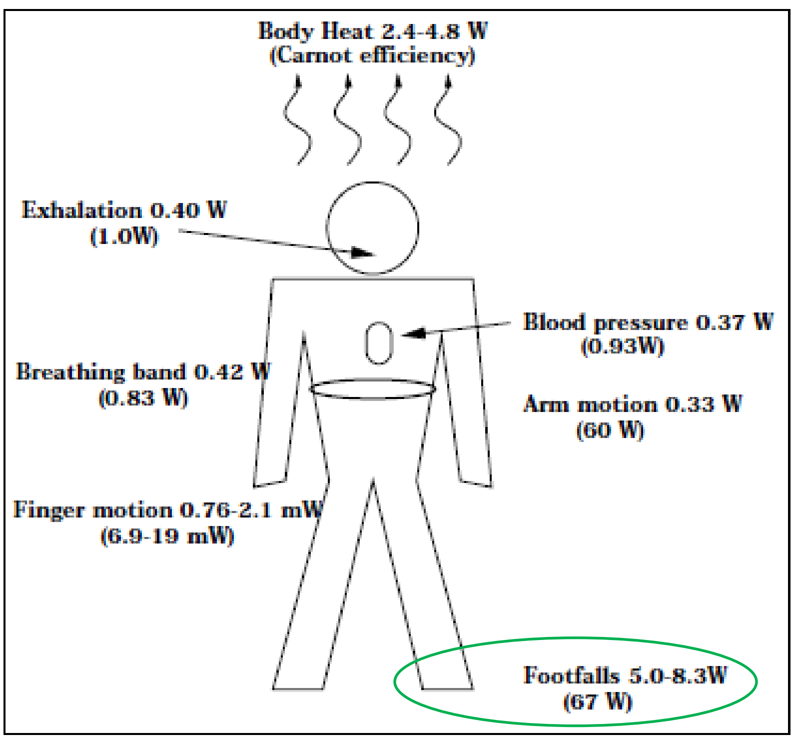

Figure 1.1 Possible reachable power from human body (footfalls can give the most power) [2].

1.3 Existing Shoe Embedded Power Generators

Generally, three methods exist to obtain electrical energy from mechanical movement [3] [12].

- **Electrostatic (capacitive) power conversion**

  The relative motion of an electrical conductor in a magnetic field causes a current to flow in the coil (Figure 1.2).

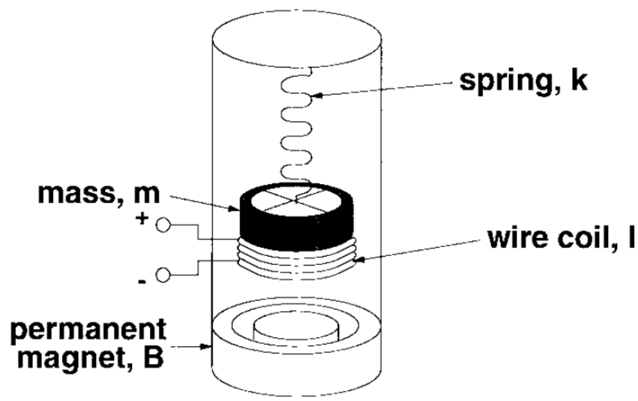

Figure 1.2 Schematic of electromagnetic power generator [13].

- **Electrostatic (capacitive) power conversion**

Two conductors, which are separated by a dielectric (i.e. a capacitor), moves relative to one another and the electrical energy is stored in the capacitor (Figure 1.3).

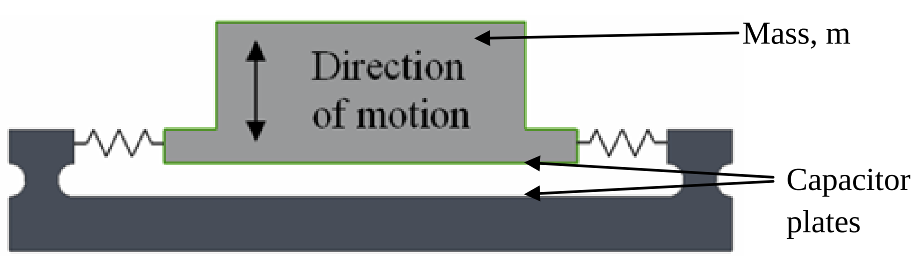

Figure 1.3 Schematic of electrostatic power generator [14].

- **Piezoelectric power conversion**

Piezoelectric materials are materials that deform in the presence of an electric field, or conversely, produce an electrical charge when mechanically deformed (Figure 1.4). Therefore, the higher the strain is produced, the higher the power is generated from the piezoelectric material. In Table 1.1, these three methods are compared.

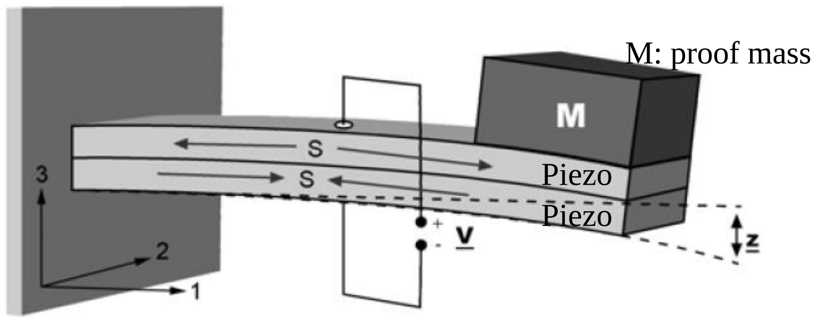

Figure 1.4 Schematic of piezoelectric power generator [3].

Table 1.1 Comparing three method of harvesting energy from vibration [1-2]

Method	Advantages	Disadvantages
Electrostatic (capacitive) power conversion	1) uses a non-resonant operating mode 2) easier to integrate with electronics and micro systems. 4) voltages of 2 to 10 volts.	1) require a separate voltage source to charge capacitor 2) more mechanical damping 3) mechanical stops is needed
Electromagnetic (inductive) power conversion	1) no separate voltage source 2) no mechanical contact or stops 3) little mechanical damping	1) low voltages. (max 0.1 V) 2) should use a small transformer
Piezoelectric power conversion	1) no separate voltage source 2) high energy density	1) difficulties to development of high quality piezoelectric thin-films

Two sets of prestressed spring metal strips with semi flexible PZT under the heel (manufactured as the $Thunder^{TM}$ by Face International) and two sets of 8 layers of stack of PVDF on the top and the bottom of plastic sheet has been used (Figure 1.5 and Figure 1.6) for the shoe insole [15]. Figure 1.7 shows the place of two sets of PZT unimorph and PVDF harvester under the shoes [15]. Two parallel DT4-028K/L piezoelectric films from MSIUSA, which inserted inside the shoe (Figure 1.8), have also been utilized for shoe power harvesting [6]. Dielectric elastomer has been mounted between bellows filled with a fluid or gel and integrated in the shoe heel [17]. This harvester is an electrostatic harvester which needs an initial voltage to apply across each face of the elastomer (Figure 1.9). A piezo (PVDF) power harvester and an electrostatic power harvester have been developed by Rocha [18]. The voltage from PVDF acts as an initial voltage for electrostatic harvester (Figure 1.10). Han and Kaajakari [19] have inserted 120 layers of microstructured piezoelectric polymer film in the shoe heel for generating electricity from footstep force (Figure 1.11).

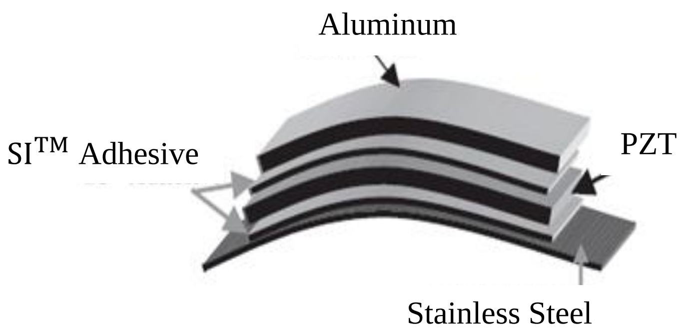

Figure 1.5 Two sets of prestressed PZT unimorph under the heel [15].

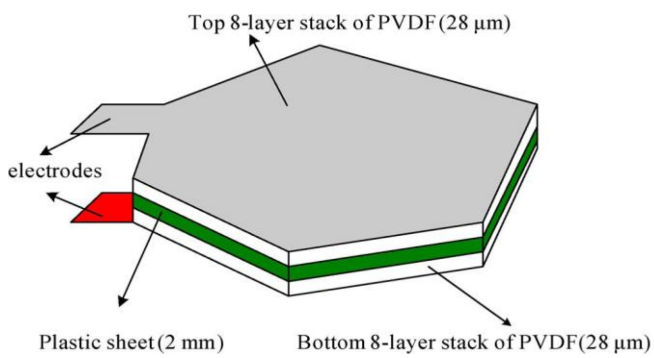

Figure 1.6 Schematic layout of PVDF harvester [15] [19].

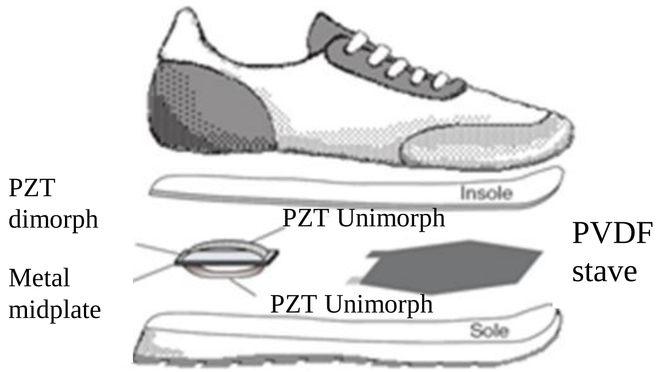

Figure 1.7 Two sets of PZT unimorph and PVDF harvester inside the shoes [15].

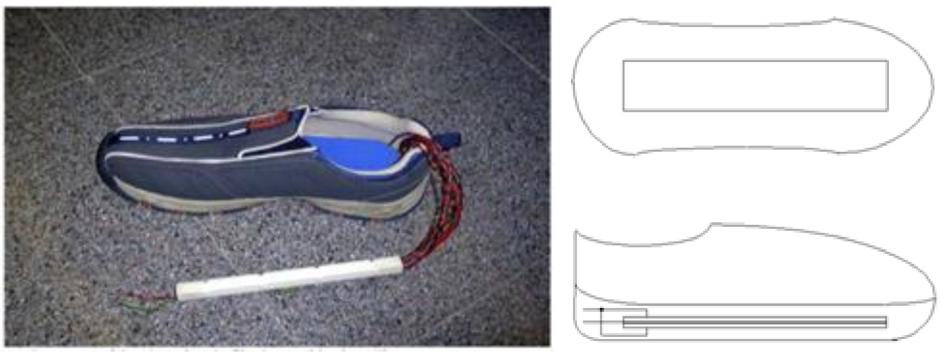
Figure 1.8 Two piezo films connected in parallel and inserted in shoes [16].

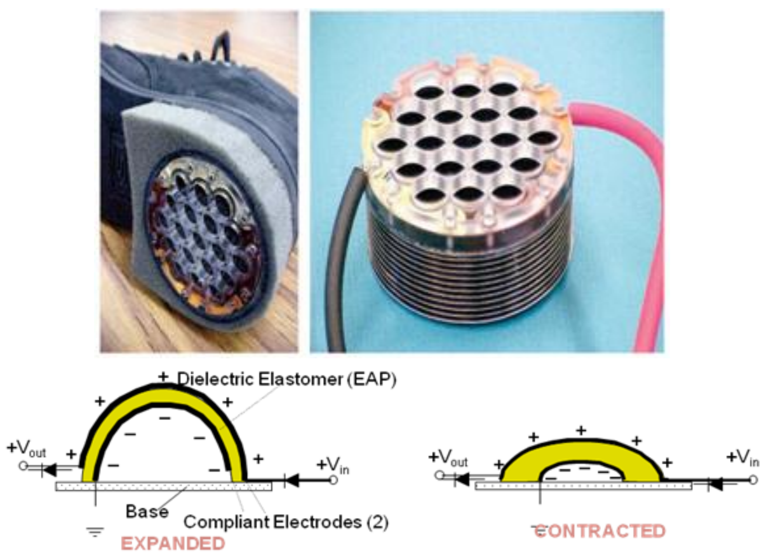

Figure 1.9 Dielectric elastomer acts as an electrostatic generator. When it deforms it produces power due to changing in plate distance [17].

Figure 1.10 Two PVDF films above the shoe sole and an electrostatic generator under the sole [18].

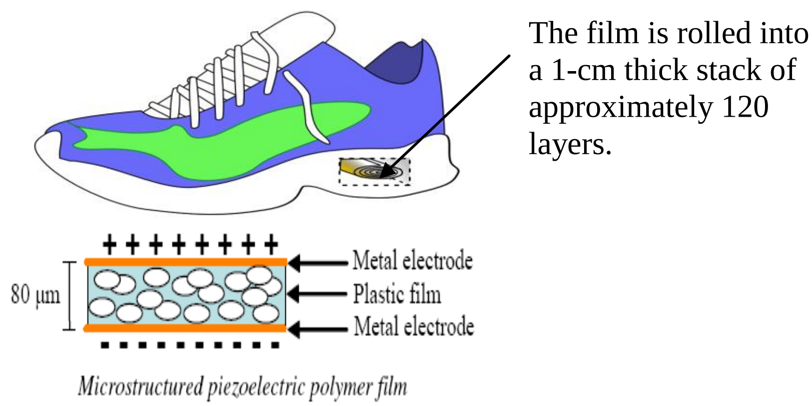

Figure 1.11 Microstructure polymer film is rolled into 120 layers of 1-cm thick [19].

Some articles discuss the piezo beam structures in shoes. Mateu and Moll [21] have analytically explained how to construct an optimum piezo beam-type harvester which is inserted in the shoe. They have introduced two types of piezo harvesters. One of them is based on the structure (homogeneous bimorph, symmetric, or asymmetric heterogeneous bimorph). The second type is based on the support. They concluded that the optimum selection for the piezoelectric is an asymmetric heterogeneous bimorph with a simply supported beam. They express that the shoe cavity dimension is also a factor to consider. Moro and Benasciutti [22] have utilized a conventional bimorph piezo beam with a proof mass in the shoes (Figure 1.12). Li [23] has used a bimorph piezo with a curved L-shaped mass (Figure 1.13) in the shoe.

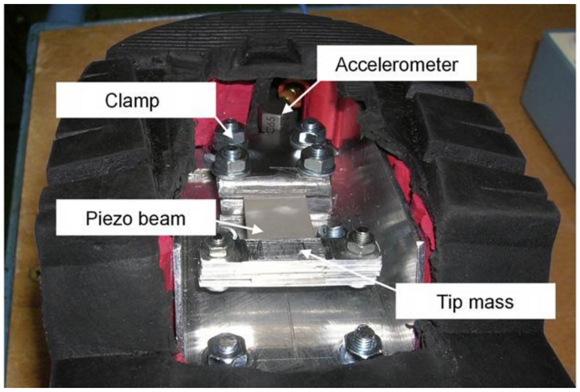

Figure 1.12 Custom clamp system with rectangular bimorph piezo beam inside the shoe [22].

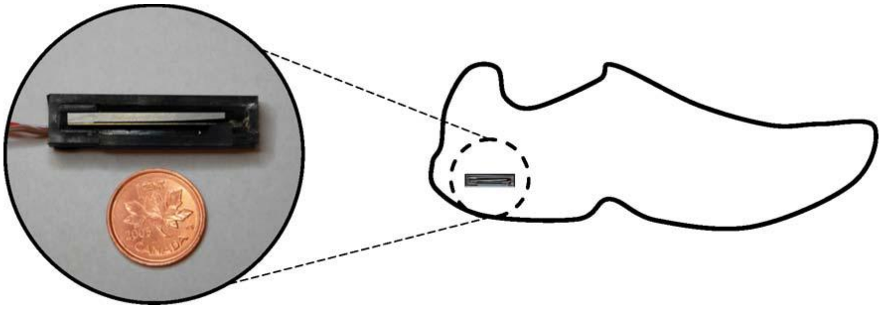
Figure 1.13 Bimorph piezo beam with the curved L-shaped mass [23].

A rotary generator has also been used to convert foot vertical movement to electrical energy [24-26]. This type of generator basically uses a rotary arm to convert a linear heel strike into rotary motion (Figure 1.14). The arm is compressed and the rotor rotates in magnetic field by a gear system and the electricity is made in the coils. Based on this idea, Paradiso and his team [26] developed a system with a simple spring, flywheel, and generator system (Figure 1.15). Hayashida [24] improved this harvester and integrated it inside the shoe heel (Figure 1.16). As rotary generators need to spin rapidly to achieve efficiency, these systems all involve significant gear ratios, which introduce considerable mechanical complexity and fairly high torque, leading to a high probability of breakage [2].

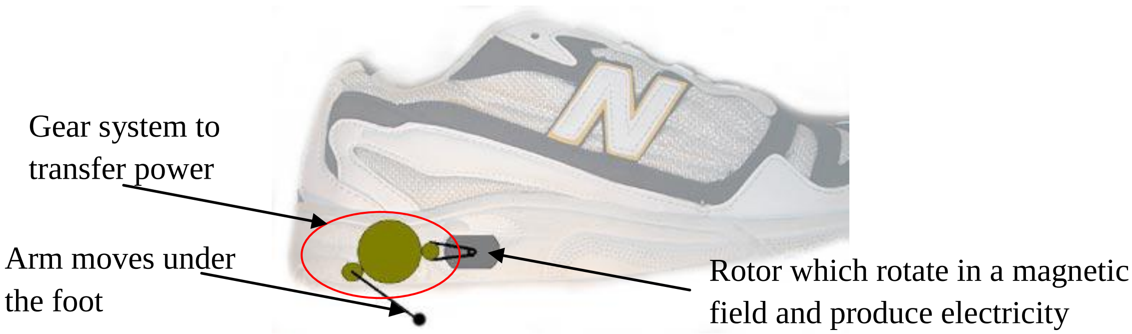

Figure 1.14 A schematic of rotary power generators [24].

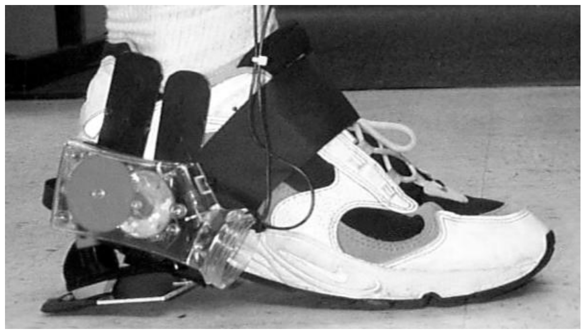
Figure 1.15 A rotary generator system [26].

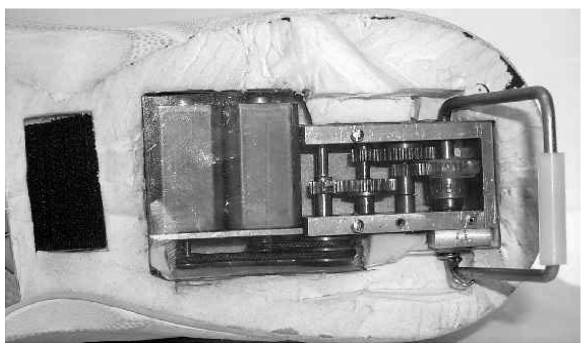
Figure 1.16 Improved rotary generator with gears and two magnetic generators [24].

Some articles (Figure 1.17, Figure 1.18, Figure 1.19, Figure 1.20, and Figure 1.21) have designed electromagnetic power generators for shoes [27-30]. In these generators, a magnet moves inside a coil.

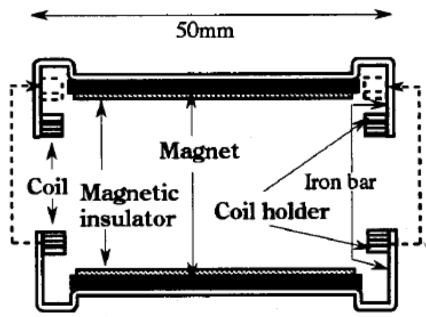

Figure 1.17 Cross section of generator with 2 magnet and 2 coils [27].

(a) (b)

Figure 1.18 Prototype of tubular linear generator. (a) Stator coils, (b) mover magnets [28].

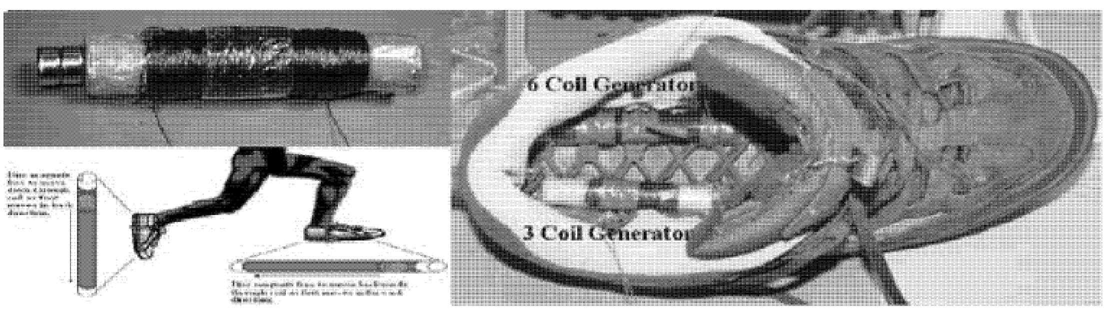

(a) (b)

Figure 1.19 (a) Generator coil, fonner and magnet, (b) Generator integrated in a shoe [29].

Figure 1.20 Demonstrator generator with 3 coils (150 turns of copper enamelled Wire) [30].

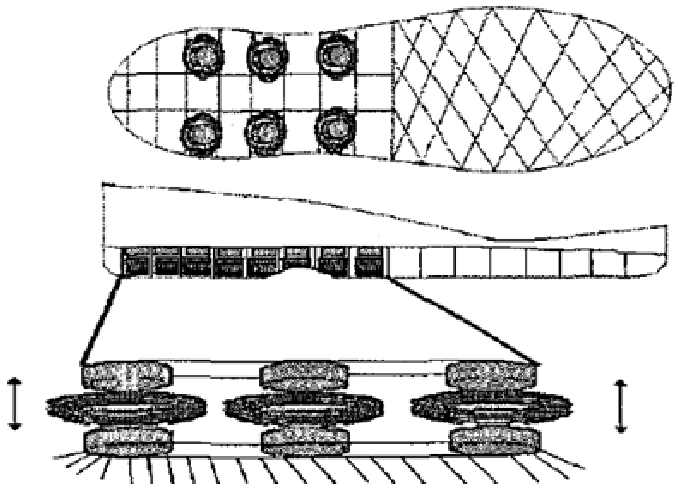

Figure 1.21 Two disk magnets facing each other in opposition: one is fixed and the other one is free to move through the coil [30].

This thesis will focus on piezo power harvesters for highest energy density in comparison with other types of power harvesters (Table 1.1) and their ability to convert directly applied strain energy into usable electric energy without any need for a separate voltage source [31] and they can easily be integrated into the shoe heel.

1.4 Problems With Existing Shoe Embedded Piezoelectric Power Generators

Literature reviews about existing shoe power harvesters have explained about difficulties in translating energy from the foot to the piezoelectric [2] [39]. Among all existing piezo materials, PZT is the main piezo material for power harvesting due to the most efficient vibration excitation [31-33] [34-38]. However, it is hard and brittle and does not have much range of motion in 3-1 direction and is not suitable for applications such as foot sole where flexibility is necessary [2]. Moreover, in the actual heel strike, the strain is concentrated at the bending point of the foot rather than distributed evenly [10].

In many shoe embedded PZT power harvesters, the high stepping static/impact force is directly acting on a PZT-metal structure, which leads to a low reliability and short life time due to the fragile nature of PZT materials and the vulnerability of the bonding between the PZT and metal under periodic impact forces. For designing a robust power harvester, the high pressure of the foot heel on the harvester should be considered. Research shows that the peak heel pressures during walking could be as high as 500~1000 Kpa.

Foot pressure distribution during walking in young and old adults is introduced by Hessert [40]. Hutton and Drabble [41] have introduced an apparatus to give the distribution of the vertical load under the foot. The foot type has also affected pressure during walking and running [42]. Zhu [43] has determined that the peak heel pressure is 665 kPa for 7 min walking at a cadence of 60 steps/min and has also mentioned that their results for peak pressures are consistent with those obtained by other researchers. It has also been found [44] that the heel peak pressures could go up to 1000 kPa when the subject was wearing shoes [44]. Soames and Clark [45] found peak pressures in the range of 600-900 kPa when the subject walked in shoes. Henning and Nilani [46] measured that the maximum foot heel pressure is 688 kPa. Nevill [47] found this measure to be 1000 kPa and Whittle [48] has reported that the heel pressure is 575 kPa.

1.5 Objectives

Shoe embedded PZT power harvesters are plagued with low reliability and short life time. This is because of the bending mode of PZT plates is often used for power harvesting. But PZT plates are brittle and fragile for bending and thus cannot take the high static and impact forces from foot stepping.

In this thesis, a novel shoe embedded air-pump type PZT power harvester is presented. The harvester can take very high static and impact forces through an air-pump design to achieve high reliability and long life time. In addition, the harvester is compact and can be easily embedded inside the shoe heel.

The thesis is organized as follows. The principle of the harvester is explained after the introduction. Then the modeling of the harvester is presented. Prototype and experimental tests are introduced next. Moreover, a method for measuring the heel force on the harvester is introduced. After that, conclusions are summarized. In Appendix A, a literature review about different configurations of the piezo power harvester and relevant piezo parameters are presented. Drawings are also given in Appendix B.

Chapter 2 Design and Modeling of the Harvester

There are some constraints to design a shoe power generator such as size limitation (especially height), comfort during walking, durability, tolerating high impact force, lightweight, and simple construction. In this harvester, an air pump is used that not only makes a relax feeling during walking but also makes air pressure to deform piezo diaphragm.

2.1 Principle of Operation

Figure 2.1 shows the air pump type shoe embedded piezoelectric power harvester. It consists of an air pump and a circular bimorph piezo diaphragm which is located in a fixed chamber. The bimorph piezoelectric diaphragm separates the fixed chamber into two parts, i.e., the upper part is connected through to the air pump and the lower part is sealed by the piezoelectric diaphragm. The air pump is sealed with a flexible rubber. The top plate of the air-pump is supported by a high stiffness spring. The harvester is embedded inside the shoe heel. When the shoe is under no stepping force, the air pressures of the upper part and lower part of the fixed chamber inside the air pump are the same and equal to atmospheric pressure. Once the foot stepping force is applied, the air inside the air pump is squeezed into the upper part of the fixed chamber and the air pressure increases, which bends the PZT diaphragm as shown in Figure 2.1(b). The piezoelectric diaphragm moves back to its normal position the foot stepping force is released. The back and forth deformation of the piezoelectric diaphragm generates electric power.

In this shoe embedded PZT power harvester design, the static/impact force from the foot stepping is taken by the housing of the fixed chamber which is made of metal such as aluminum or hard plastic and thus can take high force. The load acting on the PZT diaphragm is caused by the pressure difference between the upper and lower parts of the fixed chamber. This pressure difference is controlled by the dimension ratio of the air pump and the upper part of the fixed chamber. Hence, unlike its conventional counterpart designs, in the shoe power harvester presented in this thesis, the high static/impact force from the foot stepping does not directly apply to the PZT diaphragm. Instead the piezoelectric unit is well protected in a fixed chamber and it deforms due to the controllable air pressure difference. As a result a high reliability and long life time of the show embedded power harvester can be achieved. In addition the power harvester has a compact structure and can be easily integrated into the shoe heel without increasing the shoe size as shown in Figure 2.1(c).

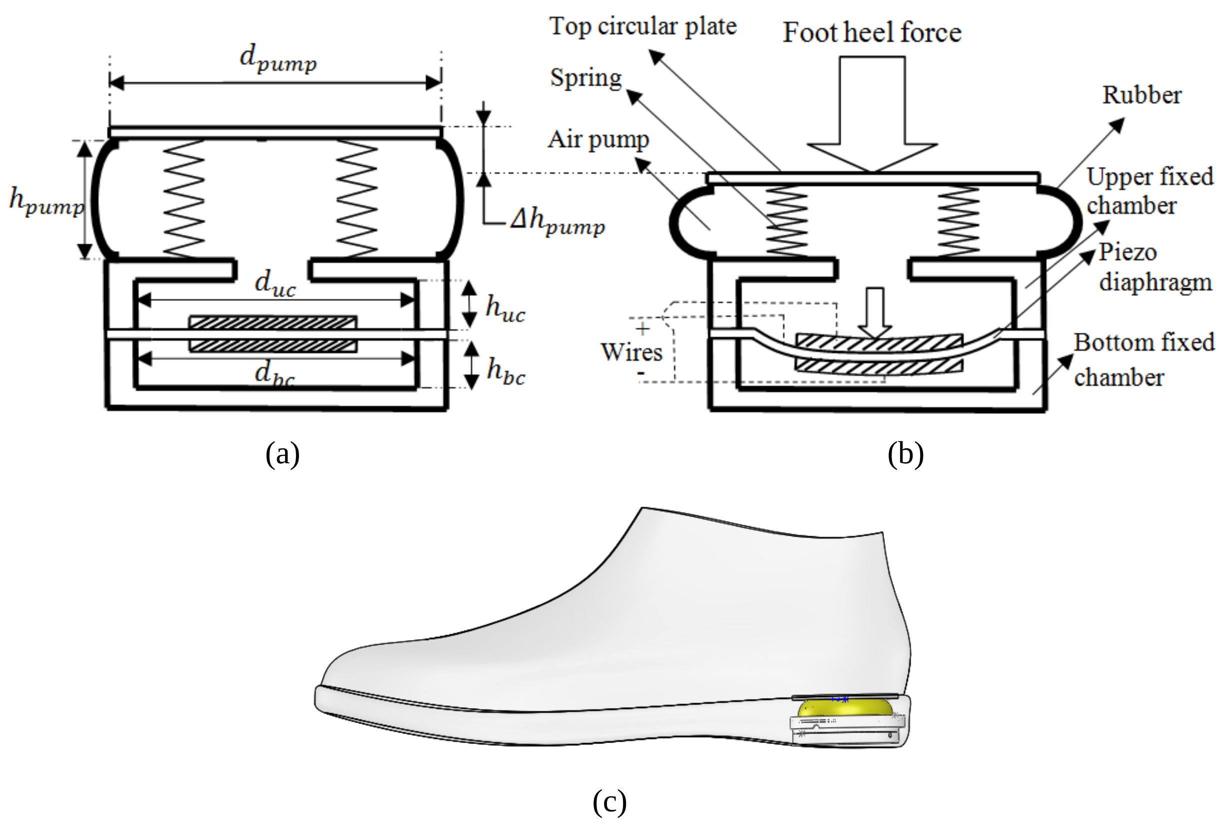

Figure 2.1 Cross section schematic of circular air pump piezo power generator with a circular bimorph piezo diaphragm before and after applying foot impact force (a) the piezo diaphragm before deformation in normal condition, (b) The Piezo diaphragm is deformed with air pressure, (c) the harvester completely embedded inside the shoe without increasing the shoe size.

This harvester can use a typical PZT plate without any damage to this fragile piezo and bonding between piezo and substrate layers. The air chamber size and the pressure on top of piezo can be adjusted based on piezo strength, shape, and configuration. The harvester also has the capability to be redesigned in a way that the air bellow is put inside the shoes and the piezo chamber part is attached outside the shoes, which means that the piezo part can be reused for different shoes.

2.2 **Piezo Diaphragm Design**

There are some researchers that have presented a theoretical analysis of unimorph piezoelectric diaphragms with simply supported and clamped boundary conditions as a potential tool for generating electrical energy from blood pressure variation for low pressure (5330 Pa) [49-59]. Moreover, Kim et al. [50-52] have developed and tested a decoupled PZT circular diaphragm with a clamped edge. The power performance of circular bimorph piezoelectric diaphragm generators (Figure 2.2) have also been analyzed [57-58]. Tang [57] has also mentioned that the bimorph diaphragm has the capability to be inserted in the heels of shoes. All above researchers tries to reach analytical models for predicting output power of diaphragm generators. However, none of them has developed and designed a real device with practical application for harvesting energy from body movement. In this design, the bimorph piezo diaphragm is practically used for deriving power from human motion.

Figure 2.2 (a) shows the cross section of the bimorph PZT diaphragm. The shim layer of brass is clamped at its edge. Two PZT plates are connected in parallel. The piezoelectric plates do not cover the whole circular area in order to avoid cancellation of the generated positive and negative charges. If the PZT plates cover the whole diaphragm, when the diaphragm deflects under a uniform pressure, there would be areas subject to negative stress and positive stress

(Figure 2.2 (b)), which generate negative and positive charges on the same side of each PZT plate. The generated positive and negative charges cancel each other [50-52].

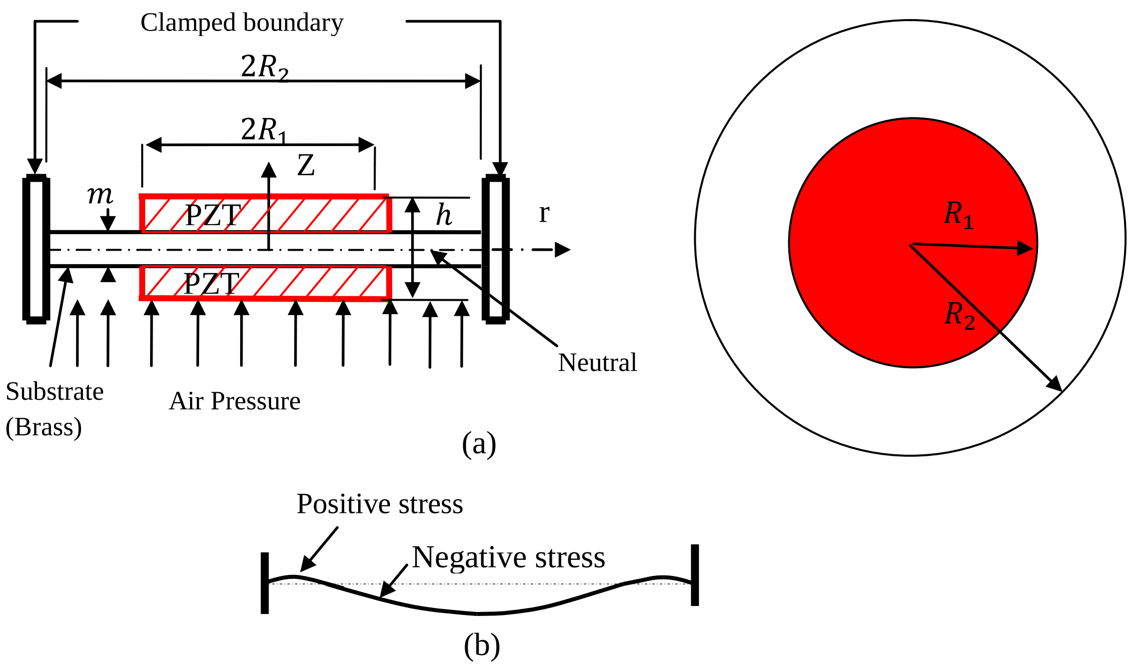

Figure 2.2 (a) Schematic of circular clamped bimorph piezo diaphragm (connected in parallel). (b) Schematic of positive and negative stress distribution on the diaphragm.

In Table 2.1 and refer to Figure 2.2, the dimensions of piezo diaphragm and material properties of PZT and brass are given.

Table 2.1 Material properties and structural parameters of the diaphragm

Parameter	PZT	Brass
Young module (N/m^2)	$E^D = 9.20E + 10$	E_m =9.72E+10
Density (kg/m^3)	ρ_C =7.90E+03	ρ_m =8.50E+03
Poison ratio	σ^D =0.31	σ_m =0.34
Piezo constant (Vm/N)	g_{31} =-7.90E-03	-
Piezo permittivity	ϵ_{33}^T=4.071E08	-
R_1 =Piezo radius (mm)	12.7	-
Thickness of each PZT plate (mm)	0.35	-
R_2=Substrate radius (mm)	-	25
m=Substrate thickness (mm)	-	0.2
Total diaphragm thickness h=0.9 (mm)	2 PZT layers	1 substrate layer

2.3 Air Chamber Design

In order to calculate the maximum deformation of the PZT diaphragm, the maximum air pressure load acting on the PZT diaphragm is calculated as follows. Refer to Table 2.2, the initial volume of the air pump is

$$V_i = h_{uc}\frac{\pi {d_{uc}}^2}{4} + h_{pump}\frac{\pi {d_{pump}}^2}{4} . \tag{2.1}$$

The final volume is

$$V_f = h_{uc}\frac{\pi {d_{uc}}^2}{4} + (h_{pump} - \Delta h_{pump})\frac{\pi {d_{pump}}^2}{4} . \tag{2.2}$$

The initial pressure inside the chamber is the atmospheric pressure. When the air pump is squeezed the pressure inside the upper part of the fixed chamber is

$$P_{upper} = P_a V_i / V_f . \tag{2.3}$$

Where Pa is the atmospheric pressure, which is 103 kPa. The lower part of the fixed chamber is assumed to remain unchanged when the air pump is squeezed because the change of the volume of the lower part of the fixed chamber due to the deformation of the PZT diaphragm is negligible. Thus the pressure load acting on the PZT diaphragm is

$$P_d = P_{upper} - P_{lower} = (P_a V_i / V_f - P_a) \tag{2.4}$$

Where P_{upper} and P_{lower} are the pressures in the upper and lower parts of the fixed chamber. Substituting the parameters into the above equations, the pressure load acting on the PZT diaphragm is 34 kPa.

Table 2.2 The dimensions of air pump and bottom and upper chambers

Parameter	Value (mm)
Pump diameter (d_{pump})	50
Pump height (h_{pump})	9.3
Spring (or pump) height deformation (Δh_{pump})	4.5
Upper chamber diameter (d_{uc})	36.3
Upper chamber height (h_{uc})	2
Bottom chamber diameter (d_{bc})	36.3
Bottom chamber height (h_{bc})	2.5

2.4 Finite Element Simulation

To verify the air chamber dimension, the air pressure on the piezo diaphragm is checked in an ANSYS simulation with the three following constraints [53]: 1) The stress of the PZT layer must be less than the PZT yield strength ($б_p < SY_{piezo}$). 2) The substrate stress must be less than the metal yield strength ($б_m < SY_{Brass}$). 3) Small deflection theory is also considered in the design of piezo diaphragm (deflection<<thickness). In other words the dimensions of chosen piezo

diaphragm should be checked for tolerating the maximum air pressure from the air pump without any possible break. The element type and mesh type are mentioned in Table 2.3.

Figure 2.3 shows the ANSYS modeling of bimorph piezo diaphragm and its maximum displacement and Figure 2.4 gives the diaphragm stress distribution. In Table 2.4, the results of applying pressure are given. As can be seen, the design for piezo diaphragm is acceptable based on the three above design constraints.

Table 2.3 Element types for piezo and substrate in ANSYS.

Type	Material	Element type
1	Piezo (PZT: DL-54HD)	Couple filed → Brick 20 node 226 (solid 226)
2	Brass (Standard C360)	Structural → solid → 20 node 186 (solid 186)

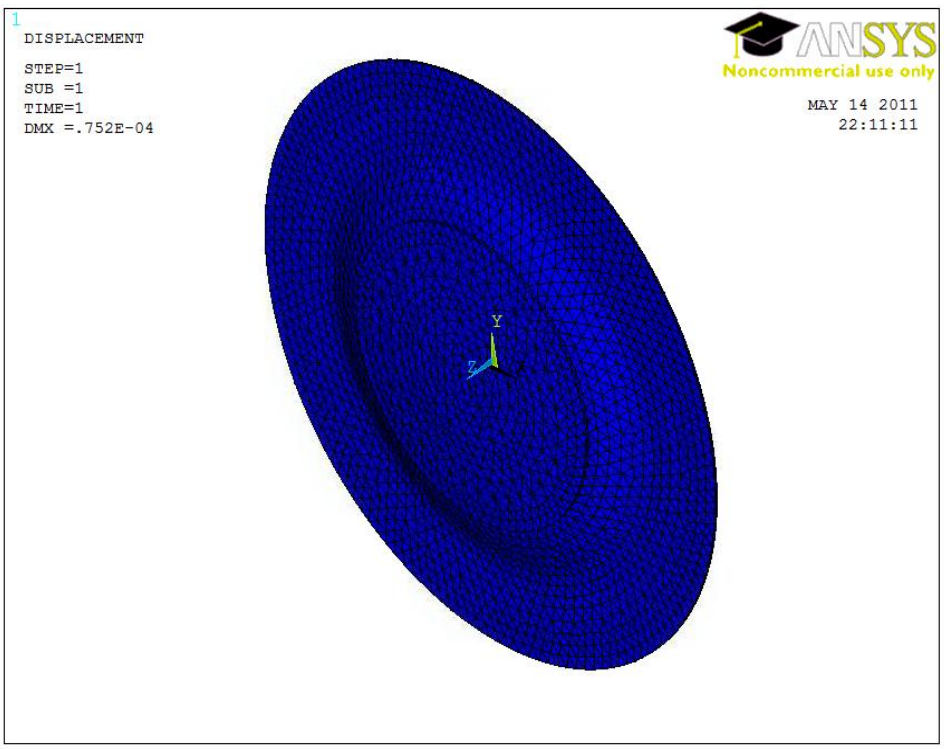

Figure 2.3 ANSYS modeling and deflection of the diaphragm after maximum deformation.

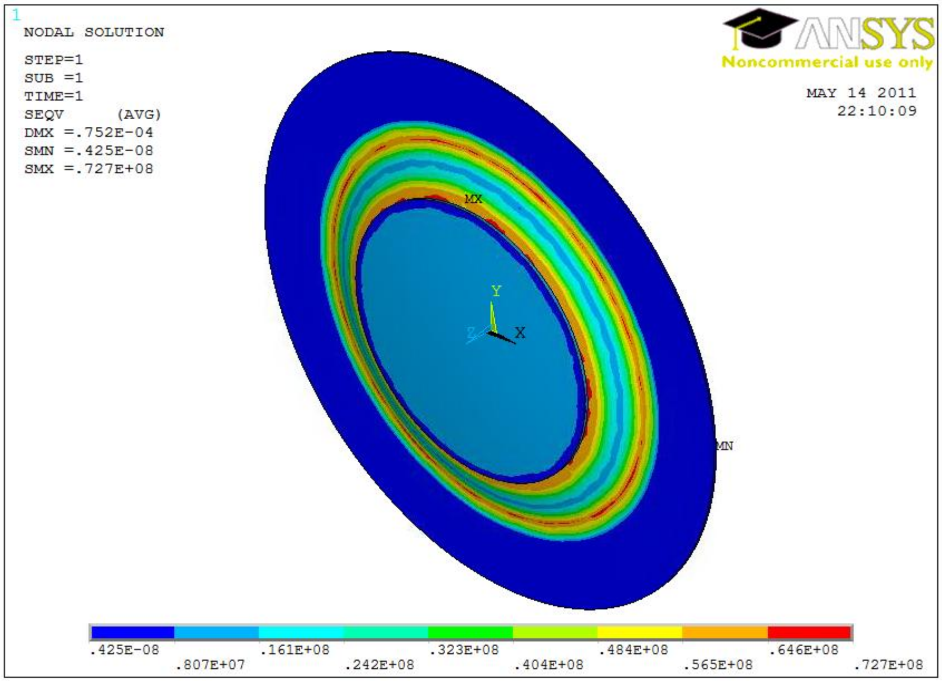

Figure 2.4. ANSYS stress analysis of the diaphragm after maximum deformation.

Table 2.4 Compared the result of ANSYS modeling with design theories.

Theory	ANSYS results	Reference value	Comparison
Small deflection theory	Deflection=75.2μm	Thickness=0.9 mm	Deflection<< Thickness
The yield strength limit(substrate)	Stress= 72.7 Mpa	Yield strength=360 Mpa	Stress<< Yield strength
The yield strength limit (piezo)	Stress= 8.07 Mpa	Yield strength=34 Mpa	Stress<< Yield strength

2.5 Theoretical Prediction of Generated Power

2.5.1 Modeling of Piezoelectric Generator

A piezoelectric energy harvester is often modeled as a mass+spring+damper+piezo structure which schematically shown in Figure 2.5 [59-60]. In this approach, an effective mass M subjected to an applied forcing function F(t) is bounded on a spring of effective stiffness k, on a damper of coefficient η, and on a piezoelectric element with capacitive C_P.

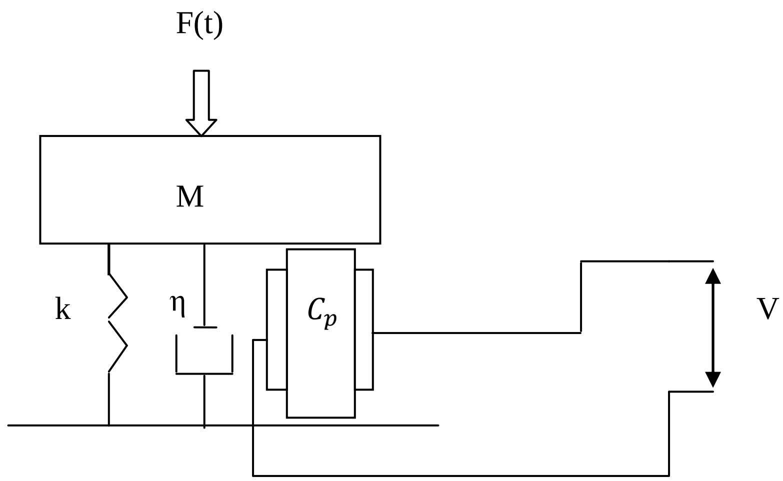

Figure 2.5 An equivalent model for a piezoelectric energy harvester.

The output power of a circular piezoelectric diaphragm depends on the material properties of piezo and substrate, diaphragm geometry parameters, working frequency, boundary conditions, external electric resistance, and external force [50-57]. Tang [57] has presented power performance equations of the circular bimorph piezoelectric diaphragm generator which is applied in this thesis to predict output power of the harvester in Figure 2.2. For an ideal piezoelectric model (no mechanical damping or $\eta = 0$), the diaphragm power output is defined as [57]:

$$P = \frac{V_{oc}^2}{2R\left(1+\frac{1}{(\omega C_f R)^2}\right)} \tag{2.5}$$

Equation (2.5) shows that the average harvester output power (P) depends on open circuit voltage (V_{oc}), piezo free capacitance (C_f), vibration or working frequency (ω) and external electrical resistance (R). The free capacitance is also a function of diaphragm dimensions. The optimal external resistance for an ideal system is defined as:

$$R_{opt} = \frac{1}{(\omega C_f)} \tag{2.6}$$

Where η is mechanical damping ratio and K is the piezoelectric coupling coefficient.

The Raleigh method is applied [57] to obtain the deflection shape of the diaphragm during uniform periodical vibration. Then this deflection function is substituted in the piezo constitutive equations to reach the open circuit voltage (V_{oc}) as well as power in Equation (2.5).

Understanding of the theory and its parameters is important, so it was decided that the steps for deriving the voltage and power equations are simply explained. First the principle of piezoelectric composite diaphragm is given. Then the Kinetic and potential energy theory and Raleigh method are applied to give the natural frequency as well as the transverse displacement function of bimorph piezo power harvester. After that, open circuit voltage equation and its relation with transverse displacement and applied pressure power are presented. This voltage equation can be substituted in Equation (2.5) to find the average output power.

2.5.2 Principle of Piezoelectric Composite Diaphragm

The constitutive equations in the polar coordinates and voltage and charge equations of the piezoelectric membrane for a piezo actuator or harvester are generally defined as follows [57-58] [61-63]:

$$T_1 = \frac{E^D}{1-(\sigma^D)^2}(S_1 + \sigma^D S_2) - \frac{g_{31}E^D}{1-\sigma^D} D_3 \tag{2.7}$$

$$T_2 = \frac{E^D}{1-(\sigma^D)^2}(S_2 + \sigma^D S_1) - \frac{g_{31}E^D}{1-\sigma^D} D_3 \tag{2.8}$$

$$E_3 = -g_{31}(T_1 + T_2) + \beta_{33}^T D_3 \tag{2.9}$$

$$dU_c = \frac{1}{2}(T_1S_1 + T_2S_2) + \frac{1}{2}D_3E_3 \tag{2.10}$$

$$V = \int E_3 dz \tag{2.11}$$

$$Q = \int D_3 2\pi r dr \tag{2.12}$$

$$V_{oc} = \frac{Q}{C_f} \tag{2.13}$$

In above equations, $E^D$and $\sigma^D$are the young's modulus and poison's ratio of the piezoelectric membrane; $D_3$and E_3 are the electric field and the electric displacement in the z-displacement, respectively; $\beta_{33}^T = \frac{1}{\in_{33}^T}$ is the impermeability; $\in_{33}^T$ is the permittivity in the z-direction; the subscript D stand for the constant electric displacement; g_{31} is the piezoelectric voltage constant; T_1 and T_2 are the stresses in the radial and angular directions; respectively; and $S_1 = z\frac{d^2w}{dr^2}$ and $S_2 = \frac{z}{r}\frac{dw}{dr}$ are the strains in the radial and angular directions; dU_c is the potential-energy density for the piezoelectric membrane; V is the external voltage and Q is the charge generated on the piezoelectric membrane. Moreover, C_f is the free capacitance of the piezo membranes and V_{oc} is open circuit voltage.

Equations (2.7) to (2.13) show that when a piezo material (as a harvester) is stressed, the electric charge is generated. This charge is restored in the piezo membrane (as a capacitor) and a voltage is produced across the piezo electrodes (open circuit voltage (V_{oc})). In simple words, an external force or pressure on the piezo causes a stress, which this stress can produce a voltage and power.

For the substrate plate, there is not an electromechanical coupling effect, so the stress is simplified to:

$$T_1 = \frac{E_m}{1-(\sigma_m)^2}(S_1 + \sigma_m S_2) \tag{2.14}$$

$$T_2 = \frac{E_m}{1-(\sigma_m)^2}(S_2 + \sigma_m S_1) \tag{2.15}$$

$$dU_m = \frac{1}{2}(T_1S_1 + T_2S_2) \tag{2.16}$$

Where E_m, σ_m are young's modulus and Poisson's ratio of the substrate plate, respectively. Moreover, dU_m is the potential-energy density for the substrate membrane.

For using the piezo as a power generator, there is no external voltage (E_3=0). For the two circular piezo layers, which are connected in parallel and use as a power harvester, the electric field and charge and open circuit voltage can be rewritten with respect to Equation (2.9), Equation (2.11), Equation (2.12), and Equation (2.13):

$$\beta_{33}^{T} D_3 = g_{31}(T_1 + T_2) \tag{2.17}$$

$$V = \int_{\alpha h/2}^{h/2} E_3 dz = 0 \tag{2.18}$$

$$Q_o = 2\int_0^{\beta a} D_3 2\pi r dr \tag{2.19}$$

$$V_{oc} = \frac{2\int_0^{\beta a} D_3 2\pi r dr}{C_f} \tag{2.20}$$

Where V is the external voltage and Q_o is the total charge generated on the two parallel-connected piezoelectric membranes and $C_f = \frac{4\pi(a\beta)^2}{[\beta_{33}^{s}\, h\,(1-\alpha)]}$ and $\beta_{33}^{s} = \beta_{33}^{T}\left[1 + \frac{2\, {g_{31}}^2 E^D}{\beta_{33}^{T}\,(1-\sigma^D)}\right]$. Refer to Figure 2.1, parameters a, h,α, β are the substrate radius ($R_2 = a$), the total thickness of the diaphragm, the substrate to total thickness ratio, and the substrate to piezo diameter ratio, respectively. Equation (2.17) clearly shows that the electric displacement (or charge) is related to stress from external force or external pressure. To find the stress, the deflection function of the piezo membrane is derived and replaced in Equation (2.14) and Equation (2.15).

2.5.3 Transverse Displacement of the Piezo Diaphragm

Transverse displacement of the bimorph piezo diaphragm can be obtained by [57]:

$$w(r) = \xi \sum_{i=0}^{n} a_i \left(\frac{r}{a}\right)^i \tag{2.21}$$

Where $w(r)$ is the deflection of the piezoelectric composite diaphragm in the z-direction; r is the distance from the center of the diaphragm to the point of the deflection; a is defined as the radius of the diaphragm; a_i is the coefficient; and $\xi = \xi_o \exp(j\omega t)$ is the vibration amplitude factor of the neutral surface of the diaphragm center. If i=4, then the calculation precision is enough for a practical application [57]. Given$w(r)|_{r=0} = \xi$, there will be $a_o = 1$. The boundary condition $\frac{dw}{dr}|_{r=0} = 0$ leads to $a_1 = 0$. Thus the deflection function of an oscillation can be written as

$$w(r) = \xi \left[1 + a_2 \left(\frac{r}{a}\right)^2 + a_3 \left(\frac{r}{a}\right)^3 + a_4 \left(\frac{r}{a}\right)^4\right] \tag{2.22}$$

For very low frequencies ($\omega \rightarrow 0$) such as walking condition, the deflection function (ξ) can be considered as a constant and will not be influenced by the driving frequency [57]. This deflection is measured in static mode of ANSYS by applying uniform pressure on one side of the diaphragm. This uniform pressure is the maximum air pump pressure after complete squeeze of the pump. Refer to Equation (2.22) for clamped boundary conditions, we have

$$w(r)|_{r=a} = \xi\,[1 + a_2 + a_3 + a_4] = 0 \tag{2.23}$$

$$\frac{dw}{dr}|_{r=a} = \xi\,[2a_2 + 3a_3 + 4a_4] = 0 \tag{2.24}$$

a_3, a_4 are obtained by solving Equations (2.23) and (2.24):

$$\begin{cases} a_3 = -4 - 2a_2 \\ a_4 = 3 - a_2 \end{cases} \tag{2.25}$$

In the following sections the kinematic and potential energy of bimorph piezo diaphragm are explained and by the Raleigh method the natural frequency of the bimorph piezo diaphragm as well as a_2, a_3, a_4 are found out [57]. Based on the Raleigh method, in the ideal condition (without any type of damping) the maximum values of potential energy and kinematic energy for the piezo diaphragm should be equal.

2.5.4 Total Kinetic Energy of Bimorph Piezo Diaphragm

The kinetic energy densities of the substrate layer and piezo layer is define $\rho_m \dot{w}^2(r)/2$ and $\rho_c \dot{w}^2(r)/2$, respectively. The total kinetic energy of the diaphragm can be calculated based on separate calculation of the substrate and piezo kinetic energies:

$$T_{total} = T_m + 2T_P \tag{2.26}$$

$$T_{total} = \frac{1}{2}\left\{\int_0^a \int_{-\alpha h/2}^{\alpha h/2} \rho_m \dot{w}^2(r) 2\pi r dr\, dz + 2\int_0^{a\beta} \int_{\alpha h/2}^{h/2} \rho_c \dot{w}^2(r) 2\pi r dr\, dz\right\} \tag{2.27}$$

Where T_m is the substrate kinetic energy and T_P is the kinetic energy of each piezo layer and w(r) is the transverse displacement of the diaphragm and ρ_m and ρ_C are the densities of the substrate plate and piezoelectric membrane, respectively. Subscript or superscript m and c stand for the substrate and piezoelectric membrane.

Substituting Equation (2.22) in Equation (2.27), Tang [57] has proved that the total kinetic energy of the diaphragm can be written as follows:

$$T_{total} = \frac{\pi \xi'^2 h\, a^2}{2}\left[\alpha \rho_m K_1 + (1+\alpha)\rho_C K_2\right] \tag{2.28}$$

Where$\xi' = j\omega\xi_o \exp(j\omega t)$; and K_1 and K_2 are kinetic-energy factors as follows:

$$K_1 = 1 + a_2 + \frac{4}{5}a_3 + \frac{2}{3}a_4 + \frac{1}{3}{a_2}^2 + \frac{4}{7}a_2a_3 + \frac{1}{2}a_2a_4 + \frac{1}{4}{a_3}^2 + \frac{4}{9}\, a_3a_4 + \frac{1}{5}{a_4}^2 \tag{2.29}$$

$$K_2 = \beta^2\left[1 + a_2\beta^2 + \frac{4}{5}a_3\beta^3 + \frac{1}{3}(2a_4 + {a_2}^2)\beta^4 + \frac{4}{7}a_2a_3\beta^5 + \frac{1}{4}(2a_2a_4 + {a_3}^2)\beta^6 + \frac{4}{9}\, a_3a_4\beta^7 + \frac{1}{5}{a_4}^2\beta^8\right] \tag{2.30}$$

2.5.5 Total Potential Energy of Bimorph Piezo Diaphragm

Substituting Equation (2.9) to Equation (2.10), the potential energy density can be written as:

$$dU_c = \frac{1}{2}\left[(T_1S_1 + T_2S_2) - g_{31}(T_1 + T_2)D_3 + \beta_{33}^T {D_3}^2\right] \tag{2.31}$$

To reach natural frequency, it is assumed that all kinetic energy is converted to potential energy which means the electric displacement is not changed ($D_3 = 0$). As a result, the potential energy density and the potential energy of the two piezo diaphragms with constant electric displacement are:

$$dU_c{}^D = \frac{1}{2}[(T_1S_1 + T_2S_2)] \tag{2.32}$$

$$U_C^D = 2\int_0^{a\beta}\int_{m/2}^{h/2} 2\pi r\, dU_C^D\, dz\, dr \tag{2.33}$$

Substituting Equation (2.7) and Equation (2.8) into Equation (2.32) and then into Equation (2.33), Tang [57] has proved that potential energy of the two piezo diaphragms with constant electric displacement ($D_3 = 0$) is:

$$U_C^D = \frac{2\,\pi}{3}\,\frac{E^D\xi^2}{1-(\sigma^D)^2}\,\frac{h^3(1-\alpha^3)}{a^2}\,\Lambda_C^D \tag{2.34}$$

Where Λ_C^D is the potential-energy factor of the piezoelectric membrane:

$$\Lambda_C^D = \left\{\frac{(1+\sigma^D)a_2}{2}\left[a_2 + 3a_3\beta + 4a_4\beta^2\right] + \frac{9}{8}\left(\frac{5}{4}+\sigma^D\right)a_3{}^2\beta^2 + 3\left(\frac{7}{5}+\sigma^D\right)a_3a_4\beta^3 + 2\left(\frac{5}{3}+\sigma^D\right)a_4{}^2\beta^4\right\}\beta^2 \tag{2.35}$$

Refer to Equation (2.16) the potential energy of the substrate plate is obtained:

$$U_m = \int_0^a\int_{-\alpha h/2}^{\alpha h/2} 2\pi r\, dU_m\, dz\, dr \tag{2.36}$$

The final equation for potential energy is given by [57]:

$$U_m = \int_0^a\int_{-\alpha h/2}^{\alpha h/2} 2\pi r\, dU_m\, dz\, dr = \frac{2\,\pi}{3}\,\frac{E_M\xi^2}{1-(\sigma_m)^2}\,\frac{h^3\alpha^3}{a^2}\,\Lambda_m \tag{2.37}$$

$$\Lambda_m = \left\{\frac{(1+\sigma_m)}{2}\,a_2[a_2 + 3a_3 + 4a_4] + \frac{9}{8}\left(\frac{5}{4}+\sigma_m\right)a_3{}^2 + 3\left(\frac{7}{5}+\sigma_m\right)a_3a_4 + 2\left(\frac{5}{3}+\sigma_m\right)a_4{}^2\right\} \tag{2-38}$$

Finally, the total potential energy of the bimorph piezoelectric composite diaphragm with constant electric displacement is obtained as follows:

$$U^D = U_m + U_C^D = \frac{2\,\pi}{3}\,\frac{E^Dh^3\xi^2}{[1-(\sigma^D)^2]a^2}\,\Lambda_{eff}^D \tag{2.39}$$

$$\Lambda_{eff}^D = \frac{E_m}{E^D}\frac{1-(\sigma^D)^2}{1-(\sigma_m)^2}\,\alpha^3\Lambda_m + (1-\alpha^3)\Lambda_C^D \tag{2.40}$$

According to Raleigh's energy principle, the maximum kinetic and potential energies for piezoelectric composite should be equal ($U^{D}{}_{max} = T^{D}_{Total\ max}$). The natural frequency of the piezoelectric composite diaphragm can be denoted by Raleigh's method and Equation (2.28) and Equation (2.39) as [57]:

$$\omega^2 = \frac{4}{3}\frac{E^D}{(1-(\sigma^D)^2)}\frac{h^2}{a^4}\frac{\Lambda^D_{eff}}{[\alpha\rho_m K_1 + (1-\alpha)\rho_C K_2]} \tag{2.41}$$

Where Λ^D_{eff} is the potential-energy factor of the whole composite diaphragm. In the above equations and refer to Figure 2.1, $\rho_C, \rho_m, \alpha, \beta, h, a, \sigma_m, E_m$ are piezo density, substrate (shim) plate density, thickness ratio, diameter ratio, total thickness, and substrate (or shim) diameter, substrate poison's ratio, and substrate modules of elasticity, respectively.

In Equation (2.41) the natural frequency is a function of a_2 ($\omega^2 = f(a_2)$). To solve Equation (2.41), the approximate Raleigh method is applied. Based on this method, the natural frequency is minimized as follows:

$$\frac{d\omega^2}{da_2} = \left[\alpha K_1 + (1-\alpha)\frac{\rho_C}{\rho_m}K_2\right]\frac{\partial\Lambda^D_{eff}}{\partial a_2} - \Lambda^D_{eff}\left(\alpha\frac{\partial K_1}{\partial a_2} + (1-\alpha)\frac{\rho_C}{\rho_m}\frac{\partial K_2}{\partial a_2}\right) = 0 \tag{2.42}$$

Solving Equation (2.42) with respect to a_2 and substituting the result into Equation (2.25), parameters a_2, a_3, a_4 and deflection function (w_r) in Equation (2.22) is obtained. Then the transfer displacement (w_r) is replaced in Equation (2.7) and Equation (2.8) to find radial stress (T_1) and angular stress (T_2). After that these results are put into Equation (2.17) to find electric displacement (D_3) and the charge collected on the electrode surface (Q_o) is reached by Equation (2.19).

2.5.6 Generated Voltage and Charge for a Clamped Bimorph Piezo Diaphragm

(Q_o) is reached by Equation (2.19) as follows [57]:

$$Q_o = \frac{\pi\, g_{31} E^D h(1+\alpha)\xi}{\beta^S_{33}\,(1-\sigma^D)}\,\beta^2(2a_2 + 3a_3\beta + 4a_4\beta^2) \tag{2.43}$$

For the bimorph piezo diaphragm in ideal conditions, the open circuit voltage (V_{oc}) can be obtained by substituting Equation (2.43) in Equation (2.19) [57]:

$$V_{oc} = -\frac{h(1-\alpha^2)\, g_{31} E^D \xi}{4\,(1-\sigma^D)a^2}\,(2a_2 + 3a_3\beta + 4a_4\beta^2) \tag{2.44}$$

Equation (2.5) and Equation (2.44) are used to predict the output power of designed harvester [57].

Chapter 3 Prototype of Air Pump Piezo Power Generator

3.1 Prototype and Fabrication

A prototype of the shoe embedded air pump type piezoelectric power harvester was fabricated (Figure 3.1). Materials and dimensions of the parts used in the harvester are listed in Table 2.2 and Table 3.1. A wave spring was chosen to keep the height low. The polycarbonate and spring parts are glued using a vibration resistant epoxy. The PZT diaphragm was glued to the polycarbonate fixed chamber at its edge. One of the main challenges here was how to seal the air pump with the top plate of the pump to be able to move up and down. A latex material was chosen to seal the air pump and a ring (Item 6) was used to keep the latex material tightly glued. The total height of the harvester without load is 24 mm. Once stepped on, the height of the harvester becomes 19.5 mm.

Table 3.1 Different parts of the harvester (refer to Figure 3.1)

Item No.	Item Name	Sizes	Material
1	Wave spring	d= 34.3mm	Smalley(C150-L1)
2	Spring connection plate	d= 40mm	Poly carbonate (t=0.094”)
3	rubber		Latex (t=0.03”)
4	Upper circular plate (air chamber)	d= 50mm	Poly carbonate (t=0.22”)
5	Bottom plate (connect to ambient air)	d= 50mm	Poly carbonate (t=0.22”)
6	Seal ring	d= 50mm	Poly carbonate (t=0.22”)
7	Top circular plate	d= 50mm	Poly carbonate (t=0.094”)
8	Bimorph piezo circular diaphragm	d= 50mm	PZT reinforced by Brass

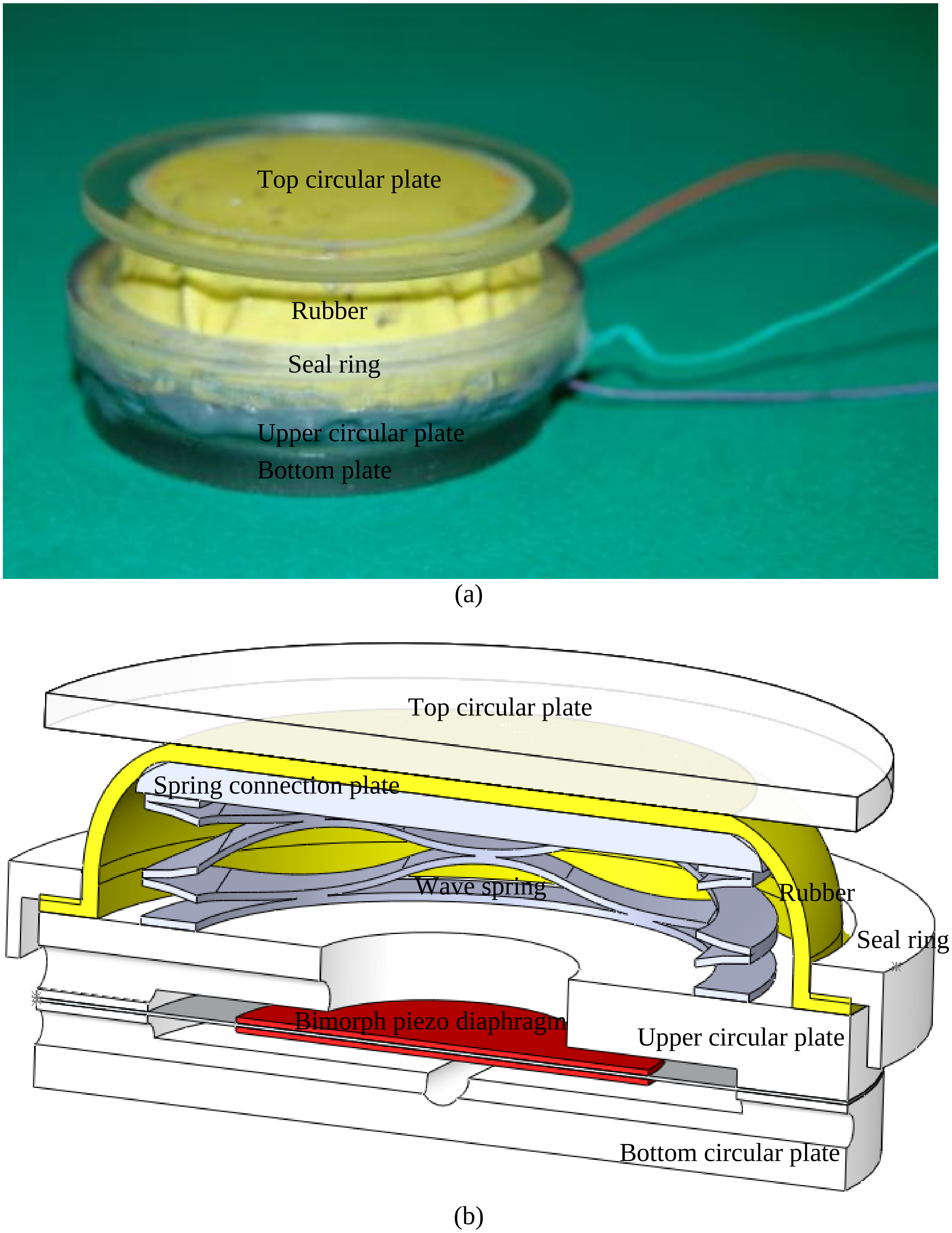

Figure 3.1 Prototype of the harvester. (a) Outside looking of the harvester. (b) Internal view of the harvester (also look at Table 3.1).

The fixed chamber has two plates: the upper circular plate (Item 4) and the bottom circular plate (Item 5). The bottom plate (Figure 3.2a) has two slots to access to ambient atmosphere and for a path for wires. A circular chamber with 36.3 mm diameter and 2 mm depth was made in the bottom plate for piezo deformation. The upper circular plate (Figure 3.2b) with thickness 5 mm and diameter 5 cm is an air chamber. The diameter and depth of the upper and bottom chambers are defined based on piezo thickness, piezo deformation, wire thickness, and air pressure. The piezo diaphragm is sandwiched and protected between Item 4 and 5.

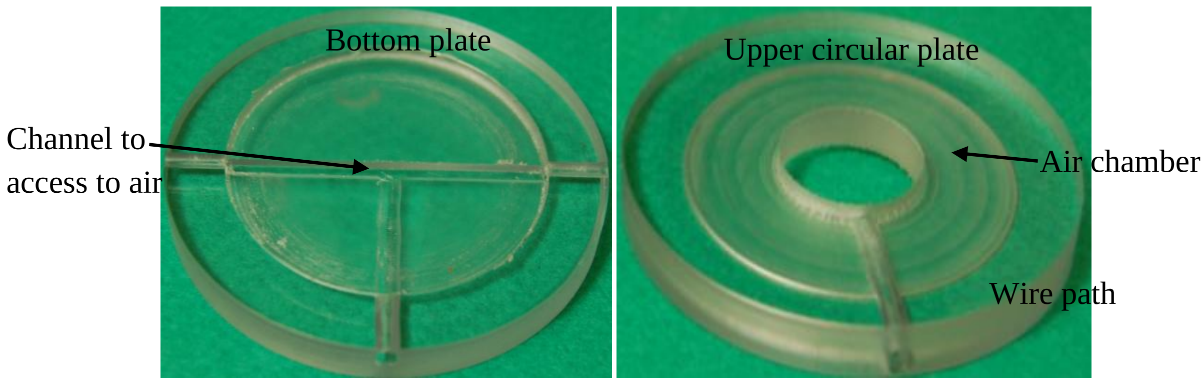

(a) (b)

Figure 3.2 (a) the bottom circular plate of the harvester (part 5) (b) the upper circular plate of the harvester (Item 4).

A wave spring (Item 1) model Smalley C150-L1 has been used which has reduced the installation space up to 50% with the same load and deflection in comparison with ordinary compression springs. The spring connection plate (Item 2) with 40 mm diameter and 2.4 mm thickness is placed on the spring plate (Figure 3.4a).

Figure 3.3a shows the top circular plate (Item 7) with 50 mm diameter and thickness 2.4 mm, which has direct contact with the foot’s heel. The rubber is sandwiched between Items 2 and 7. A seal ring is also used to keep and seal the bottom of the rubber (Figure 3.4).

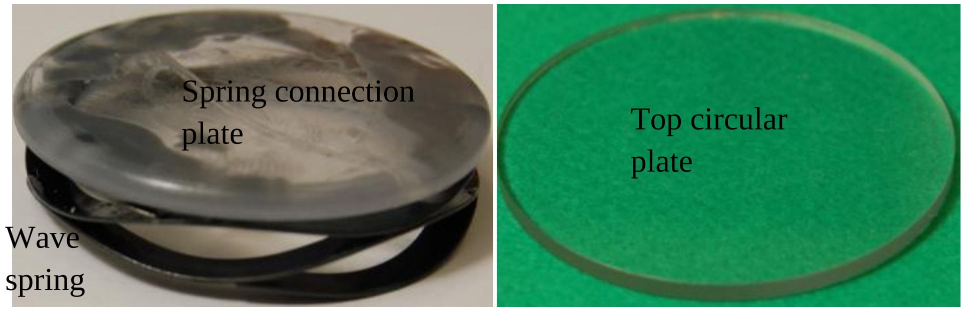

(a) (b)

Figure 3.3 (a) the wave spring (Item 1) and the spring connection plate (Item 2), (b) the top circular plate (Item 7).

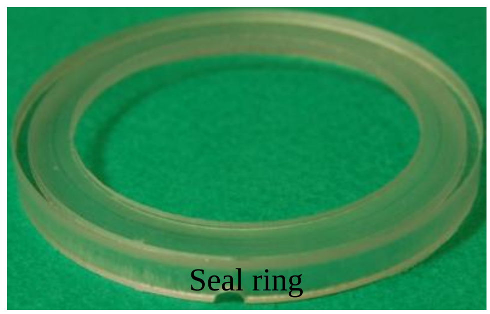

Figure 3.4 The seal ring (Item 6) to keep and seal the rubber bottom surrounding.

A bimorph circular piezo diaphragm with two layers PZT (DL-54HD) and a layer of brass (standard C360) is used from Dell Piezo Company [64], which has been connected in parallel with three wires (Figure 3.5). An epoxy vibration resistant model McMaster 7508A43 is used for polycarbonate, spring parts. Another epoxy model Loctite E-20 HP is also used for connecting piezo diaphragm to polycarbonate parts.

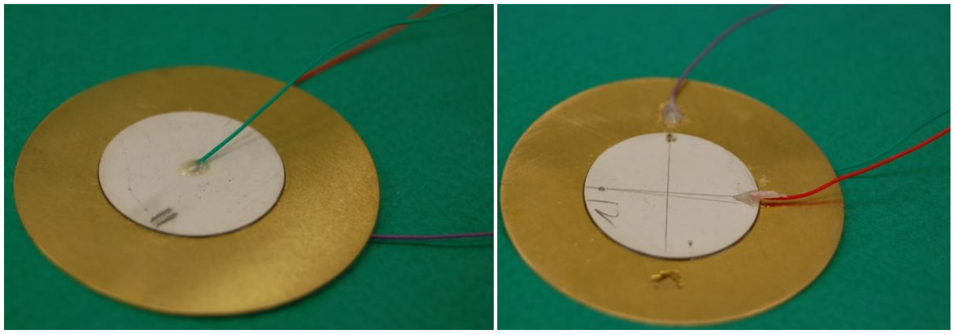

(a) (b)

Figure 3.5 Bimorph piezo diaphragm with shim plate (Item 8) is parallel extension operation which means three wires are connected (two of them to Piezo layers and one to brass shim). (a) Upside of piezo diaphragm. (b) Downside of the piezo diaphragm

3.2 Modification of the Power Harvester

During the experimental tests, the spring epoxy was damaged due to a weak epoxy connection. As a result, the spring was freely moving and cutting the rubber. For solving the problem, the following possible solution was executed.

1. The wave spring had no shim plate which had not made a strong epoxy connection (Figure 3.6). Therefore a new wave spring with two end shim plates was used for a stronger epoxy connection (Figure 3.7).

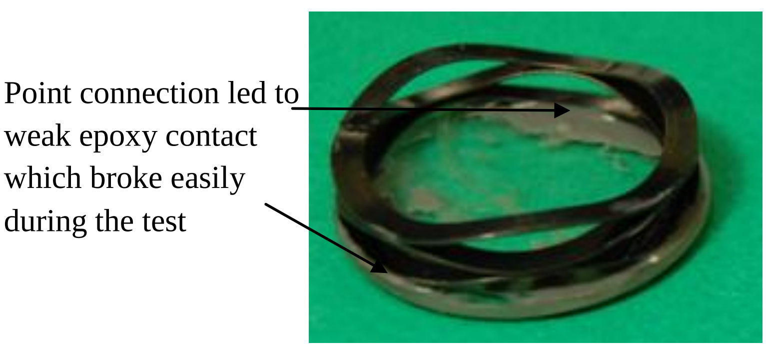

Figure 3.6 The initial wave spring without end shim plate (model C-150 Smalley Co.)

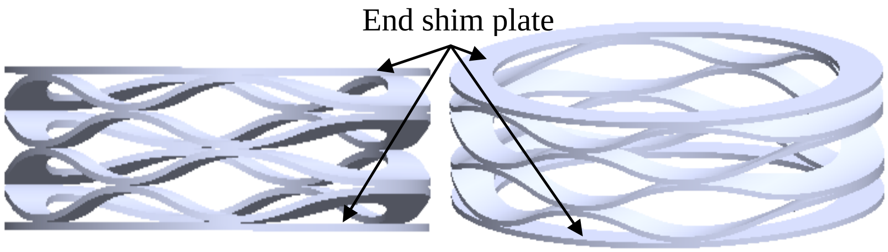

Figure 3.7 The wave spring with end shim plate (model CS-137 Smalley Co.).

2. A new wave spring with smaller diameter (diameter 1.37”) was utilized, which never touches the rubber.
3. Two aluminum rings were designed to keep the spring in its position. Even if the epoxy is broken again, these rings don’t let the spring move against the rubber (Figure 3.8).
4. Two aluminum plates with 50 mm diameter were made and replaced with the initial top circular plate and the spring connection plate (Figure 3.9).
5. A new epoxy model 3M Scotch-Weld DP 460 was used to reach stronger epoxy connections as well.

Table 3.2 Added parts to the harvester after modification (Figure 3.9).

Item No.	Item name	Sizes	Material
9	Upper aluminum ring	d= 38.1mm	Aluminum
10	Lower aluminum ring	d= 40mm	Aluminum
11	Top aluminum circular plate	d= 44.5mm	Aluminum
12	New spring connection aluminum plate	d= 50mm	Aluminum
13	Wave spring	d= 30 mm	Smalley model CS-137

(a) (b)

Figure 3.8 (a) The bottom aluminum ring to keep the bottom of spring, (b) The top aluminum ring to fix the top of spring.

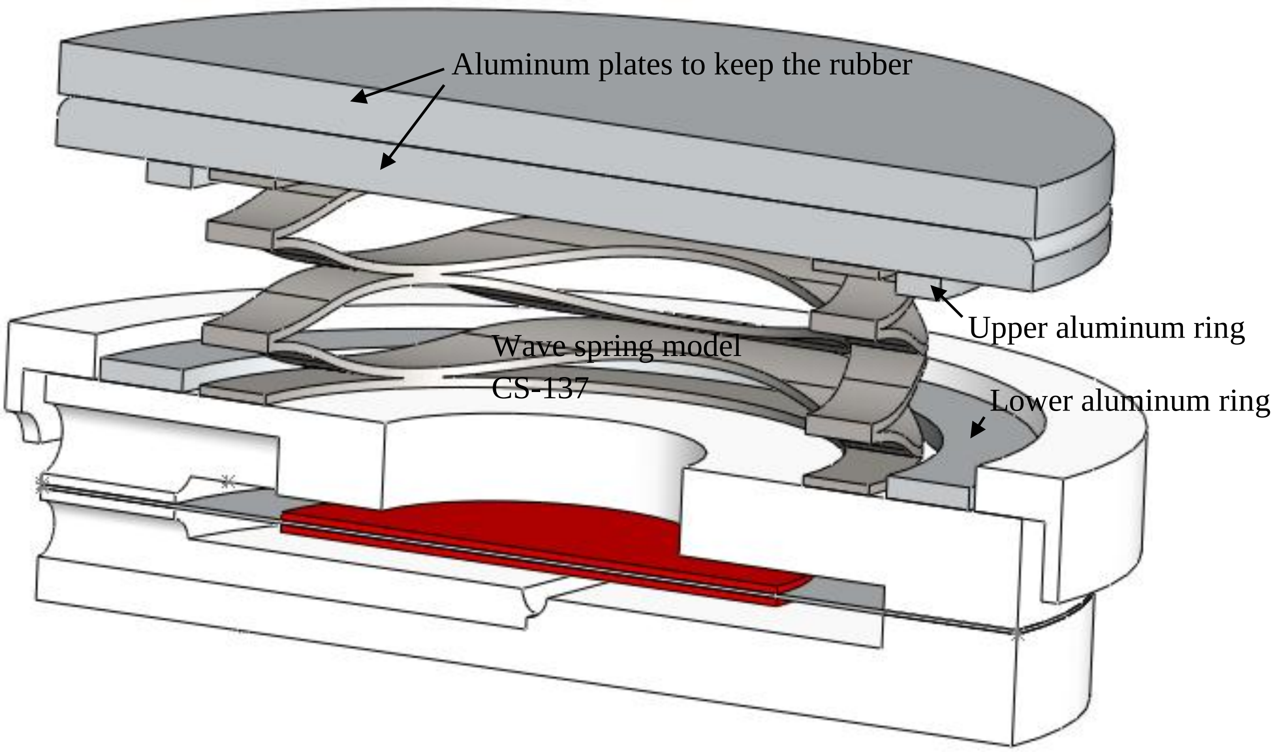

Figure 3.9 Cross section of modified power harvester.

3.2.1 Fabrication and Assembly Process of New Parts

Refer to Figure 3.10, first lower aluminum ring (Item 10) is being epoxy on the bottom plate (Item 5). Then the upper aluminum ring (Item 9) is attached on the center of the new spring connection aluminum plate (Item 13). Next the new spring is centralized inside upper aluminum ring (Item 12) and being epoxy on part No. 13. After that, the rubber is attached by epoxy (model 3M Scotch-Weld DP 460) on the surface of seal ring (Item 6). Then the spring, which has already connected to part No. 9, 12, and 13, is being epoxy inside the lower aluminum ring (Item 10) on bottom plate (Item 5). Finally, the rubber is sandwiched and being epoxy between the top aluminum circular plate (Item 11) and part No. 12.

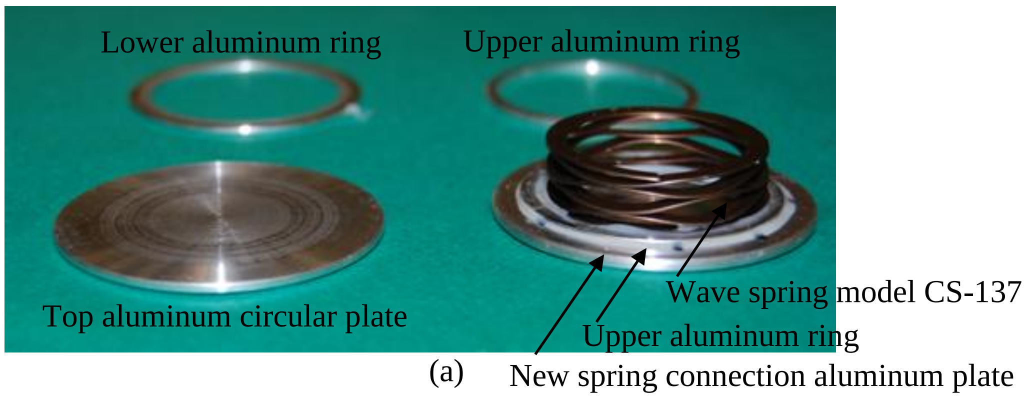

(a)

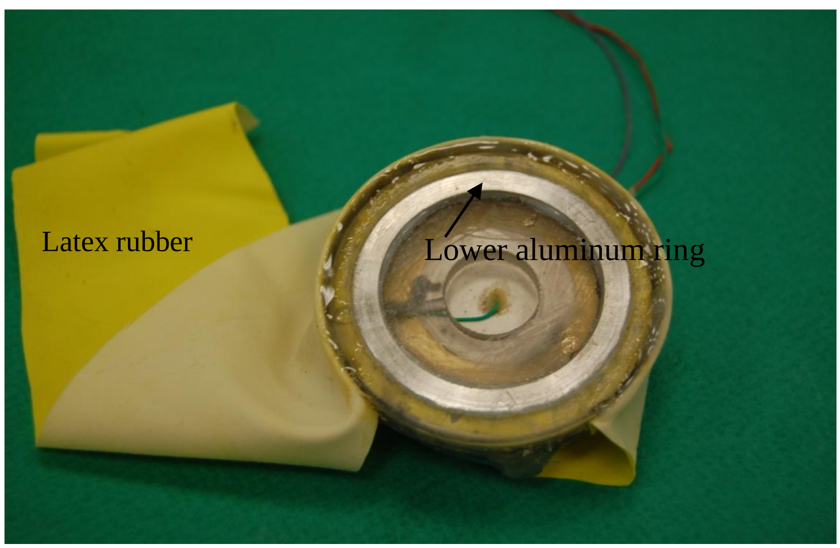

(b)

Figure 3.10 Fabrication process of the harvester parts; the cure time between each step is 24 hours due to required time for epoxy hardness.

3.3 Integration in a Shoe

A typical formal shoe was selected to insert the harvester. First a hole with diameter 55 mm was opened inside the shoe heel (Figure 3.11 a). Moreover, at the back of the shoe a hole was made for wires (Figure 3.11 b). The power generator is inserted inside the hole and then the shoe pad is placed in its position (Figure 3.12).

(a)

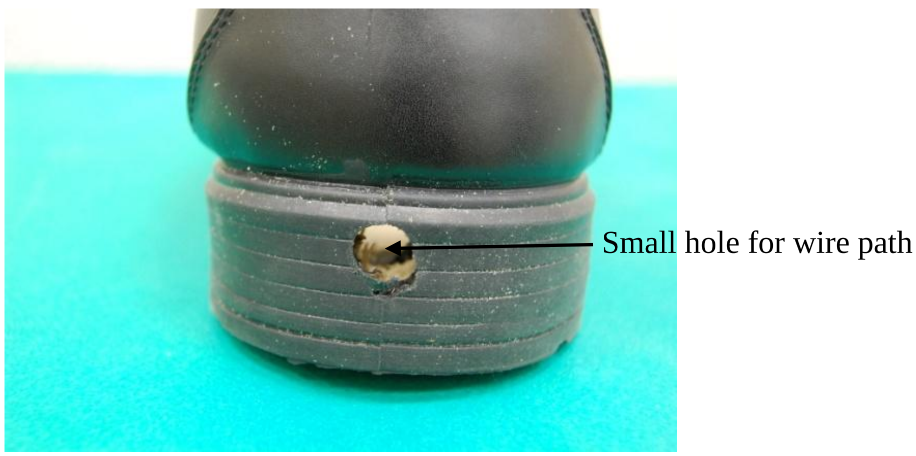

(b)

Figure 3.11 (a) A 55 mm hole inside the heel for placing the power generator, (b) A hole for wire path.

(a)

(b)

Figure 3.12 (a) The harvester is embedded in the shoe heel, (b) The level of harvester is the same as shoe pad level.

Chapter 4 Experimental Tests and Results Analysis

Two types of experimental tests have been performed on the treadmill for measuring output power and for measuring impact force. In the following sections the experimental test setup and the results are reported.

4.1 Voltage and Power Measurement Tests

4.1.1 Experimental Test Setup for Measuring Voltage

The shoe embedded power harvester was tested when the shoe was worn and the wearer walked on a treadmill with the speed ranging from 1 mph to 4 mph (Figure 4.1). The wearer is 1.75m tall and weighs 92 kg. Various resistive loads are connected to the output of the harvester (Figure 4.2). The generated power was calculated using the following equation.

$$P = \frac{V_{rms}^{2}}{R} \qquad (5.1)$$

Where P is the generated average power, V_{rms} is the output voltage (root mean square) and R is the resistance.

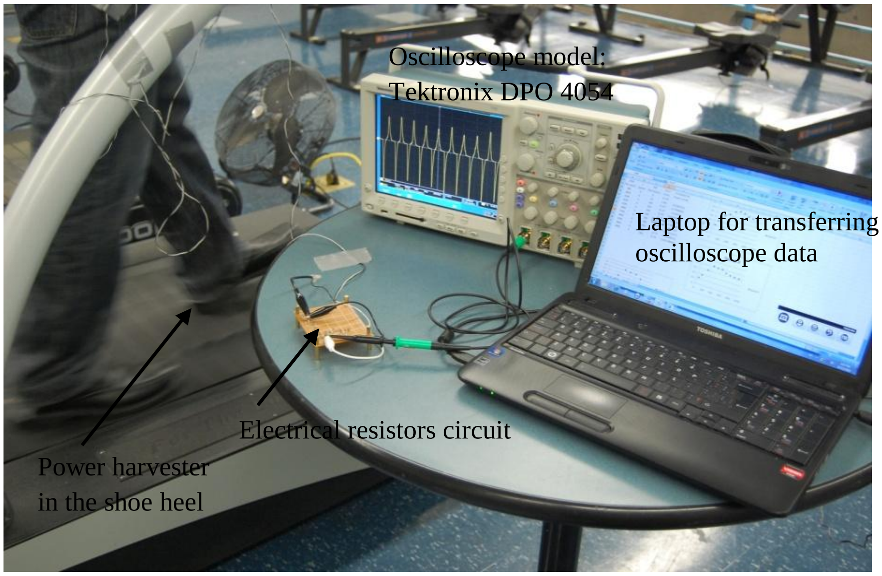

Figure 4.1 Experimental test set up on treadmill for measuring the voltage: The wearer walks with speed ranging from 1mph to 4 mph.

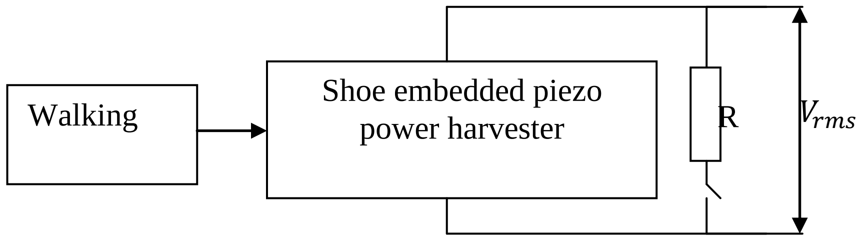

Figure 4.2 Experimental test set up on treadmill: Electrical connection of the testing setup.

4.1.2 First Trial With Hand Impact Force

Before doing the test in real conditions on the treadmill, the impact force is applied by hands for resistors 20 KΩ to 200 KΩ. Table 4.1 illustrates that power can reach 0.8 mW.

Table 4.1. Test results by applying hand force.

Resistance(KΩ)	V_{rms}(volt)	f(mHz)	P (mW) $=\frac{V_{rms}{}^2}{R}$
20	3.579	483.1	0.64
40	4.383	843.1	0.48
60	6.249	470.6	0.65
80	7.066	966.2	0.62
100	7.112	456.6	0.51
110	7.463	456.6	0.51
120	7.88	881.1	0.52
130	8.43	451.5	0.55
150	10.39	546.4	0.72
160	10.96	527.7	0.75
170	11.5	136	0.78
180	12	531.9	0.80
200	11.66	461.9	0.68

4.1.3 First Experimental Test on a Treadmill

Figure 4.3 provides the experimental results of average output power on a treadmill for resistances 20 kΩ to 200 kΩ for five different speeds (1 mph, 2 mph, 3 mph, 4 mph, 5 mph). It can be seen from the data that the output power increases with speed rise and the maximum power is 0.8 mW (R=200 kΩ) for a speed of 5 miles/hour. It is analytically expected that for every walking speed the power reaches a maximum amount in an optimum resistance; then the power gradually decreases. However, the graph does not follow this expected pattern.

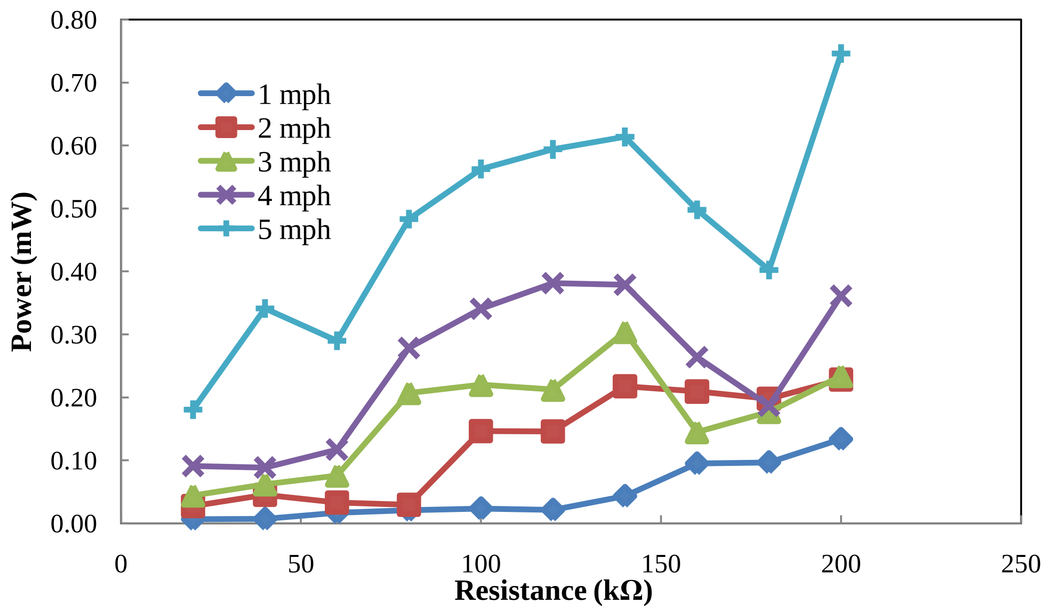

Figure 4.3 Power versus resistance in different speeds (first experimental test on treadmill).

4.1.4 More Experimental Tests on a Treadmill

Figure 4.4 and Figure 4.5 provide two more experimental test data on a treadmill for speed 1 mph, 2 mph, 3 mph, 4 mph, and 5 mph. These two graphs show that for each electrical resistance the power increases with speed rise. Comparing maximum power of the same speed in these graphs also reveals that the output power has decreased in different tests. For example, the maximum power of a speed 5 mph in Figure 4.4 is 0.76 mW, but the maximum power of a speed 5 mph in Figure 4.5 has reduced to 0.1 mW. In contrast with the theoretical prediction, there are also unexpected fluctuations in the output power with respect to increasing electrical resistance. This output power variations come from some problems in the harvester, which have been explained and solved in section 3.2 .

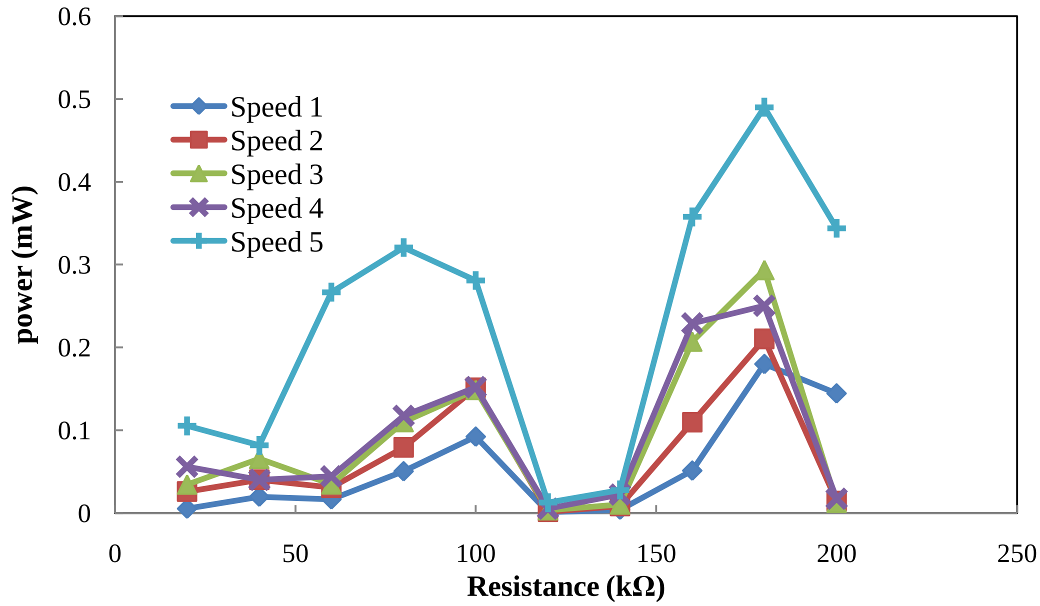

Figure 4.4 Power versus resistance (second test).

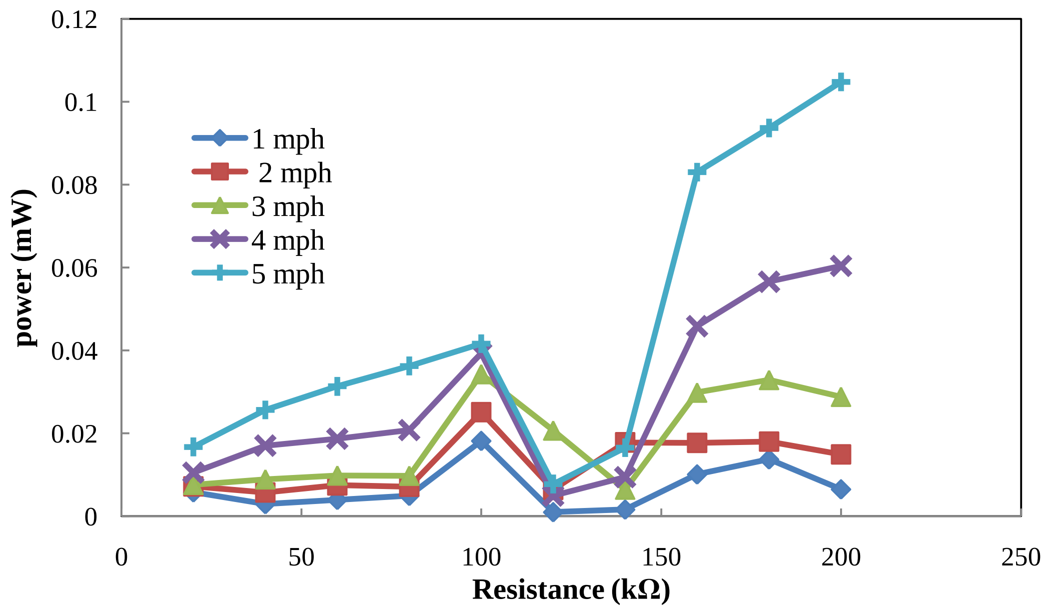

Figure 4.5 Power versus resistance (third test).

4.1.5 Experimental Tests after Harvester Modification

Previous tests were performed for a speed of 1 mph, 2 mph, 3 mph, 4 mph, and 5 mph. Speed 1 mph is very slow walking; speed 4 mph is fast walking; and speed 5 mph is a running condition. So it was decided to do the next tests only for speed 1 mph to 4 mph. Moreover, more electrical resistances between ranges 50 kΩ to 900 kΩ were picked. Figure 4.6 illustrates the output power versus resistance in different walking speeds on the treadmill. For each speed, the power has gradually increased to a maximum amount for an optimum resistance then it has gently reduced. The maximum power is 1.14 mW (at speed 4 mile/hour). Figure 4.7 demonstrates V_{rms} versus resistance. In each speed, the voltage has increased with increasing the electrical resistances.

Again it is theoretically expected that for each resistance with increasing speed the power increases to a maximum value then it decreases. However, this theoretical prediction has not happened for all electrical load resistances and there was a discrepancy between theory and experimental results for some of electrical resistances. For instance, in electrical resistance 900 KΩ, the output power for speed 3 was less than the output power for speed 2.

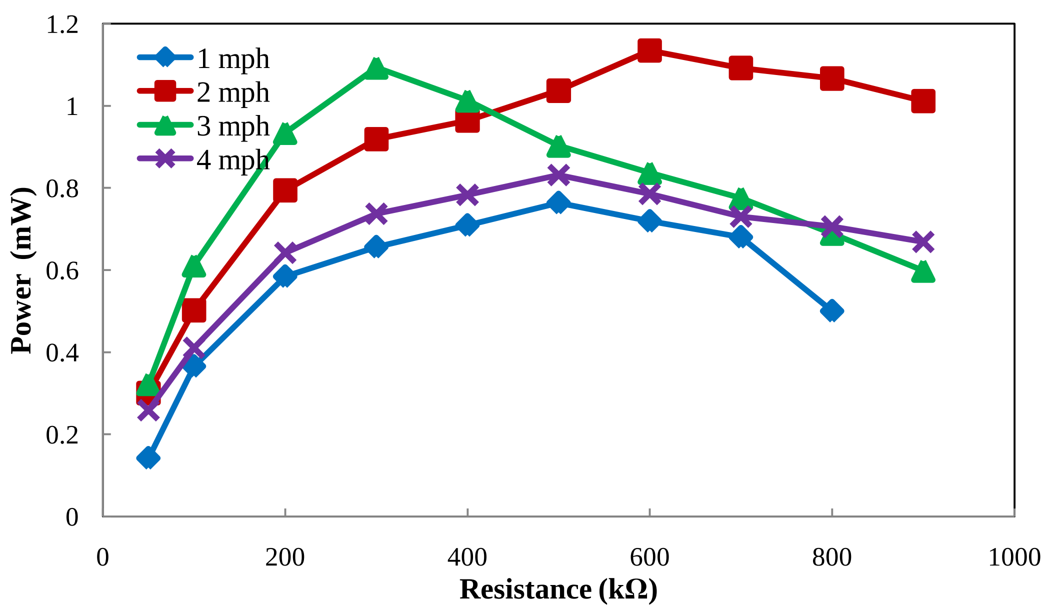

Figure 4.6 First test after modification (power versus resistance).

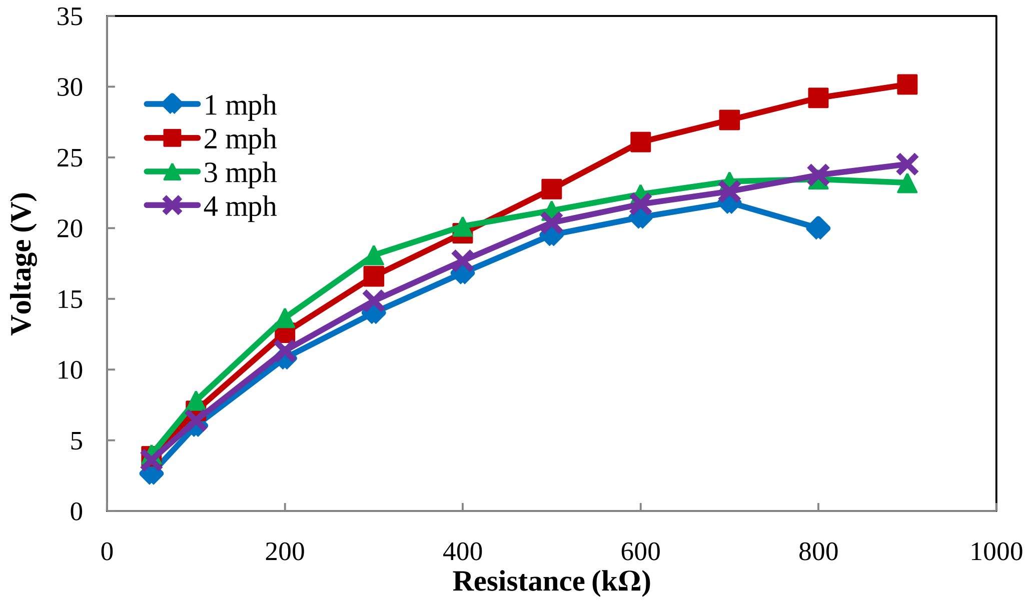

Figure 4.7 First test after modification (voltage versus resistance).

Figure 4.8 and Figure 4.9 provide more experimental test results for power and voltage. The two graphs exhibit that the voltage increases with speed rise and there is a maximum power and optimum resistance for each speed. However, comparing Figure 4.8 with Figure 4.6 reveals that the maximum power of a speed of 4 mph reduces from 1.1mW to 0.82 mW, respectively.

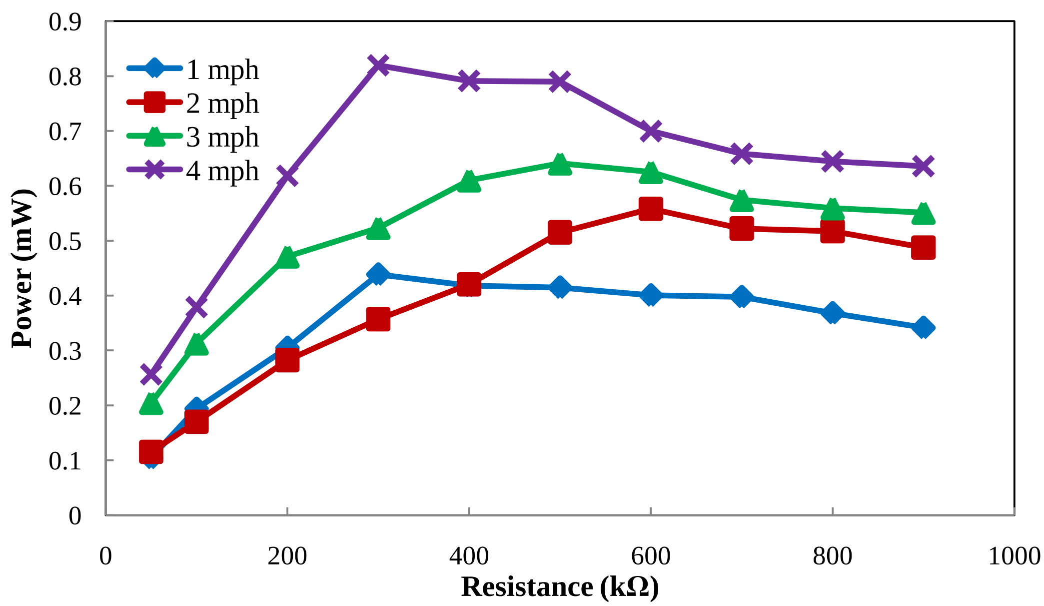

Figure 4.8 Second test after modification (power versus resistance).

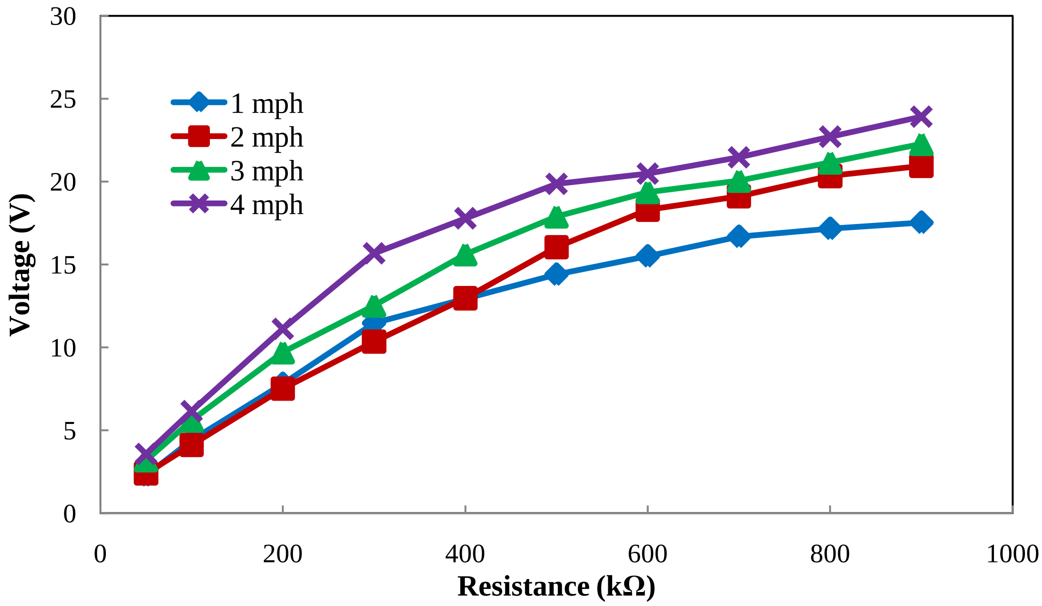

Figure 4.9 Second test after modification (voltage versus resistance).

This power reduction was due to a leakage in the harvester rubber, which made by sharp epoxy edges. This sharp edge was also removed by a file (Figure 4.10).

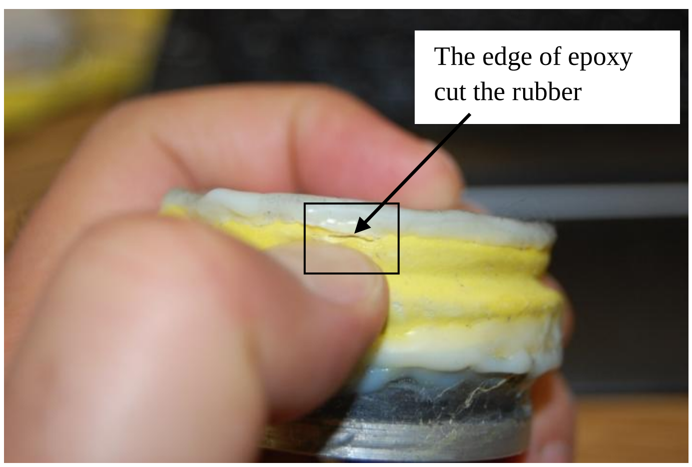

Figure 4.10 Slut was made due to edge of epoxy.

More experimental tests were performed after sealing the rubber and cutting the sharp edge of the epoxy. Figure 4.11 (a) shows the generated voltage (V_{rms}) with respect to different electrical load resistances (R) at speeds of 1 mph, 2 mph, 3 mph and 4 mph. The test results show that the voltage increases with the resistance and the speed. Figure 4.11 (b) shows the generated average power versus the resistance at different speeds. For each speed there is an optimal resistance for generating the maximum power. The maximum power of the prototype is 1.12 mW for a resistive load of 500 kΩ at the speed of 4 mph.

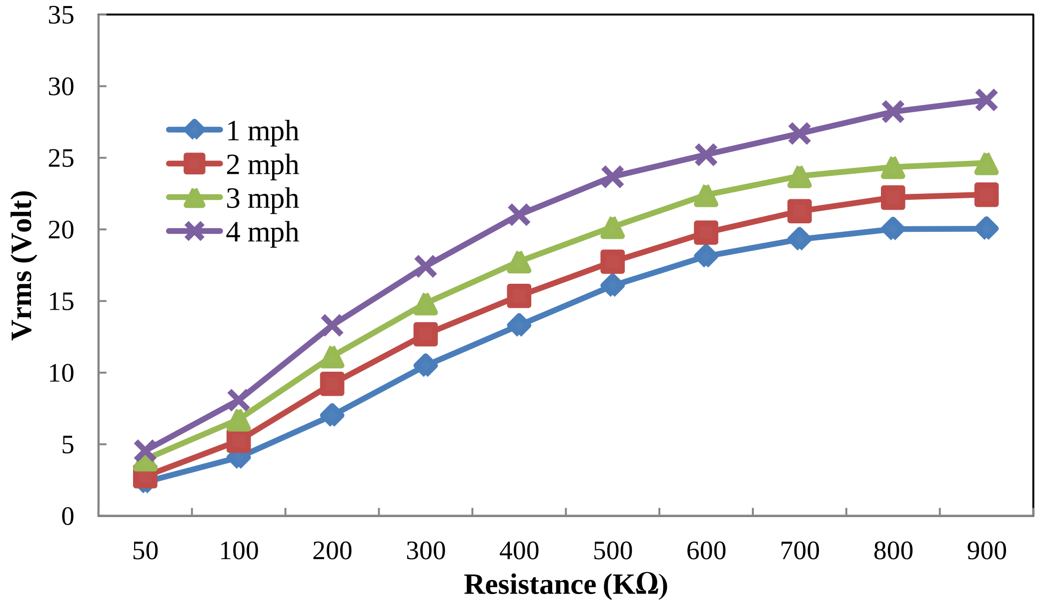

(b)

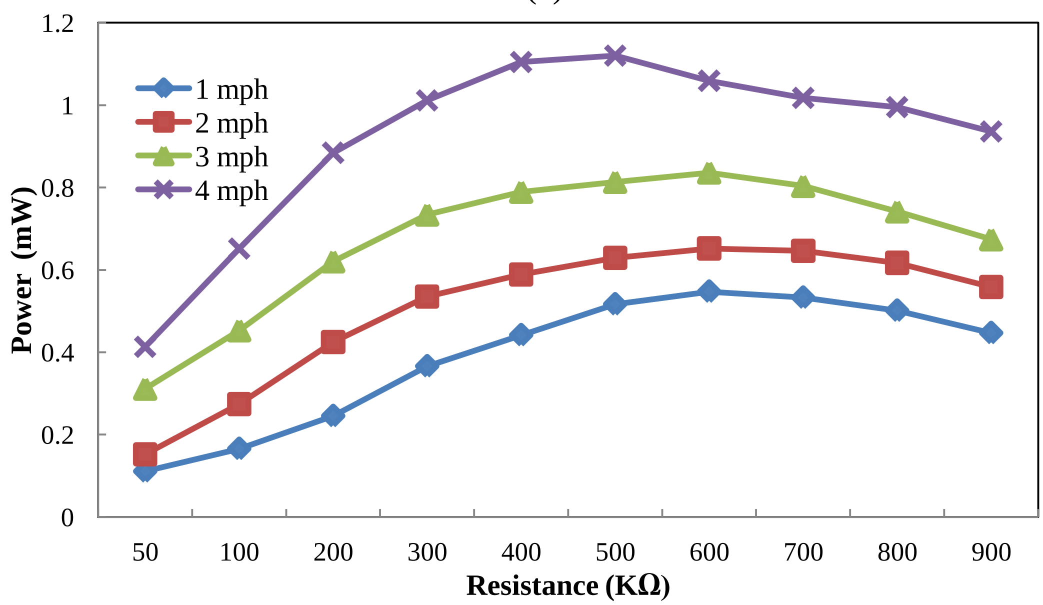

(b)

Figure 4.11 (a) Vrms (voltage) versus resistance and (b) Power versus resistance for four speeds of 1 mph, 2 mph, 3 mph, and 4 mph on the treadmill.

4.2 Theoretical Simulation and Comparison

Although Tang [57] presents an analytical model for a clamped circular bimorph piezo diaphragm, he has not performed any experimental tests to compare experimental results with the theoretical calculations.

In Figure 4.12, Figure 4.13, Figure 4.14, and Figure 4.15 the experimental results are compared with the results calculated using the model (Eqs. (2.5) and (2.44)). As calculated in ANSYS modeling, the deflection of the diaphragm center point (ξ) is 75.2 µm. The measured frequencies, which are measured by oscilloscope during experimental tests on the treadmill, are ω_1 =4.95 rad/s, ω_2 =5.52 rad/s, ω_3 =6.45 rad/s, ω_4 = 7.22 rad/s for speeds of 1mph, 2 mph, 3 mph and 4 mph, respectively. These four figures show the calculated maximum powers are higher than the tested results. For example the predicted maximum powers at speeds of 4 mph, 3 mph, 2 mph and 1 mph are 1.58 mW, 1.39 mW, 1.2 mW and 1.07 mW, respectively; while the experimental results are 1.14 mW, 0.82 mW, 0.65 mW, and 0.55 mW. The optimum experimental resistances for generating the maximum powers are also different from the calculated values.

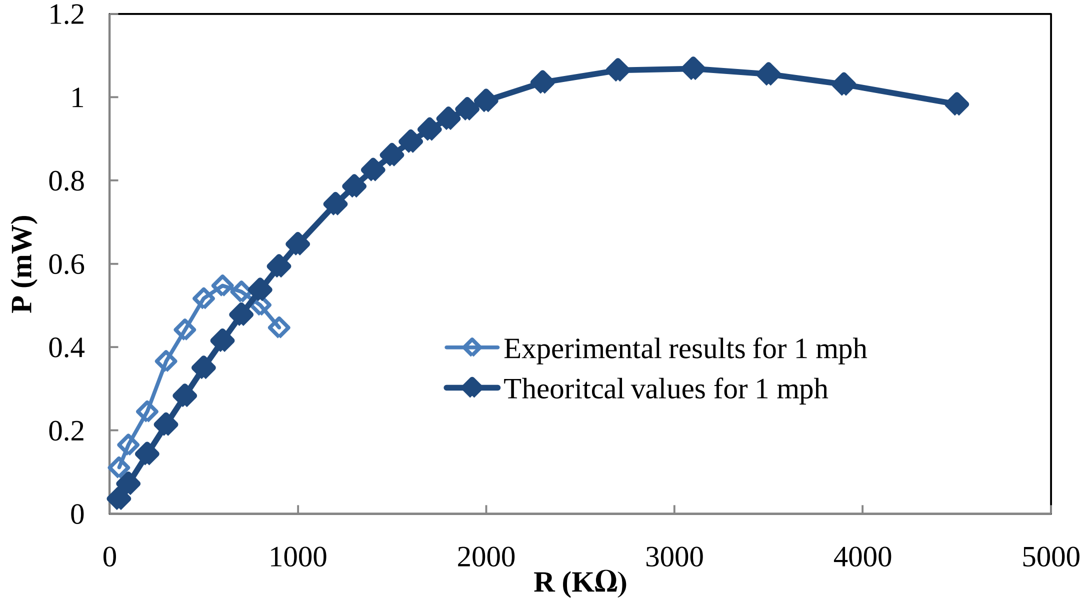

Figure 4.12 Comparing experimental output powers with predicted theoretical power values in different resistances for 1 mile/hour.

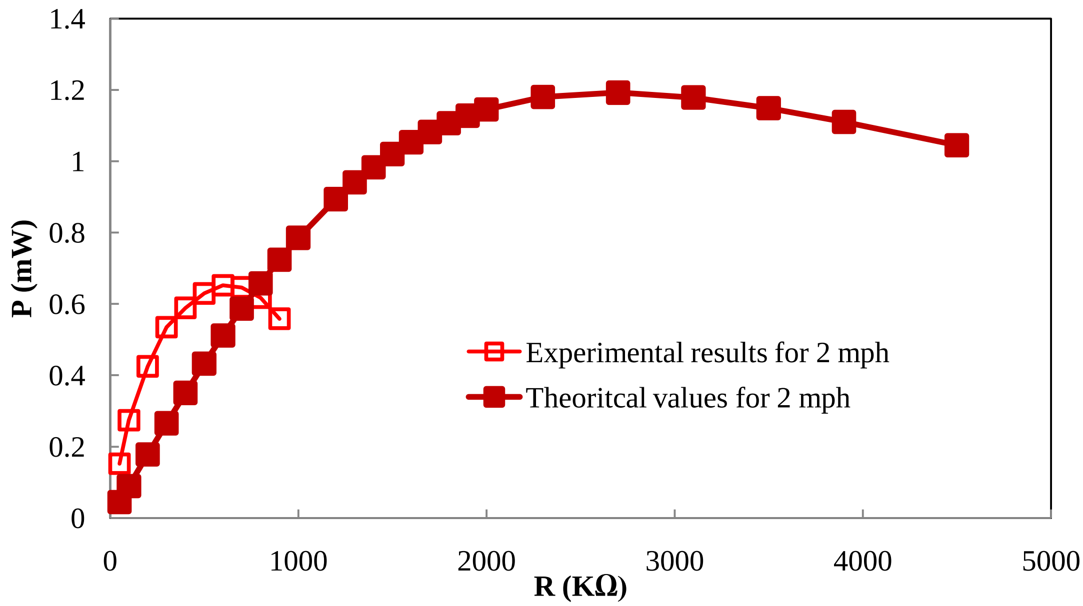

Figure 4.13 Comparing experimental output powers with predicted theoretical power values in different resistances for 2 mile/hour.

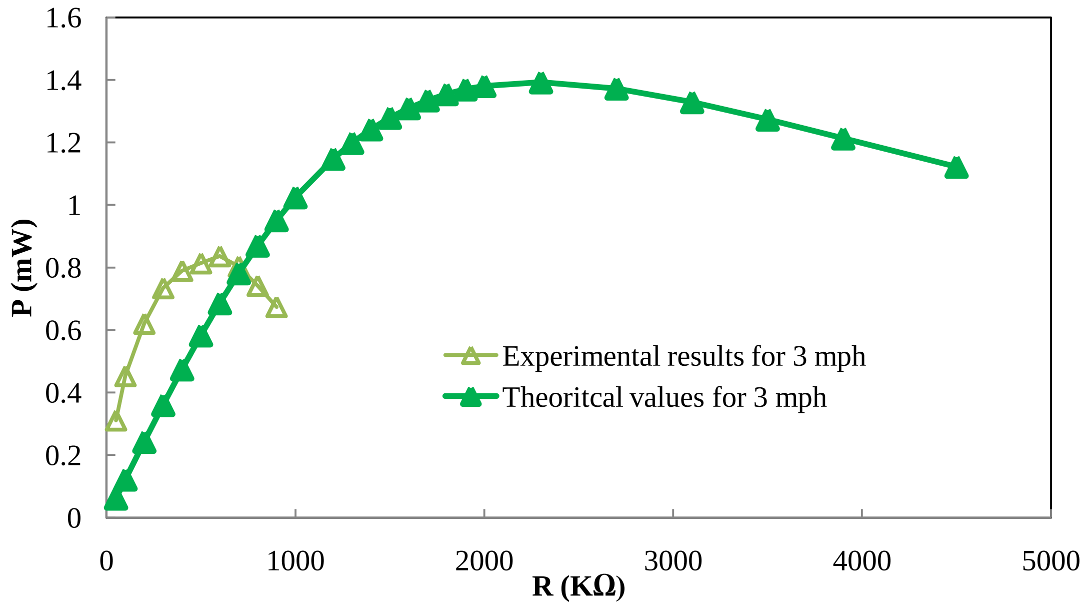

Figure 4.14 Comparing experimental output powers with predicted theoretical power values in different resistances for 3 mile/hour.

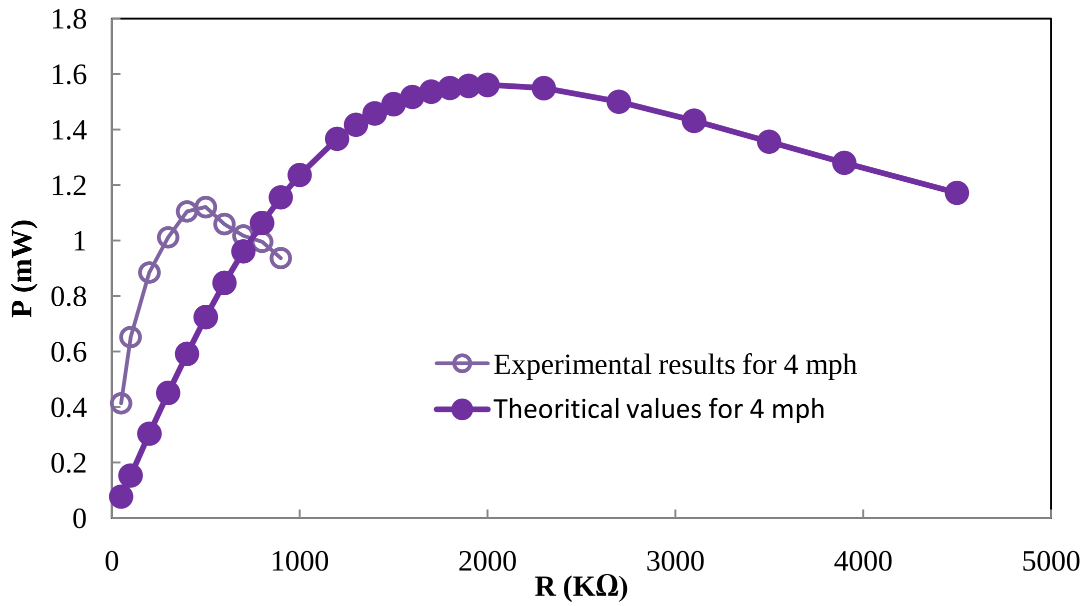

Figure 4.15 Comparing experimental output powers with predicted theoretical power values in different resistances for 4 mile/hour.

4.2.1 Results Analysis and Discussion

The discrepancy between the calculated results and experimental results are mainly attributed to the assumption of zero damping made in the model in order to simplify the process of deriving the power formula [57]. In practical harvester, the damping is not zero. It lowers the generated power and affects the optimal resistive load [1] [3] [34-35] [60-61] [78]. Theoretical equations of the power and optimum resistance for a two piezo layer cantilever with proof mass are presented by Roundy [1] [3]. He proves that power and optimum resistance not only depend on harvester dimensions and frequency but also depend on damping ratio (η) and piezoelectric coupling coefficient (k_{31}). For a real system the optimal external load is modified to [3]:

$$R_{opt} = \frac{1}{(\omega C_f)} \frac{2\eta}{\sqrt{4\eta^2 + {k_{31}}^4}} \tag{4.1}$$

Damping ratio which depends on type of piezo harvester and its dimensions and configuration [59-60] is $\eta = 0.03$ for a cantilever-beam type which operates in the {3-1} mode [60].

4.3 Foot Stepping Force

In conventional shoe embedded PZT power harvesters, the high stepping static/impact force is directly acting on a PZT-metal structure, which leads to a low reliability and short life time due to the fragility nature of PZT materials and the vulnerability of the bonding between the PZT and metal under periodic impact force. The shoe embedded PZT harvester developed in this paper can solve the problems of low reliability and short life time through an air pump design. In the following subsections, the stepping force acting on the harvester is measured.

4.3.1 Force Experimental Test Set Up

The stepping force acting on the harvester is measured using a force sensor (A401 flexi force sensor from Tekscan, INC.) with a 1 inch sensing area. A 5 mm thick poly carbonate circular plate of 1 inch in diameter (the same diameter of sensor sensing area) is glued on the sensor. Then a 5 mm thick polycarbonate plate of 50 mm in diameter is glued on the top plate of the harvester (Figure 4.16). These parts are attached by super glue. The measured signal is wirelessly transmitted to a receiver which is connected to a computer, as shown in Figure 4.17. The oscilicope also measures the open circuite voltage (V_{rms}) and piezo excitation frequency.

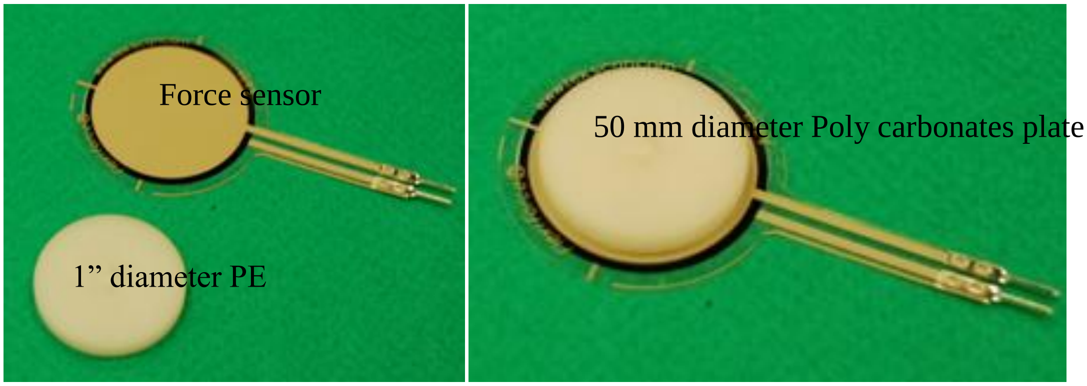

(a) (b)

Figure 4.16 (a) A force measurement sensor with a 50 mm diameter poly carbonates plate, (b) The poly carbonate plate is covered the sensing area.

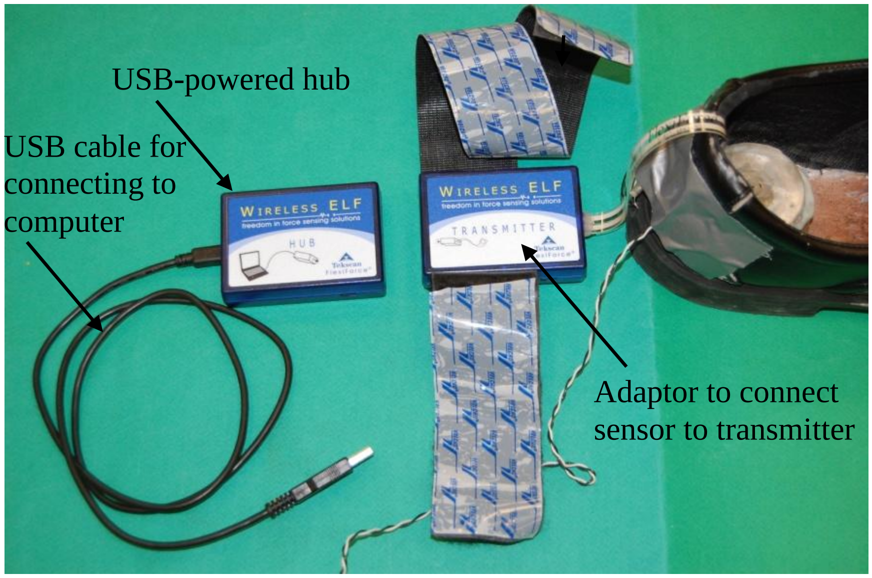

(a)

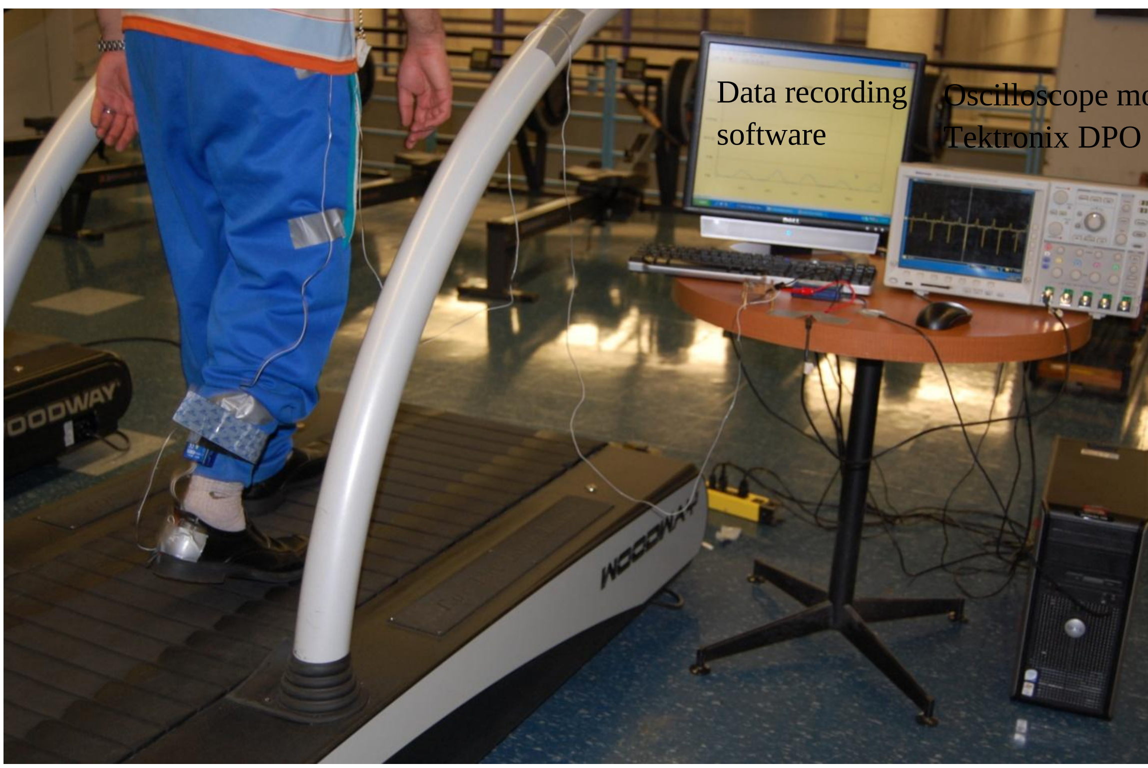

(b)

Figure 4.17 (a) Force measurement device (wireless ELF system from Tekscan, INC.), (b) Force experimental test set up on a treadmill.

4.3.2 Force Test Results

Figure 4.18 presents the measured stepping force acting on the harvester when the harvester is embedded in a shoe walking on the treadmill. As can be seen, the peak force increases with the speed as shown inTable 4.2. The maximum stepping force is more than 600 N when walking on the treadmill.

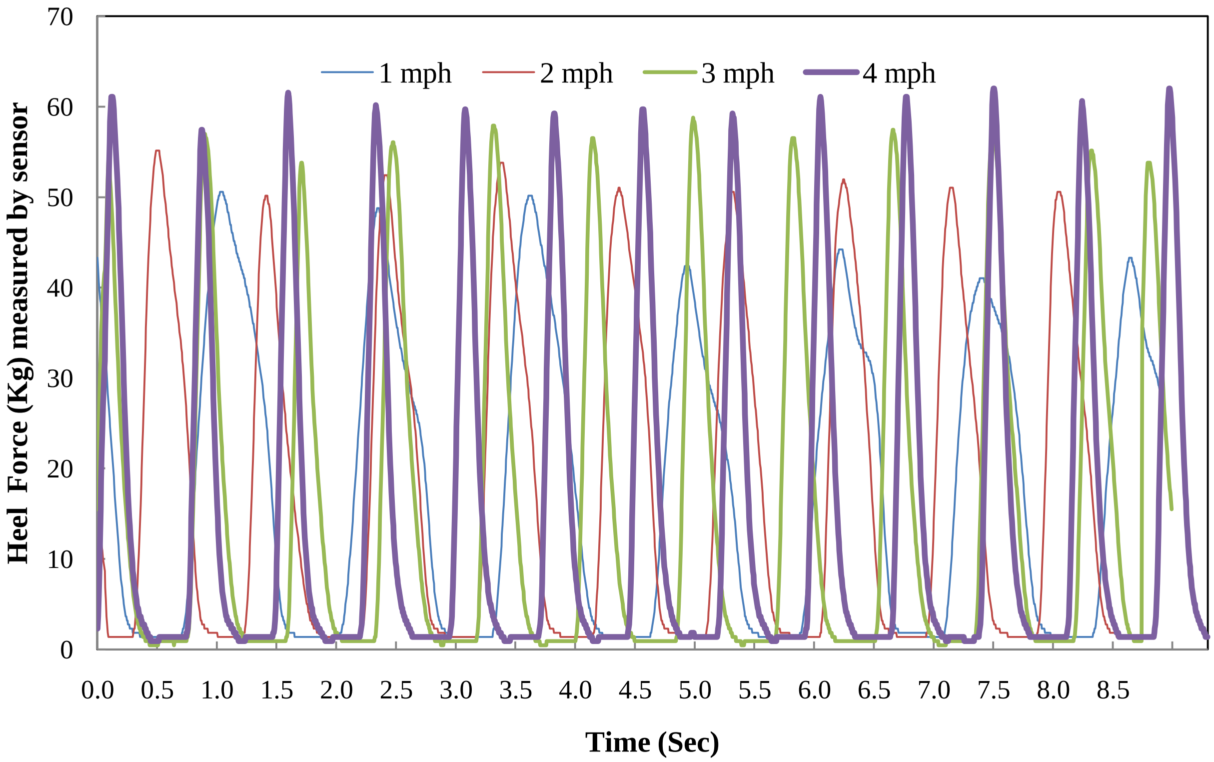

Figure 4.18 Heel force on harvester for speed 1mile/hour to 4 miles/hour.

Table 4.2. Measured maximum force when walking on the treadmill.

Speed (mile/hour)	Max Force (N)	Open circuit V_{rms} (Volt)
1	496.4	32.4
2	541.5	35.9
3	576.8	36.7
4	608.2	38.5

The stepping force was measured when stepping randomly on the floor including stepping on the floor as hard as poosible. The maximum measured stepping force was 902.5 N (460 kpa) as shown in Figure 4.19. The harvester survived all tests without degrading the performance. The measured steeping force matches the results have reported in other articles [40-48]. Actually the harvester can take even much higher force, a force as high as the harvester housing can take, according to the air pump type design as shown in Figure 2.1.

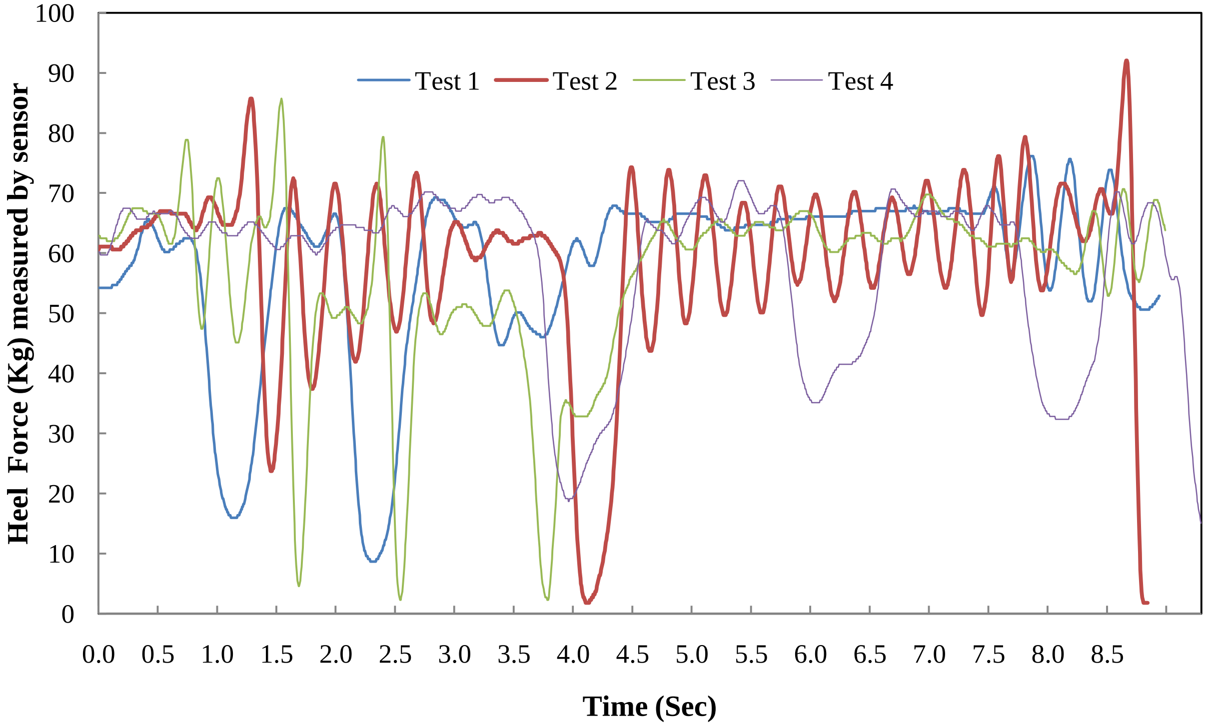

Figure 4.19 Measured steeping force for random stepping on the floor.

Chapter 5 Summary and Future Work

5.1 Summary

In all existing shoe piezo power generators, the foot pressure is directly on the piezo material, which is very fragile. Moreover, bonding between the piezo and the metal layer is weak and cannot tolerate long walking times. In this thesis, a shoe embedded air pump type piezoelectric power harvester has been developed and tested which can solve the problem of shoe piezo harvesters. In this harvester, the PZT deforms to generate electric power due to the air pressure difference caused by the air pump which is subject to the stepping force. Thus the high static/impact stepping force is not directly acting on the PZT-metal composite structure as is the case in most conventional designs, which leads to significantly improved reliability and life time. Experimental tests showed an average power of 1.12 mW was generated when the harvester is embedded in the show and the shoe wearer walked on the treadmill at a speed of 4 mph.

An existing analytical modeling for circular bimorph piezo diaphragm was also used to predict the maximum output power. This theory has significant discrepancy for finding the optimum resistance due to neglecting the system damping.

Moreover, a method was introduced for measuring the impact force on the harvester during walking, jagging, and jumping. The stepping force acting on the harvester was measured as high as 902.5 N.

This harvester has also the capability to put the air bellow inside the shoes and the piezo chamber part outside the shoes which means that the piezo part can be accessible and be used for different shoes.

5.2 Future Work

The future work of this project should focus on the following:

- The design can be improved with increasing the air pressure by modifying the chamber size. The internal pressure of the chamber should be measured by pressure sensor to find the real pressure inside the air chamber. This measurement can be used to find the difference between theoretical pressure and real pressure.
- Different rubbers should be tested to choose a more reliable rubber. Moreover, moulded bellows (Figure 5.1) can be used which is more useful for air bellows or air pump applications. This type of bellows can also help to solve the weak epoxy problem.

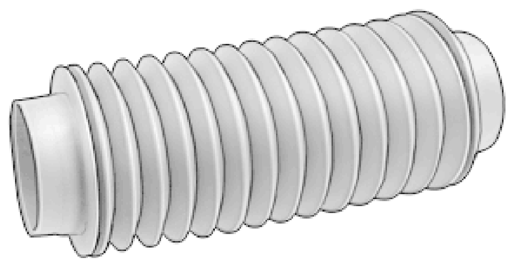

Figure 5.1 Moulded air below is applicable for air pump.

- Capacitive load tests should be performed. A circuit should be designed to rectify the AC voltage to lower DC voltage which is suitable for a real small electronic device.

Appendix A Piezoelectric Configurations

A.1Piezoelectric Materials

The material selection for the design is very critical because the maximum power output is closely related to materials properties of the piezoelectric material and the geometry. For the piezoelectric material, these fundamental properties are important [3]:

- The piezoelectric strain coefficient (d) - relates strain to electric field
- The piezoelectric voltage coefficient (g) - relates stress to voltage.
- Coupling coefficient (k) – material's ability to convert mechanical energy to electrical energy or vice versa.
- Dielectric constant (ε) – the higher it is, the lower the source impedance of the generator.
- Young's modulus – affects the stiffness of the bender.
- Tensile strength – which limits the maximum strain that a bender can withstand

There are two commercially available piezoelectric materials, PZT (Lead Zirconate Titanate) and PVDF (Polyvinlidine Fluoride). In Table A.1 these main types of piezo materials have been compared.

Table A.1 Comparison of piezoelectric materials [3].

Property	Units	PZT	PVDF
Strain coefficient (d_{31})	10^{-12} m/V	320	20
Strain coefficient (d_{33})	10^{-12} m/V	730	30
Coupling coefficient (k_{31})	-	0.41	0.11
Coupling coefficient (k_{33})	-	0.74	0.16
Dielectric constant	$\varepsilon/\varepsilon_o$	4600	12
Elastic modulus	10^{10} N/m^2	5.0	0.3
Tensile strength	10^7 N/m^2	3.4	5.2

A.2Modes of Piezoelectric

There are two common modes utilized for piezoelectric energy harvesting 33-mode (or stack) and 31-mode (bimorphs). In the 33-mode, the direction of applied stress (force) and generated voltage is the same, while in 31-mode the stress is applied in the axial direction but the voltage is obtained from the perpendicular direction as shown in Figure A.2.

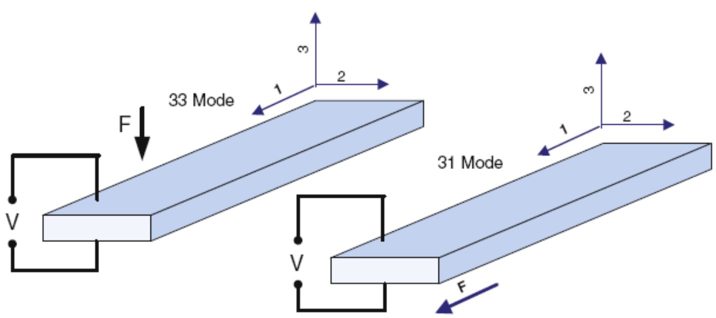

Figure A.2 Operating modes of piezoelectric transducer [12].

A.3Researches Based on Materials, Piezoelectric Patches, and Geometries

Piezoelectric materials can be configured in many different ways that improve output power. One way to improve configuration of the power harvesting device is modification of piezoelectric materials. In Table A.2, a summary of investigations and advantages/ disadvantages of mentioned materials can be seen.

The efficiency of a power harvester can also be improved by using multilayer piezoelectric materials. In Table A.3, various devices using multiple piezoelectric patches have been mentioned. Moreover, a lot of articles have focused on the geometry of power harvesters including changing shape, adding prestress and electrode pattern (Table A.4).

Table A.2 Some researches based on materials.

Author	Material	Advantages/ disadvantages	Appendix A
Lee et al [32]	PZT	Most common type, but not flexible, and susceptible to fatigue crack growing during cycle loading	Table A.5
Lee et al [33]	PVDF	Resistance to fatigue crack/ Low piezo material properties	Table A.5
Mohammadi et al [66]	Piezofiber composite	Increased flexibility	Figure A.11
Sodano et al [67]	MFC, quick pack	Flexibility and more energy capacity	Table A.5

Table A.3 Some researches based on using piezoelectric patches.

Author	Piezoelectric configuration	Advantages/ disadvantages	Appendix A
Ng and Liao [68]	Unimorph, series and parallel bimorph	Unimorph; for low excitation and load Serial bimorph: high excitation and load Parallel bimorph: medium excitation and load	Figure A.3
Mateu and Moll [69]	Homogeneous , and heterogeneous bimorph; heterogeneous unimorph	Heterogeneous unimorph and bimorph generated most power	Figure A.4 Figure A.5 Figure A.6

Table A.4 Some researches based on various geometries.

Author	Material	Advantages/ disadvantages	Appendix A
Mateu and Moll [69]	Rectangular and triangular cantilever	Triangular configuration capable of higher power generation	Figure A.4 Figure A.7
Roundy et al [1]	Trapezoidal cantilever	Trapezoidal configuration allows strain to be evenly distributed increasing efficiency and produce 30% more energy than rectangular	Figure A.6
Yoon et al [70]	Initially curved PZT unimorph	Increased harvesting capacity	Table A.5
Ericka et al [49] & Mo et al. [54-56]	Unimorph circular membrane	Capable of harvesting energy from fluctuating pressure sources	Figure A.8
Tang et al. [57] Junwu et al. [58]	Bimorph circular plate	for fluctuating pressure sources	Figure A.9
Kim et al. [47-48]	Unimorph plate with recouped electrodes	for fluctuating pressure sources	Figure A.10

Table A.5 Some bulk transducer structures for energy harvesting [1-2][12-14][45][63-66]

Transducer products	Company/Characteristics
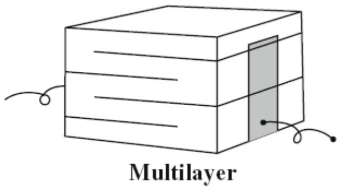	Supplier example: Morgan Electroceramics, APC International, Tokin, PI. Characteristics: low frequency (~10 Hz), suitable under large uniaxial stress condition, easy mounting.
 Macro Fiber Composite (MFC)	Supplier example: Smart Material. Characteristics: flexible, both d33 and d31 mode possible, low strain high frequency application, large area coverage, can be used as a bimorph element.
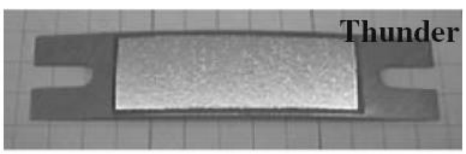	Supplier example: Face International. Characteristics: various curvatures and heights possible providing wide range of stress amplification, suitable for very low frequencies (~1 Hz).
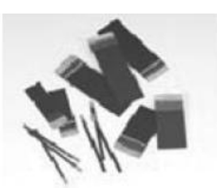 Bimorphs	Supplier example: APC International. Characteristics: resonance frequency can be tuned in the range of 5–100 Hz, used in various configuration such as cantilever, end–end clamped, etc.

	Supplier example: Mide Characteristics: similar to bimorphs but easier mounting, wide bandwidth, widely used in cantilever configuration
	Characteristics: curved surface resulting in higher charge under a given stress level, can be stacked to amplify charge.
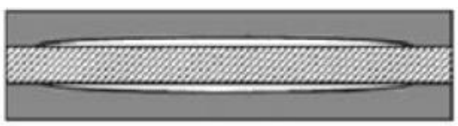 Moonie 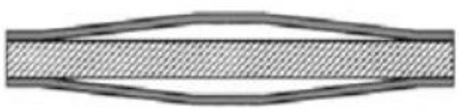 Cymbal	Supplier: Micromechatronics. Characteristics: metal caps protect ceramic allowing application under high stress levels, higher charge due to stress amplification, resonance frequency can be tuned by changing cap dimensions and material.

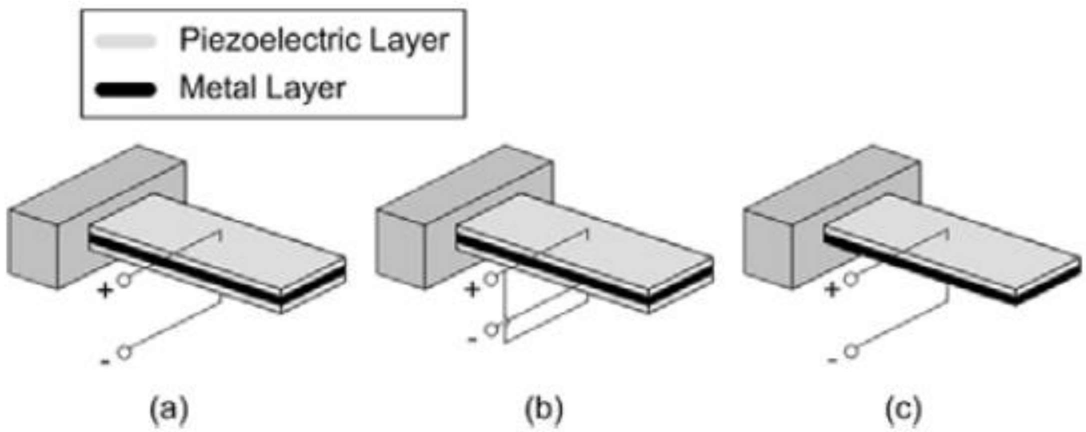

Figure A.3 (a) A series triple layer type piezoelectric sensor, (b) A parallel triple layer type piezoelectric sensor, (c) A unimorph piezoelectric sensor [3], [32].

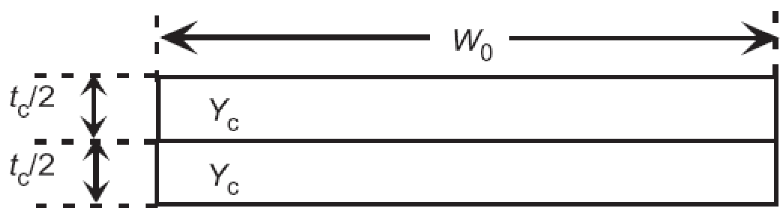

Figure A.4 Section of a homogeneous bimorph beam. tc/2 corresponds to a piezoelectric film thickness [69].

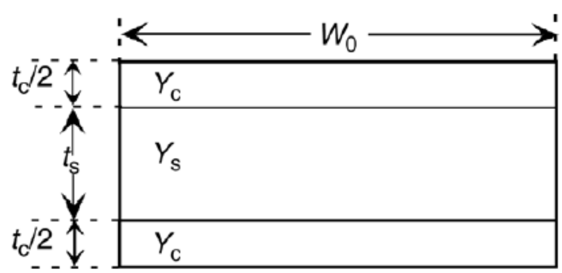

Figure A.5 Cross section of symmetric heterogeneous bimorph beam. tc/2 corresponds to piezoelectric film thickness whereas ts correspond to non-piezoelectric film thickness [69].

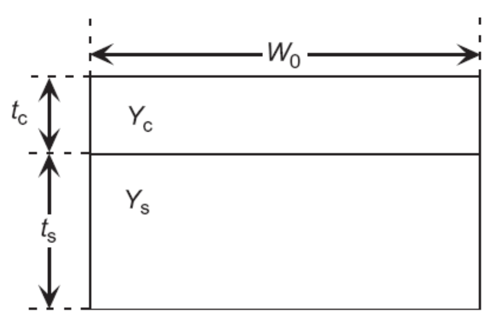

Figure A.6 Cross section of asymmetric heterogeneous bimorph beam. tc corresponds to piezoelectric film thickness whereas ts correspond to non-piezoelectric film thickness. Yc is the Young’s modulus for the piezoelectric material and Ys is the Young’s modulus for the non-piezoelectric material. W0 is the width of the beam [69].

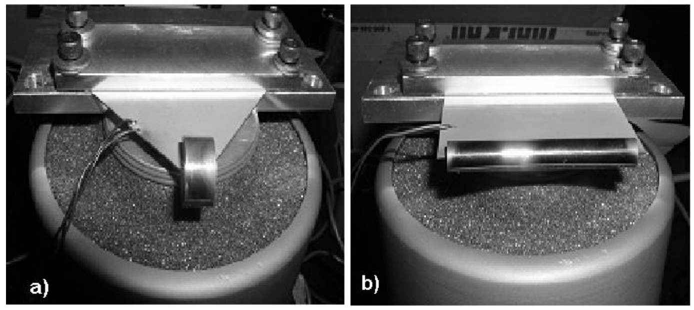

Figure A.7 Cantilever beam designs with (a) trapezoidal, and (b) rectangular footprints [1], [69].

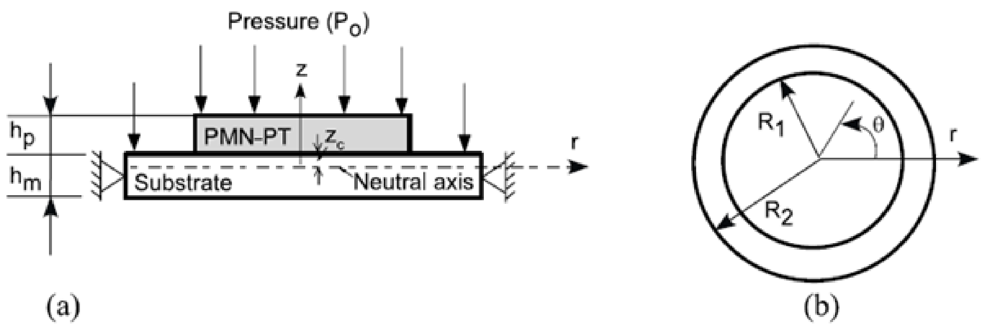

Figure A.8 Unimorph piezoelectric circular harvester: (a) Cross section view, (b) Top view [5].

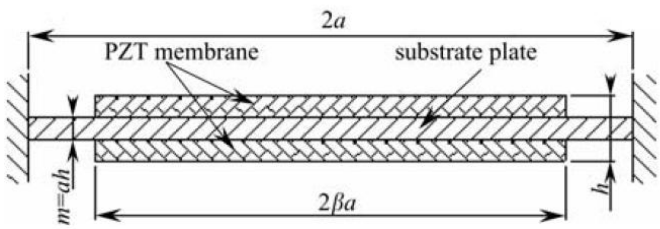

Figure A.9 Cross section of PZT composite diaphragm [57].

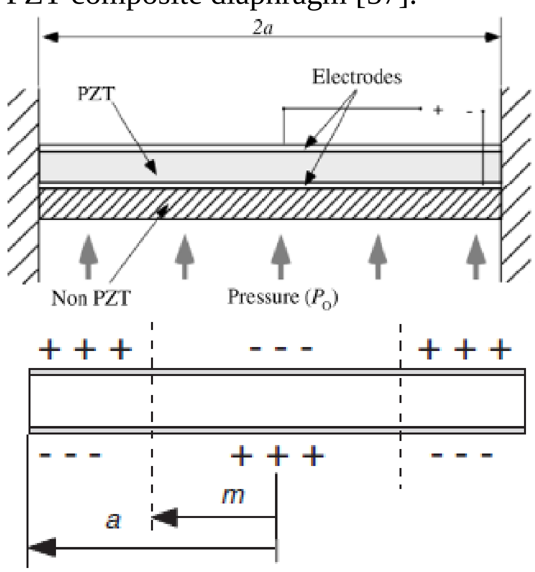

Figure A.10 Cross section of decoupled piezo diaphragm [50-52].

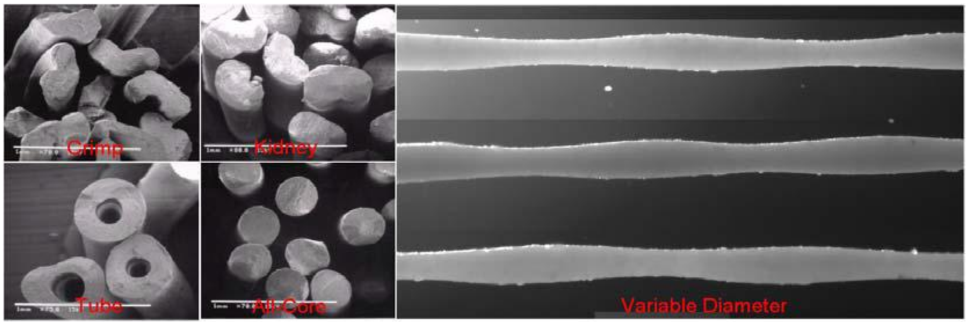

Figure A.11 Ceramic fibers of various cross-sections [66].

Appendix B The Harvester Drawings

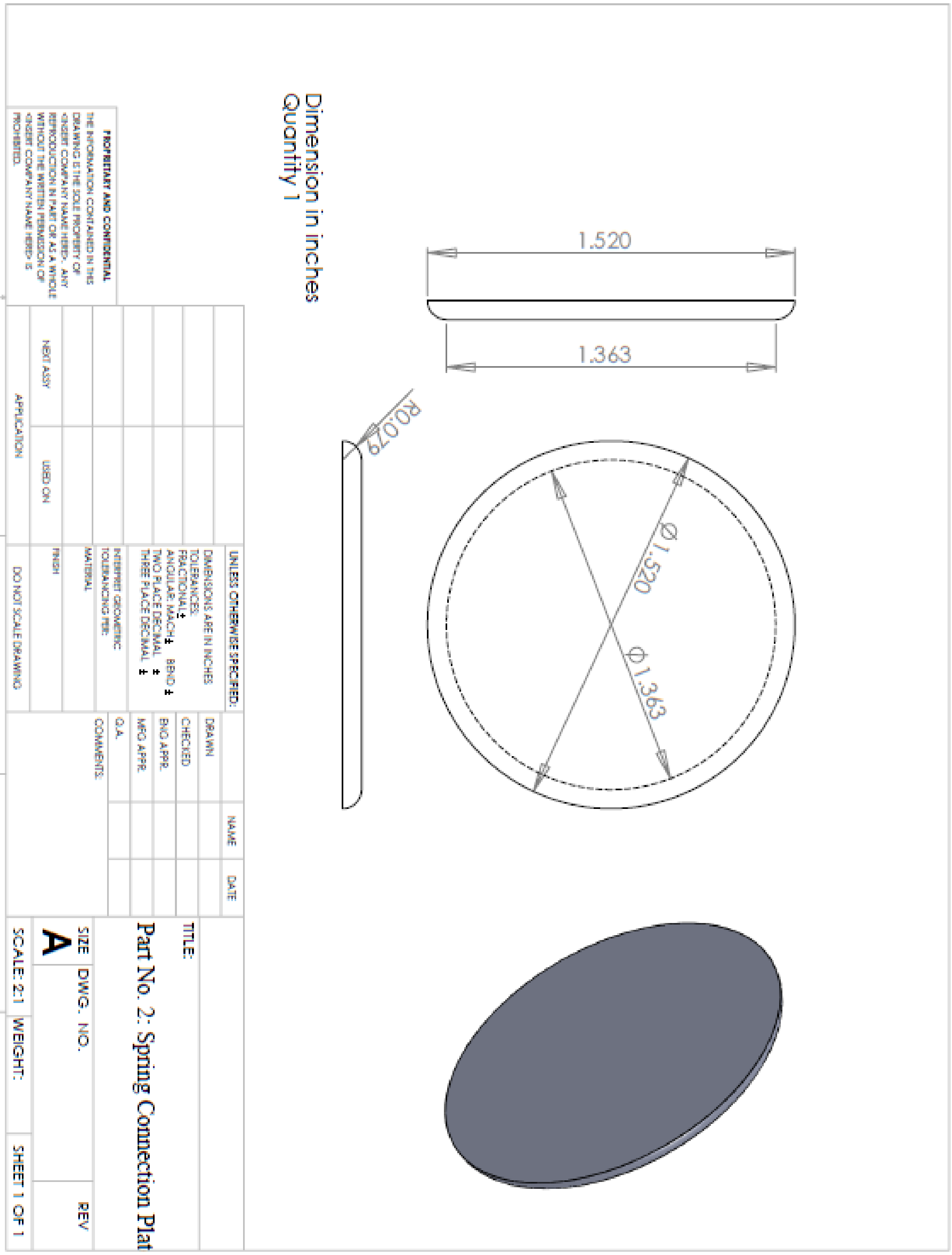

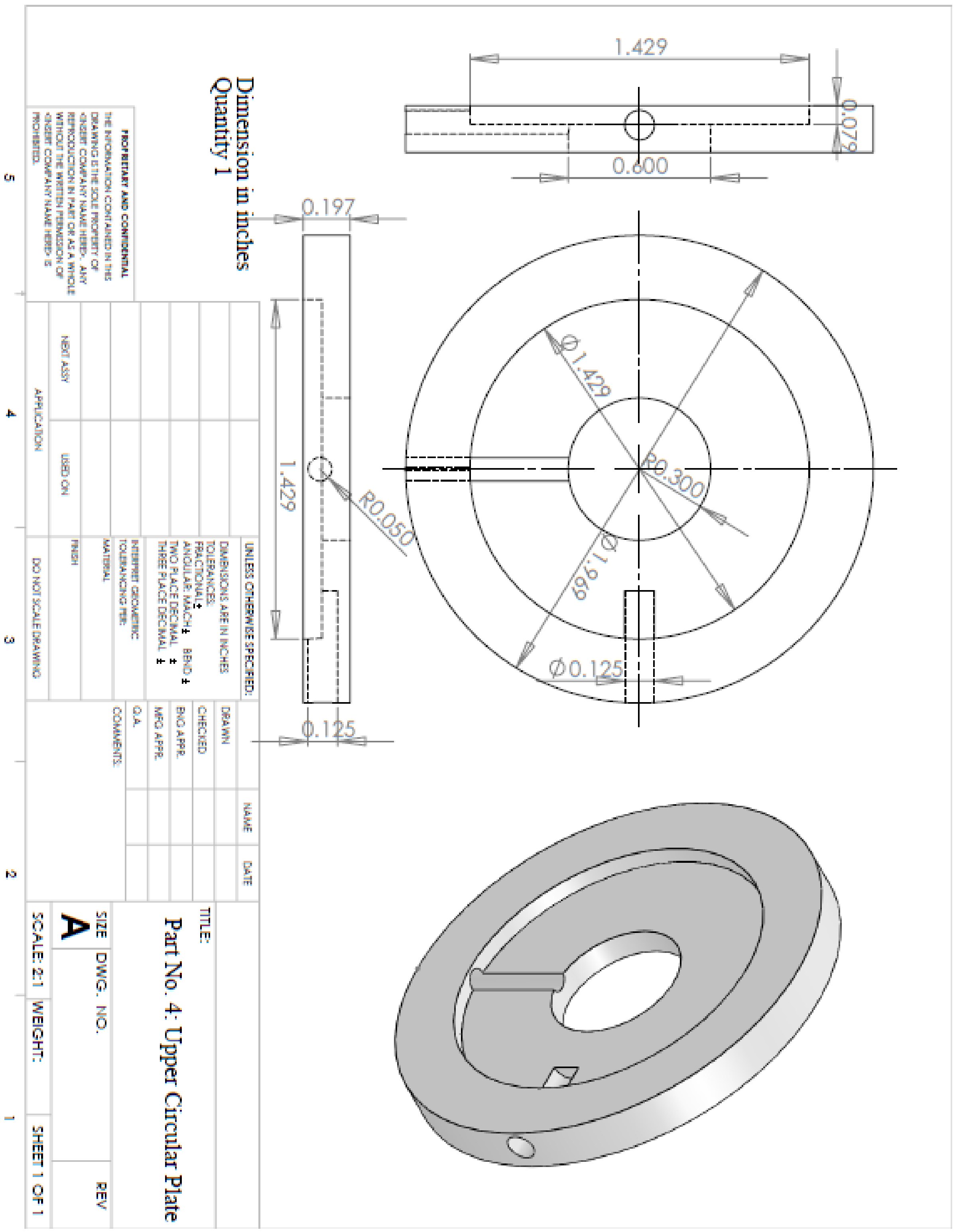

Dimension in inches
Quantity 1
1.429
0.079
0.600
0.197
Ø1.429
R0.300
Ø1.969
Ø0.125
1.429
R0.050
0.125
PROPRIETARY AND CONFIDENTIAL
APPLICATION
NEXT ASSY
USED ON
DO NOT SCALE DRAWING
UNLESS OTHERWISE SPECIFIED:
DIMENSIONS ARE IN INCHES
FINISH
MATERIAL
DRAWN
CHECKED
ENG APPR.
MFG APPR.
Q.A.
COMMENTS:
NAME
DATE
TITLE:
Part No. 4: Upper Circular Plate
SIZE
A
DWG. NO.
REV
SCALE: 2:1
WEIGHT:
SHEET 1 OF 1

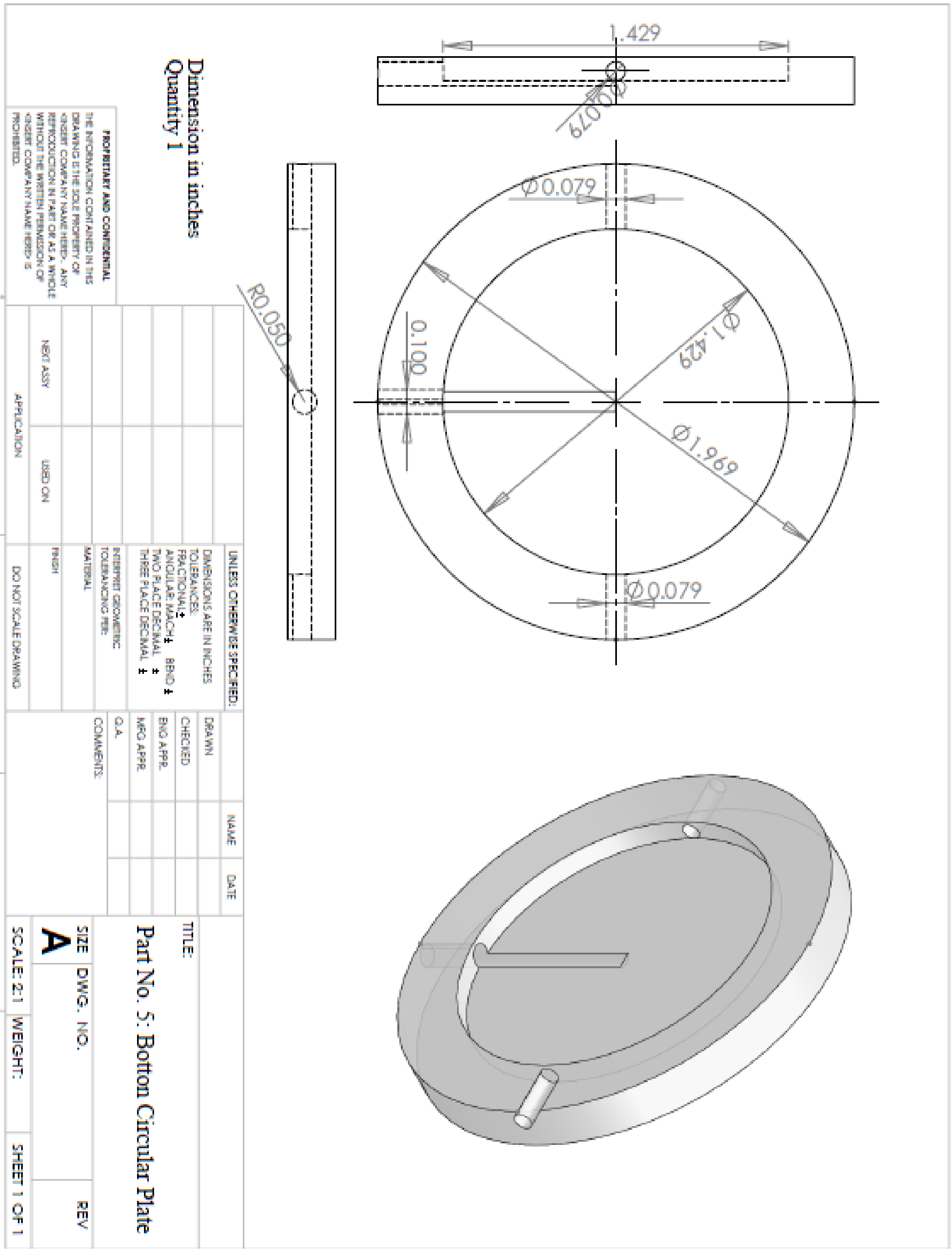

1.429
Ø0.079
Ø0.079
Ø0.079
0.100
Ø1.429
Ø1.969
R0.050
Dimension in inches
Quantity 1
PROPRIETARY AND CONFIDENTIAL
UNLESS OTHERWISE SPECIFIED:
DIMENSIONS ARE IN INCHES
TOLERANCES:
NEXT ASSY
USED ON
APPLICATION
DO NOT SCALE DRAWING
MATERIAL
FINISH
DRAWN
CHECKED
ENG APPR.
MFG APPR.
Q.A.
COMMENTS:
NAME
DATE
TITLE:
Part No. 5: Botton Circular Plate
SIZE
A
DWG. NO.
REV
SCALE: 2:1
WEIGHT:
SHEET 1 OF 1

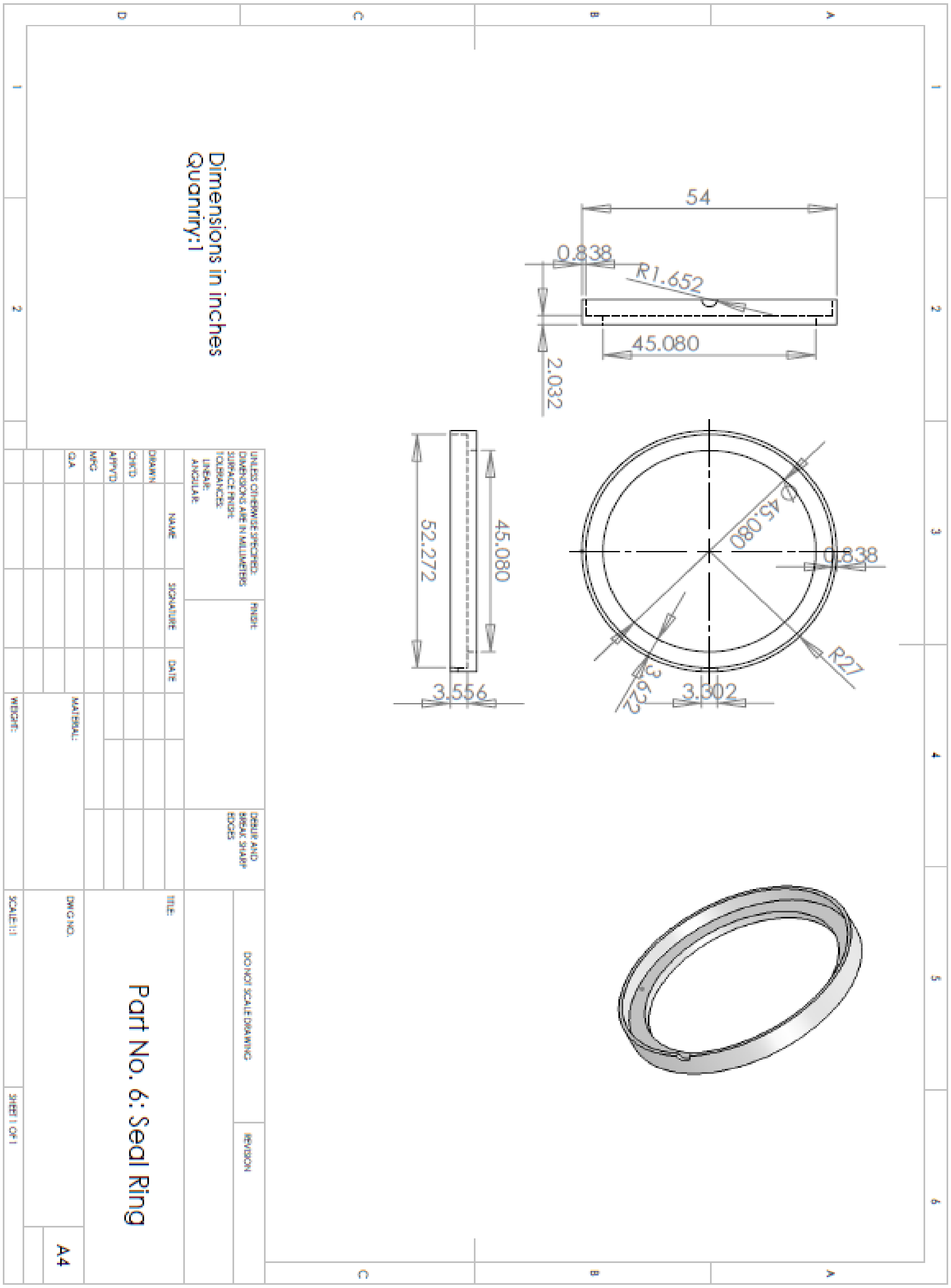

Dimensions in inches
Quanrity:1
54
0.838
R1.652
45.080
2.032
Ø 45.080
0.838
R27
3.622
3.302
52.272
45.080
3.556
UNLESS OTHERWISE SPECIFIED:
DIMENSIONS ARE IN MILLIMETERS
SURFACE FINISH:
TOLERANCES:
LINEAR:
ANGULAR:
FINISH:
DEBUR AND BREAK SHARP EDGES
DO NOT SCALE DRAWING
REVISION
NAME
SIGNATURE
DATE
DRAWN
CHK'D
APPV'D
MFG
Q.A
MATERIAL:
WEIGHT:
TITLE:
Part No. 6: Seal Ring
DWG NO.
A4
SCALE:1:1
SHEET 1 OF 1

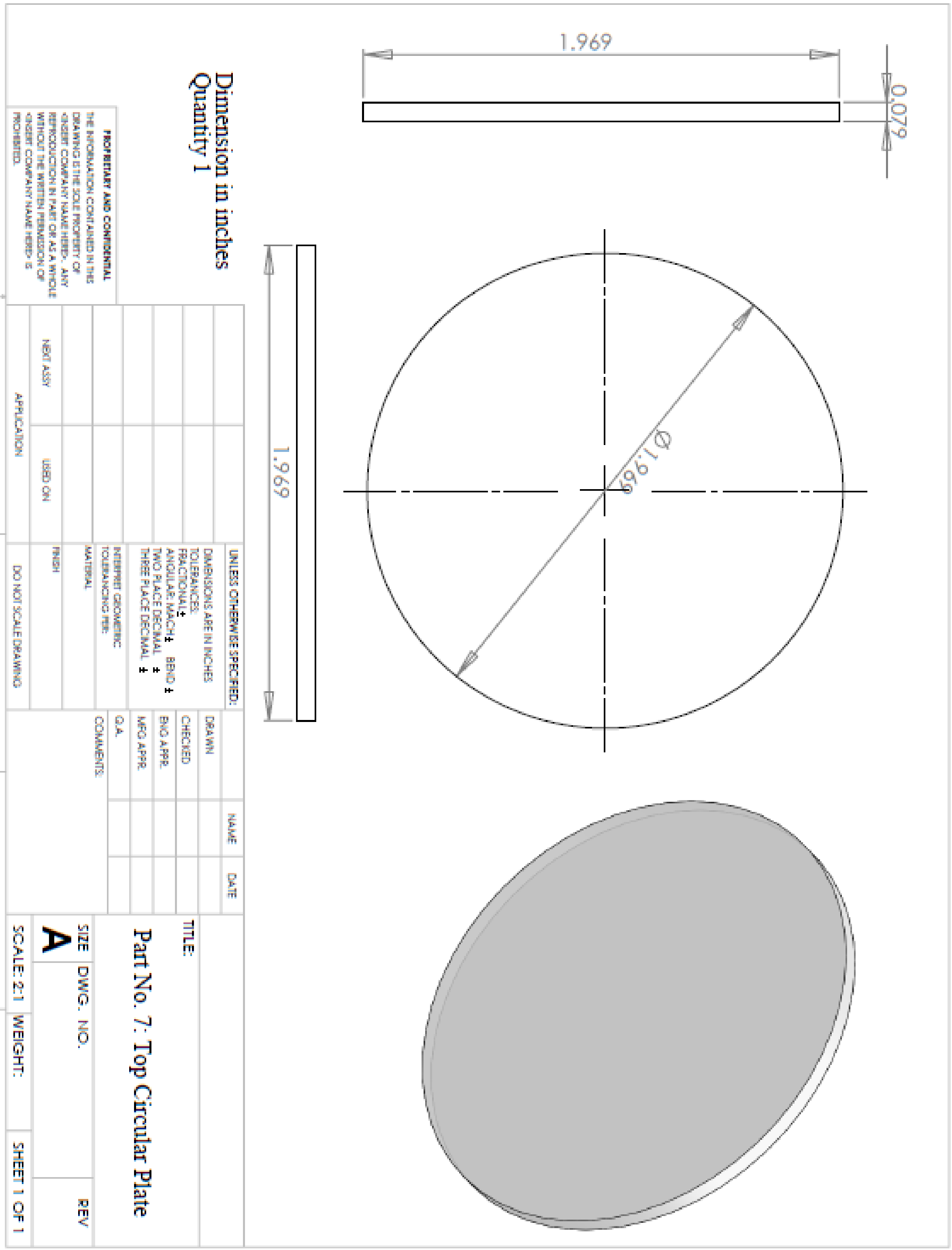
1.969
0.079
Ø1.969
1.969
Dimension in inches
Quantity 1
PROPRIETARY AND CONFIDENTIAL
UNLESS OTHERWISE SPECIFIED:
DIMENSIONS ARE IN INCHES
TOLERANCES:
FRACTIONAL ±
ANGULAR: MACH ± BEND ±
TWO PLACE DECIMAL ±
THREE PLACE DECIMAL ±
INTERPRET GEOMETRIC TOLERANCING PER:
MATERIAL
FINISH
NEXT ASSY
USED ON
APPLICATION
DO NOT SCALE DRAWING
DRAWN
CHECKED
ENG APPR.
MFG APPR.
Q.A.
COMMENTS:
NAME
DATE
TITLE:
Part No. 7: Top Circular Plate
SIZE
A
DWG. NO.
REV
SCALE: 2:1
WEIGHT:
SHEET 1 OF 1

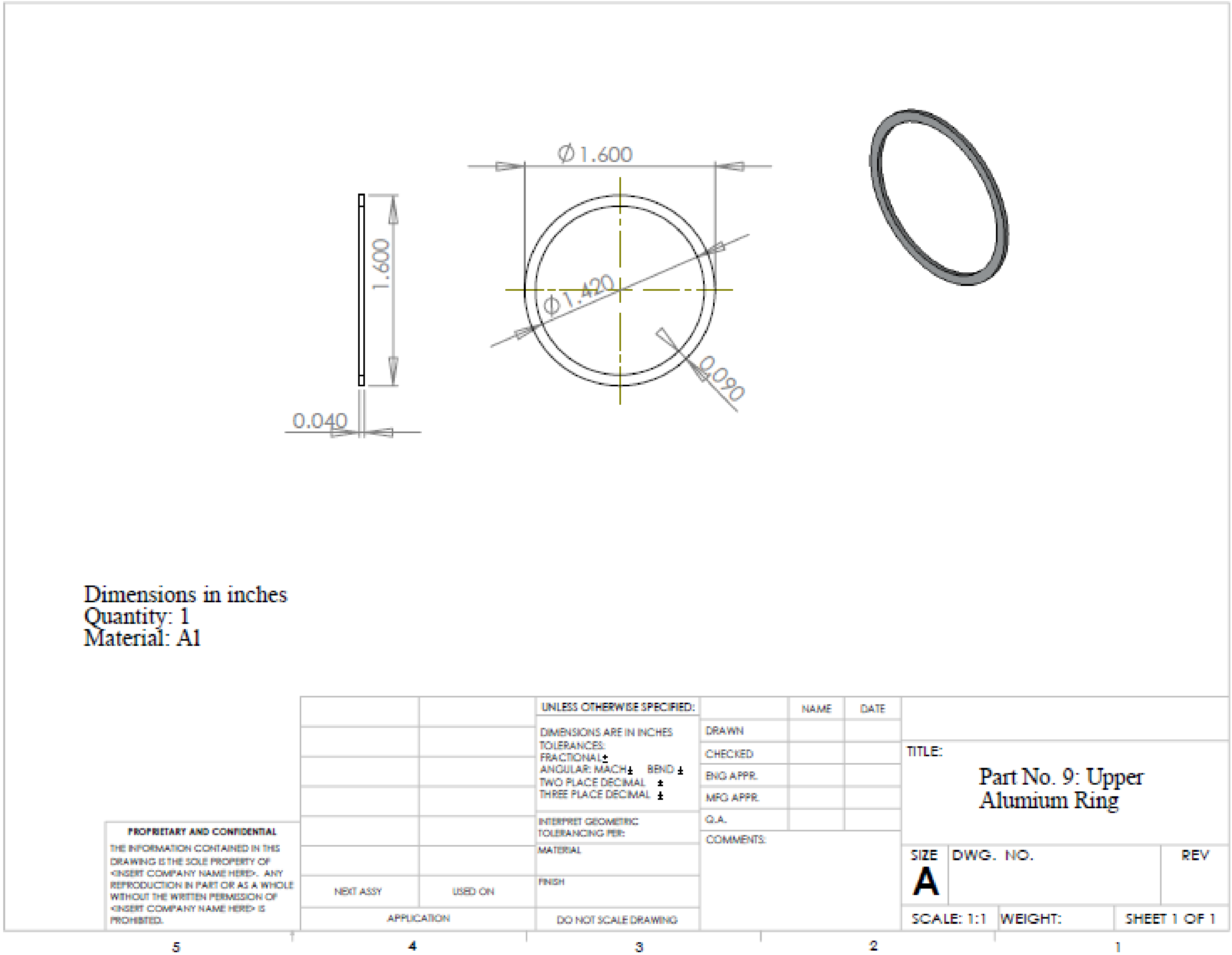
Ø1.600
1.600
Ø1.420
0.090
0.040
Dimensions in inches
Quantity: 1
Material: A1
UNLESS OTHERWISE SPECIFIED:
DIMENSIONS ARE IN INCHES
TOLERANCES:
FRACTIONAL±
ANGULAR: MACH± BEND ±
TWO PLACE DECIMAL ±
THREE PLACE DECIMAL ±
INTERPRET GEOMETRIC TOLERANCING PER:
MATERIAL
FINISH
DO NOT SCALE DRAWING
NEXT ASSY
USED ON
APPLICATION
NAME
DATE
DRAWN
CHECKED
ENG APPR.
MFG APPR.
Q.A.
COMMENTS:
TITLE:
Part No. 9: Upper Alumium Ring
SIZE
A
DWG. NO.
REV
SCALE: 1:1
WEIGHT:
SHEET 1 OF 1
PROPRIETARY AND CONFIDENTIAL
THE INFORMATION CONTAINED IN THIS DRAWING IS THE SOLE PROPERTY OF <INSERT COMPANY NAME HERE>. ANY REPRODUCTION IN PART OR AS A WHOLE WITHOUT THE WRITTEN PERMISSION OF <INSERT COMPANY NAME HERE> IS PROHIBITED.
5
4
3
2
1

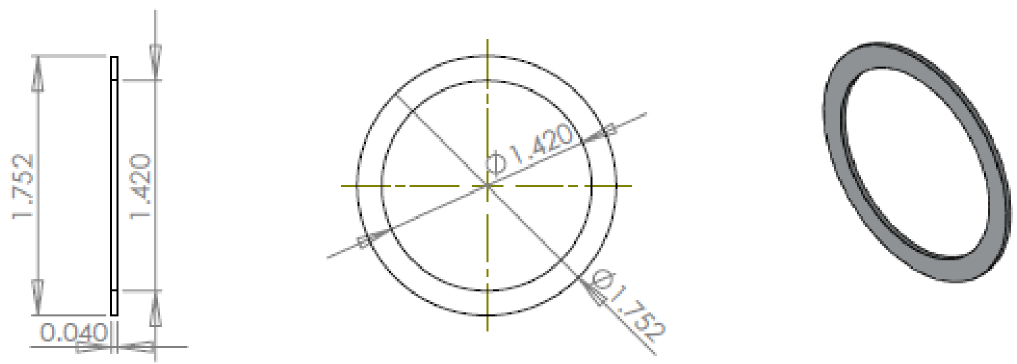

Dimension in inches
Quantity: 1
Material: Al

PROPRIETARY AND CONFIDENTIAL

THE INFORMATION CONTAINED IN THIS DRAWING IS THE SOLE PROPERTY OF <INSERT COMPANY NAME HERE>. ANY REPRODUCTION IN PART OR AS A WHOLE WITHOUT THE WRITTEN PERMISSION OF <INSERT COMPANY NAME HERE> IS PROHIBITED.

NEXT ASSY	USED ON
APPLICATION	

UNLESS OTHERWISE SPECIFIED:
DIMENSIONS ARE IN INCHES
TOLERANCES:
FRACTIONAL ±
ANGULAR: MACH ± BEND ±
TWO PLACE DECIMAL ±
THREE PLACE DECIMAL ±
INTERPRET GEOMETRIC TOLERANCING PER:
MATERIAL
FINISH
DO NOT SCALE DRAWING

	NAME	DATE
DRAWN		
CHECKED		
ENG APPR.		
MFG APPR.		
Q.A.		
COMMENTS:		

TITLE:
Part No. 10: Lower Al Ring

SIZE A | DWG. NO. | REV
SCALE: 1:1 | WEIGHT: | SHEET 1 OF 1

5 4 3 2 1

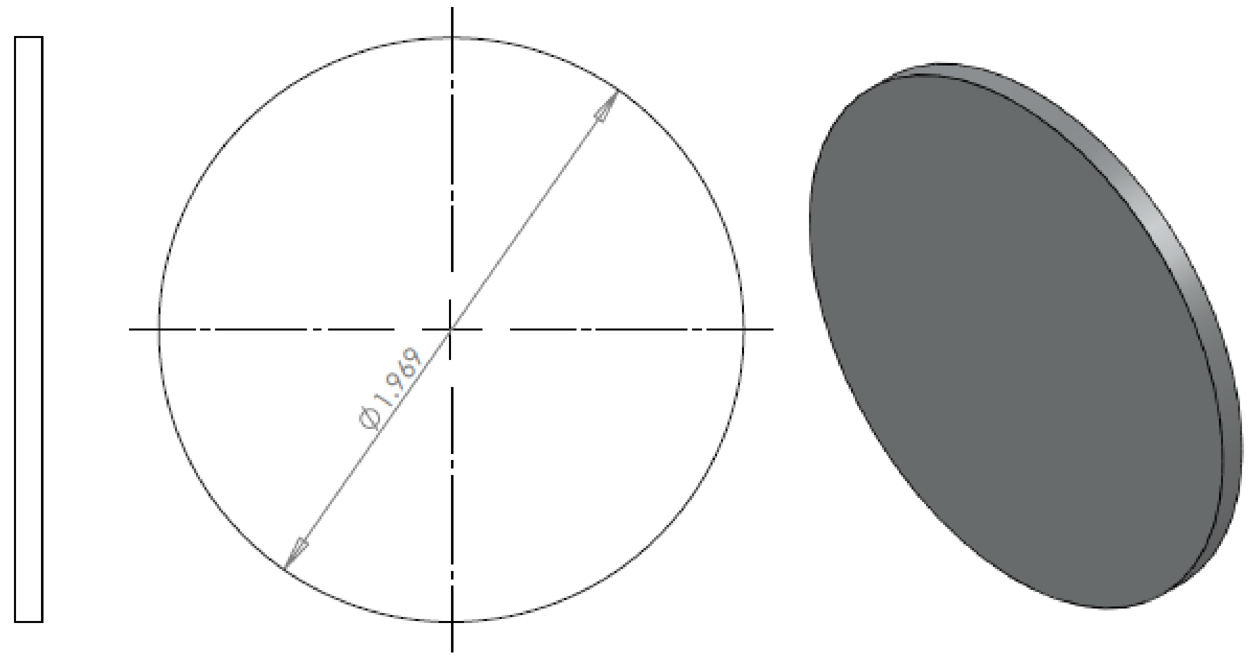

Dimesnions: inches
Quantity: 1
Material: Polycarbonate

PROPRIETARY AND CONFIDENTIAL

THE INFORMATION CONTAINED IN THIS DRAWING IS THE SOLE PROPERTY OF <INSERT COMPANY NAME HERE>. ANY REPRODUCTION IN PART OR AS A WHOLE WITHOUT THE WRITTEN PERMISSION OF <INSERT COMPANY NAME HERE> IS PROHIBITED.

NEXT ASSY	USED ON
APPLICATION	

UNLESS OTHERWISE SPECIFIED:
DIMENSIONS ARE IN INCHES
TOLERANCES:
FRACTIONAL ±
ANGULAR: MACH ± BEND ±
TWO PLACE DECIMAL ±
THREE PLACE DECIMAL ±
INTERPRET GEOMETRIC TOLERANCING PER:
MATERIAL
FINISH
DO NOT SCALE DRAWING

	NAME	DATE
DRAWN		
CHECKED		
ENG APPR.		
MFG APPR.		
Q.A.		

COMMENTS:

TITLE:
Part No. 11: Top Al Plate

SIZE A | DWG. NO. | REV
SCALE: 2:1 | WEIGHT: | SHEET 1 OF 1

5 4 3 2 1

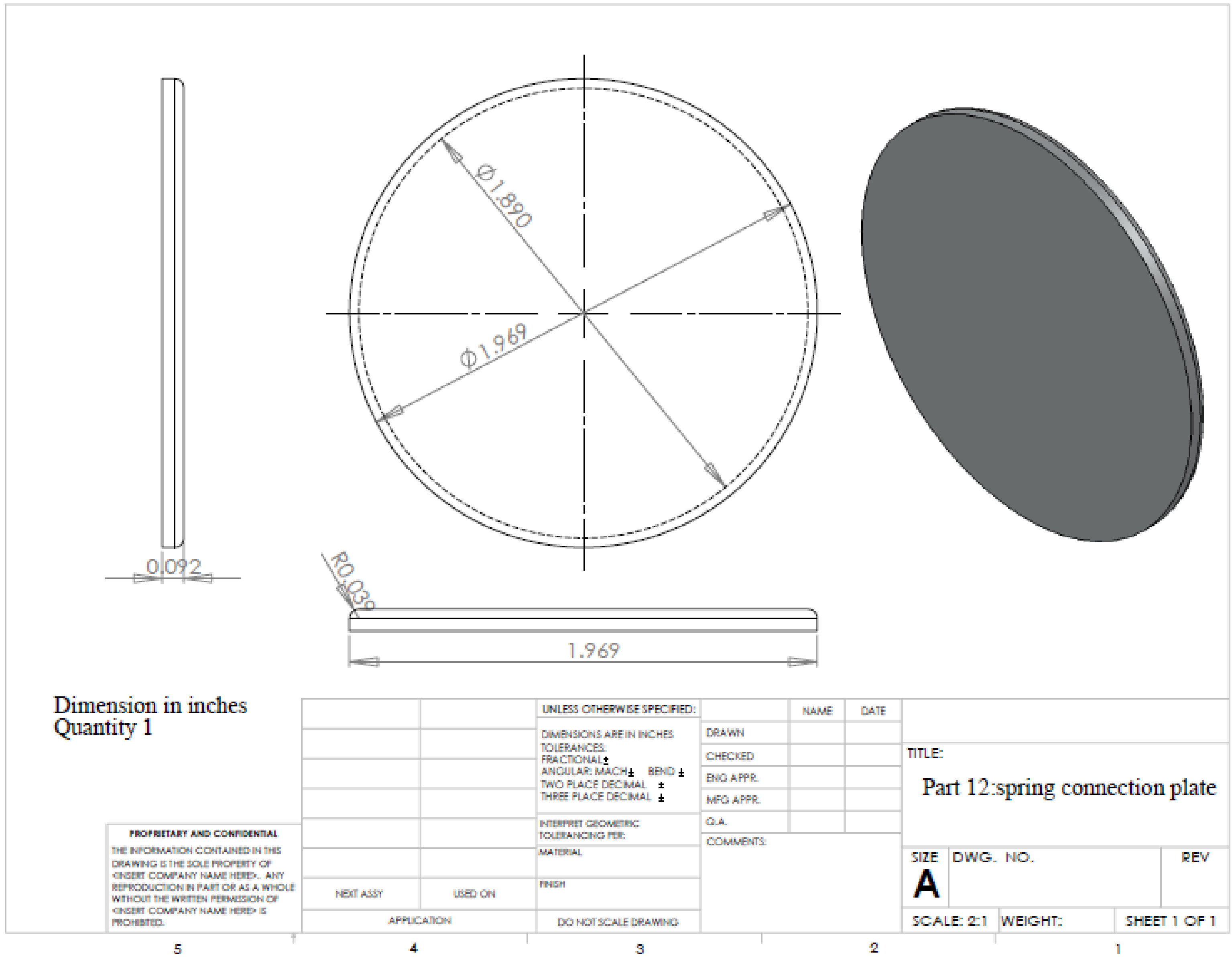

0.092
Ø1.890
Ø1.969
R0.039
1.969
Dimension in inches
Quantity 1
PROPRIETARY AND CONFIDENTIAL
THE INFORMATION CONTAINED IN THIS DRAWING IS THE SOLE PROPERTY OF <INSERT COMPANY NAME HERE>. ANY REPRODUCTION IN PART OR AS A WHOLE WITHOUT THE WRITTEN PERMISSION OF <INSERT COMPANY NAME HERE> IS PROHIBITED.
NEXT ASSY
USED ON
APPLICATION
UNLESS OTHERWISE SPECIFIED:
DIMENSIONS ARE IN INCHES
TOLERANCES:
FRACTIONAL ±
ANGULAR: MACH ± BEND ±
TWO PLACE DECIMAL ±
THREE PLACE DECIMAL ±
INTERPRET GEOMETRIC TOLERANCING PER:
MATERIAL
FINISH
DO NOT SCALE DRAWING
NAME
DATE
DRAWN
CHECKED
ENG APPR.
MFG APPR.
Q.A.
COMMENTS:
TITLE:
Part 12:spring connection plate
SIZE
A
DWG. NO.
REV
SCALE: 2:1
WEIGHT:
SHEET 1 OF 1
5
4
3
2
1

References

[1] S. Roundy, E. S. Leland, J. Baker *et al*., "Improving power output for vibration-based energy scavengers," *IEEE Pervasive Computing*, vol. 4, no. 1, pp. 28-36, 2005.

[2] T. Starner, and J.A. Paradiso, "Human generated power for mobile electronics, low-power electronics design," *(C. Piguet, Ed.)Power, CRC Press*, vol. 1990, pp. 1–35, 2004.

[3] S. J. Roundy, P. Wright, and J. Rabaey, "Energy scavenging for wireless sensor networks with special focus on vibrations," *Springer*, 2003.

[4] J. Kymissis, C. Kendall, J. Paradiso, and N. Gershenfeld, "Parasitic power harvesting in shoes piezoelectric cantilevers," *Smart Materials and Structures*, vol. 19, no. 11, 1998.

[5] P. Niu, R. Chapman, R. Riemer, and X. Zhang, "Evaluation of motions and actuation methods for biomechanical energy harvesting," *35th Annual IEEE Power Electronics Specialists Conference*, vol. 3, pp. 2100-2106, 2004.

[6] S.R. Platt, S. Farritor, K. Garvin, and H. Haider, "The use of piezoelectric ceramics for electric power generation within orthopaedic implants," *IEEE/ASME Transactions on Mechatronics*, vol. 10, no. 4, pp. 455-461, 2005.

[7] J. M. Donelan, Q. Li, V. Naing, *et al*., "Biomechanical energy harvesting: generating electricity during walking with minimal user effort," *Science*, vol. 319, no. 5864, pp. 807-810, 2008.

[8] L. C. Rome, L. Flynn, E.M. Goldman, *et al*., "Generating electricity while walking with loads," *Science*, vol. 309, pp. 1725-1728, 2005.

[9] H. A. Sodano, "Harvesting energy from the straps of a backpack using piezoelectric materials" *Springer Science+Business Media, LLC*, Energy Harvesting Technologies, Chapter 17, 2009.

[10] P. Niu, and P. Chapman, "Design and performance of linear biomechanical energy conversion devices," *37th IEEE Annual Power Electronics Specialists Conference*, pp. 1-6, 2006.

[11] P. Niu, P. Chapman, L. DiBerardino *et al*., "Design and optimization of a biomechanical energy harvesting device," *IEEE Annual Power Electronics Specialists Conference*, pp. 4062-4069, 2008.

[12] H. Kim, Y. Tadesse, S. Priya, "Piezoelectric energy harvesting," *Springer Science+Business Media, LLC*, Energy Harvesting Technologies, Chapter 1 , 2009.

[13] R. Amirtharajah, and A.P. Chandrakasan, "Self-powered signal processing using vibration-based power generation," *IEEE Journal of Solid-State Circuits*, vol. 33, no. 5, pp. 687-695, 1998.

[14] B. O. H. Veld, D. Hohlfeld, and V. Pop, “Harvesting mechanical energy for ambient intelligent devices,” *Information Systems Frontiers*, vol. 11, no. 1, pp. 7-18, 2009.

[15] N.S. Shenck, and J.A. Paradiso, “Energy scavenging with shoe-mounted piezoelectrics,” *IEEE Micro*, vol. 21, no. 3, pp. 30-42, 2001.

[16] L. Mateu, F. Fonellosa, and F. Moll, “Electrical characterization of a piezoelectric film-based power generator for autonomous wearable devices” *Proceedings of 18th Conference on Design of Circuits and Integrated Systems (Ciudad Real)*, pp. 677–82, 2003.

[17] R. Kornbluh, R. Pelrine, Q. Pei, *et al.*, “Electroelastomers: applications of dielectric elastomer transducers for actuation, generation and smart structures,” *Smart Structures and Materials conference: Industrial and Commercial Applications of Smart Structures Technologies, Proc. SPIE* vol. 4698, pp. 254-270, 2002.

[18] J. G. Rocha, L. M. Gonçalves, P. F. Rocha *et al.*, “Energy harvesting from piezoelectric materials fully integrated in footwear,” *IEEE Transactions on Industrial Electronics*, vol. 57, no. 3, pp. 813-819, 2010.

[19] D. Han, and V. Kaajakari, “Microstructured polymer for shoe power generation,” *IEEE Solid-State Sensors, Actuators and Microsystems Conference, Transducers*, 2009.

[20] [20] A. Khaligh, P. Zeng, and C. Zheng, “Kinetic energy harvesting using piezoelectric and electromagnetic technologies-state of the art,” *Industrial Electronics, IEEE Transaction*, vol. 57, no. 3, pp. 850-860, 2009.

[21] L. Mateu, and F. Moll, “Optimum piezoelectric bending beam structures for energy harvesting using shoe inserts,” *Journal of Intelligent Material Systems and Structures*, vol. 16, no. 10, pp. 835-845, 2005.

[22] L. Moro, and D. Benasciutti, “Harvested power and sensitivity analysis of vibrating shoe-mounted piezoelectric cantilevers,” *Smart Materials and Structures*, vol. 19, no. 11, 2010.

[23] W. G. Li, S. He, and S. Yu, “Improving power density of a cantilever piezoelectric power harvester through a curved L-shaped proof mass,” *IEEE Transactions on Industrial Electronics*, vol. 57, no. 3, pp. 868-876, 2010.

[24] J. Hayashida, “Unobtrusive integration of magnetic generator systems into common footwear,” Bachelor’s Thesis, MIT Department of Mechanical Engineering, 2000.

[25] J. A. Paradiso, “Systems for human-powered mobile computing,” *Proceedings of the 43rd ACM/IEEE annual Design Automation Conference*, pp. 645-650, 2006.

[26] J. A. Paradiso, and T. Starner, “Energy scavenging for mobile and wireless electronics,” *IEEE Pervasive Computing*, vol. 4, no. 1, pp. 18-27, 2005.

[27] K. Watanabe, K. Nagano, T. Kimoto *et al.*, “A new kind of small generator embedded inside the heel of a shoe,” *IEEE Power Electronics and Motion Control Conference*, vol. 2, pp. 548, 2000.

[28] C. Wang, D. Miao, P. C. Luk, *et al*., "A shoe-equipped linear generator for energy harvesting," IEEE *International Conference on Sustainable Energy Technologies, ICSET*, pp. 1, 2010.

[29] D. Carroll, and M. Duffy, "Demonstration of wearable power generator," *IEEE Power Electronics and Applications*, pp. 10, 2005.

[30] D. Carroll, and M. Duffy, "Electromagnetic generators for power harvesting," *35th IEEE Power Electronics Specialists Conference*, vol. 3, pp. 2075, 2004.

[31] S. R. Anton, and H.A. Sodano, "A review of power harvesting using piezoelectric materials (2003-2006)," *Smart Materials and Structures*, vol. 16, no. 3, pp. R1-R21, 2007.

[32] B. S. Lee, J. He, W. J. Wu, and W. P. Shih, "MEMS generator of power harvesting by vibrations using piezoelectric cantilever beam with digitate electrode," *Procceedings of Smart Structures and Materials Conference, Proc. SPIE,* pp. 6169-6190B, 2006.

[33] C. S. Lee, J. Joo, S. Han, and S. K. Koh, "Multifunctional transducer using poly(vinylidene fluoride) active layer and highly conducting poly(3,4-ethylenedioxythiophene) electrode: actuator and generator," *Applied Physics Letters*, vol. 85, pp. 1841-3, 2004.

[34] H. A. Sodano, J. Lloyd, and D. J. Inman, "An experimental comparison between several active composite actuators for power generation," *Proceeding of Smart Structures and Materials Conference, Proc. SPIE,* vol. 5390370–8, 2004.

[35] H. A. Sodano, G. Park, and D. J. Inman, "A review of power harvesting using piezoelectric materials," *Shock Vibration Digest*, vol. 36, pp. 197–206, 2004.

[36] H. A. Sodano, G. Park, and D. J. Inman, "Estimation of electric charge output for piezoelectric energy harvesting," *Strain*, vol. 40, pp. 49–58, 2004.

[37] H. A. Sodano, D. J. Inman, and G. Park, "Comparison of piezoelectric energy harvesting devices for recharging batteries," *Journal of Intelligent Material Systems and Structures*, vol. 16, pp. 799–807, 2005.

[38] H. A. Sodano, D. J. Inman, and G. Park, "Generation and storage of electricity from power harvesting devices," *Journal of Intelligent Material Systems and Structures*, vol. 16, pp. 67–75, 2005.

[39] S. W. Arms, C.P. Townsend, M. J. Churchill *et al*., "Energy harvesting wireless sensors," *Springer Science+Business Media, LLC,* Energy Harvesting Technologies, Chapter 7, 2009.

[40] M. J. Hessert, M. Vyas, J. Leach *et al*. "Foot pressure distribution during walking in young and old adults," *BMC Geriatrics*, vol. 5, 2005.

[41] W. C. Hutton, and G. E. Drabble, "An apparatus to give the distribution of vertical load under the foot," *Rheumatology*, vol. 11, no. 6, pp. 313-317, 1997.

[42] B. Chuckpaiwong, J. A. Nunley, N.A. Mall *et al*., "The effect of foot type on in-shoe plantar pressure during walking and running," *Gait Posture*, vol. 28, no. 3, pp. 405-411, 2008.

[43] H. Zhu, N. Maalej, J. G. Webster *et al*., "Microprocessor-based data-acquisition system for monitoring foot pressures," *IEEE/Engineering in Medicine and Biology Society Annual Conference*, vol. 10, no. 4, pp. 1599-1600, 1988.

[44] P. R. Cavanagh, and M. Ae, "A technique for the display of pressure distributions beneath the foot," *Journal of Biomechanics*, vol. 13, no. 2, pp. 69-75, 1980.

[45] R. W. Soames, and C. Clark, "Heel height-induced changes in metatarsal loading patterns during gait," *Biomechanics IX-A*, pp. 446–450, 1985.

[46] E. M. Hennig, and T. L. Nilani, "In-shoe pressure distribution for running in various types of footwear," *Journal of Applied Biomechanics*, vol. 11, no. 3, pp. 299-310, 1995.

[47] A. J. Nevill, M. G. Pepper, and M. Whiting, 1995. "In-shoe feet pressure measurement system utilizing piezselectric film transducers," *Medical and Biological Engineering and Computing*, vol. 33, no. 1, pp. 76, 1995.

[48] M. W. Whittle, "Generation and attenuation of transient impulsive forces beneath the foot: A review," *Gait Posture*, vol. 10, no. 3, pp. 264-275, 1999.

[49] M. Ericka, D. Vasic, F. Costa *et al*., "Energy harvesting from vibration using a piezoelectric membrane," *J. Physique. Coll. IV*, vol. 128, pp. 187–93, 2005.

[50] H. W. Kim, S. Priya, K. Uchino *et al*., "Piezoelectric energy harvesting under high pre-stressed cyclic vibrations," *Journal of Electronics*, vol. 15, no. 1, pp. 27-34, 2005.

[51] S. Kim, W. W. Clark, and Q. M. Wang, "Piezoelectric energy harvesting using a bimorph circular plate: analysis," *Journal of Intelligent Material Systems and Structures*, vol. 16, no. 10. pp. 847–854, 2005.

[52] S. Kim, W. W. Clark, and Q. M. Wang, "Piezoelectric energy harvesting using a bimorph circular plate: experimental study," *Journal of Intelligent Material Systems and Structures*, vol. 16, no. 10, pp. 855-864, 2005.

[53] C. Mo, L. J. Radziemski, and W. W. Clark, "Analysis of PMN-PT and PZT circular diaphragm energy harvesters for use in implantable medical devices," *Active and Passive Smart Structures and Integrated Systems, Proc. SPIE*, vol. 6525, pp. 652507, 2007.

[54] C. Mo, L. J. Radziemski, and W. W. Clark, "Analysis of piezoelectric circular diaphragm energy harvesters for use in a pressure fluctuating system," *Smart Materials and Structures*, vol. 19, no. 2, 2010.

[55] C. Mo, L. J. Radziemski, and W. W. Clark, "Experimental validation of energy harvesting performance for pressure loaded piezoelectric circular diaphragms," *Smart Materials and Structures*, vol. 19, no. 7, 2010.

[56] W. W. Clark, and C. Mo, “Piezoelectric energy harvesting for Bio-MEMS applications,” *Springer Science+Business Media, LLC,* Energy Harvesting Technologies, Chapter 16, 2009.

[57] K. Tang, J. Kan, T. Peng *et al*., “Power performance of circular piezoelectric diaphragm generators,” *Frontiers of Mechanical Engineering in China*, vol. 3, no. 4, pp. 434-440, 2008.

[58] J. Kan, Q. Jinhao, K. Tang *et al*., “Modeling and simulation of piezoelectric composite diaphragms for energy harvesting,” *International Journal of Applied Electromagnetics and Mechanics*, vol. 30, no. 1-2, pp. 95-106, 2009.

[59] Y. C. Shu, and I. C. Lien, “Analysis of power output for piezoelectric energy harvesting systems,” *Journal of Intelligent Material Systems and Structures*, vol. 15, pp. 1499–1512, 2006.

[60] Y. C. Shu, and I. C. Lien, “Efficiency of energy conversion for a piezoelectric power harvesting systems,” *Journal of Micromachining and Microengineering*, vol. 16, pp. 2429-2438, 2006.

[61] A. Erturk, and D. J. Inman, “Electromechanical modeling of cantilevered piezoelectric energy harvesters for persistent base motions,” *Springer Science+Business Media, LLC*, Energy Harvesting Technologies, Chapter 2, 2009.

[62] L. Demin, “Princple of transducer,” Qingdao: Ocean University of Qingdao, 2001.

[63] IEEE std. 176, “IEEE standards on piezoelectricity,” *The Institute of Electrical and Electronics Engineers*, 1978.

[64] Del Piezo Specialties. http://delpiezo.com/yahoo_site_admin/assets/docs/Matrixes_of_DL-50HD.36192159.pdf. Accessed August 2010.

[65] S. Roundy, and P. K. Wright, “A piezoelectric vibration based generator for wireless electronics,” *Smart Materials and Structures*, vol. 13, no. 5, pp. 1131-1142, 2004.

[66] F. Mohammadi, A. Khan, and R. B. Cass, “Power generation from piezoelectric lead zirconate titanate fiber composites,” *Proceedings of Materials Research Symposium*, pp. 736, 2003.

[67] H. A. Sodano, D. J. Inman, and G. Park, “Comparison of piezoelectric energy harvesting devices for recharging batteries,” *Journal of Intelligent Material Systems and Structures*, vol. 16, pp. 799–807, 2005.

[68] T. H. Ng, and W. H. Liao, “Feasibility study of a self-powered piezoelectric sensor,” Proc. Smart Structures and Materials Conference, Proc. SPIE, vol. 5359, pp. 377-388, 2004.

[69] L. Mateu, and F. Moll, “Optimum piezoelectric bending beam structures for energy harvesting using shoe inserts,” *Journal of Intelligent Material Systems and Structures*, vol. 16, no. 10, pp. 835-845, 2005.

[70] H. S. Yoon, G. Washington, and A. Danak, “Modeling, optimization, and design of efficient initially curved piezoceramic unimorph for energy harvesting applications,” *Journal of Intelligent Material Systems and Structures*, vol. 16, no. 10, pp. 877-888, 2005.

[71] T. H. Ng, and W. H. Liano, “Sensitivity analysis and energy harvesting for a self-powered piezoelectric sensor,” *Journal of intelligent material system and structure*, vol. 16, pp. 785-797, 2005.

[72] E. Klimiec, K. Zaraska, and W. Zaraska, “Micropower source based on piezoelectric polymers,” *Advances in Applied Ceramics*, vol. 109, no. 3, pp. 152-155, 2010.

[73] B. Richter, J. Twiefel, and J. Wallaschek, “Piezoelectric equivalent circuit models,” *Springer Science+Business Media, LLC*, Energy Harvesting Technologies Chapter 4, 2009.

[74] B. E. Lewandowski, K. L. Kilgore, and K. J. Gustafson, “Feasibility of an implantable, stimulated muscle-powered piezoelectric generator as a power source for implanted medical devices,” *Springer Science+Business Media, LLC*, Energy Harvesting Technologies Chapter 15, 2009.

[75] D. Jia, J. Liu, and Y. Zhou, “Harvesting human kinematical energy based on liquid metal magnetohydrodynamics,” *Physics Letters, Section A: General, Atomic and Solid State Physics*, vol. 373, no. 15, pp. 1305-1309, 2009.

[76] M. Papila, M. Sheplak, and L. N. Cattafesta, “Optimization of clamped circular piezoelectric composite actuators” *Sensor and Actuators A: Physical*, vol. 147, pp. 310-323, 2008.

[77] M. Brissaud, “Theoretical modeling of non-symmetric circular piezoelectric bimorphs,” *Journal of Micromechanics and Microengineering*, vol. 16, pp. 876-8, 2006.

[78] V. R. Challa, M. G. Prasad, Y. Shi *et al.*, “A vibration energy harvesting device with bidirectional resonance frequency tenability,” *Smart Materials and Structures*, vol. 17, no. 1, 2008.

[79] V. H. Hasselquist, “Pneumatic bellows pump,” U.S. Patent No. 2,686,006, 1954.

[80] D. F. Meschan, “Shock Absorbing Athletic Shoe,” U.S. Patent No. 6,996,923 B2, 2006.

[81] R. Chin, E. Loth, and E. T. Hsiao-Wecksler, “Fluid-power harvesting by pneumatic bellow during human giant,” *8th International symposium on Fluid Power, ASME Fluids Engineering Conference*, Jacksonville, FL, 2008.

[82] Canada GPS. http://www.canadagps.com/Holux_GR241.html. Accessed January 2011.

[83] Air Conditioned Shoes. http://www.dailymail.co.uk/news/article-495399/Smelly-feet-Try-pair-air-conditioned shoes.html. Accessed November 2007.

[84] Nike Air Pump shoes. http://www.freewebs.com/twix_182/willsrandomreview.htm, .

[85] Smalley Steel Ring Company. http://www.smalley.com/whats_new/2010_feb_08.asp. Accessed February 2009.

[86] D. Benasciutti, L. Moro, S. Zelenika *et al*., “Vibration energy scavenging via piezoelectric bimorphs of optimized shapes,” *Microsystem Technologies*, vol. 16, no. 5, pp. 657-668, 2010.